Mon. Not. R. Astron. Soc. **275,** 255–300 (1995)

The soft gamma repeaters as very strongly magnetized neutron stars – I. Radiative mechanism for outbursts

Christopher Thompson[1] and Robert C. Duncan[2]
[1] *Canadian Institute for Theoretical Astrophysics, 60 St George St, Toronto, Canada M5S 1A7*
[2] *Department of Astronomy, University of Texas, Austin, TX 78712, USA*

Accepted 1995 January 11. Received 1995 January 6; in original form 1994 October 26

ABSTRACT

A radiative model for the soft gamma repeaters and the energetic 1979 March 5 burst is presented. We identify the sources of these bursts with neutron stars the external magnetic fields of which are much stronger than those of ordinary pulsars. Several independent arguments point to a neutron star with $B_{\rm dipole} \sim 5 \times 10^{14}$ G as the source of the March 5 event. A very strong field can (i) spin down the star to an 8-s period in the $\sim 10^4$-yr age of the surrounding supernova remnant N49; (ii) provide enough energy for the March 5 event; (iii) undergo a large-scale interchange instability the growth time of which is comparable to the ~ 0.2-s width of the initial hard transient phase of the March 5 event; (iv) confine the energy that was radiated in the soft tail of that burst; (v) reduce the Compton scattering cross-section sufficiently to generate a radiative flux that is $\sim 10^4$ times the (non-magnetic) Eddington flux; (vi) decay significantly in $\sim 10^4$–10^5 yr, as is required to explain the activity of soft gamma repeater sources on this time-scale; and (vii) power the quiescent X-ray emission $L_{\rm X} \sim 7 \times 10^{35}$ erg s^{-1} observed by *Einstein* and *ROSAT* as it diffuses through the stellar interior.

We propose that the 1979 March 5 event was triggered by a large-scale reconnection/interchange instability of the stellar magnetic field, and the soft repeat bursts by cracking of the crust. The hard initial spike of the March 5 event is identified with an expanding pair fireball, and the soft tail of that burst, together with the short, soft repeat bursts, with a pair plasma trapped in the stellar magnetosphere. We construct a detailed radiative model that describes the cooling of such a plasma. The opacity is dominated by the electron–baryon contaminant in a cold surface layer, and the plasma releases energy as the edge of the pair-dominated region propagates inward, in a cooling wave. The rate at which the plasma volume contracts is limited either by the rate of advection of heat toward the stellar surface (where the field is strongest and the scattering opacity weakest), or by ablation of ions and electrons from the stellar surface.

The effective temperature of the surface radiation depends only on the surface magnetic field strength in the regime where the radiative flux is limited by ablation from the neutron star surface (which is the regime of interest in the March 5 event), and otherwise is weakly dependent on the plasma energy density. We argue that the deposition of equivalent energy in a much weaker magnetic field (characteristic of ordinary pulsars) necessarily generates a very high scattering depth which chokes off the radiative flow on the observed ~ 0.1-s time-scale of soft gamma repeater bursts. Indeed, we suggest that the same basic magnetospheric emission mechanism operates at lower field strengths ($B \sim 10^{12}$ G) in Type II X-ray bursts, which have much lower luminosities than soft gamma repeater bursts.

Important magnetic radiative effects include the suppression of Compton scattering in the extraordinary polarization mode, and stimulated photon splitting. We derive the Boltzmann equations for the photon occupation number which describe stimulated photon splitting, as well as *photon merging*. We show that the net splitting

rate vanishes in thermal equilibrium. Radiative diffusion occurs primarily in the E-mode, although rapid scattering of the O-mode ensures convergence of the photon distribution function to a Bose–Einstein form. This allows us to write down diffusion equations for the photon energy flux and number flux as linear superpositions of gradients in the temperature and chemical potential. The transition from a Planck to a Bose–Einstein spectrum occurs at $T \sim 10$ keV. Photon splitting at higher temperatures can impede free-streaming of photons across the magnetic field lines, but splitting of high-energy photons is impeded by the inverse process of photon merging.

We demonstrate that only a small fraction of the pair bubble energy can be conducted into the crust during the lifetime of the burst. We discuss the radiative ablation of matter from the heated stellar surface after the magnetospheric pair plasma is dissipated. The ensuing surface afterglow is typically ~ 1 per cent of the burst luminosity. Direct pair neutrino cooling of the plasma is shown to be unimportant for soft gamma repeater bursts, but may help to determine the light curve of the March 5 event. Finally, we make a critical comparison between this model and models in which the soft gamma repeater bursts are triggered by accretion and/or involve surface cooling.

Key words: magnetic fields – radiation mechanisms: thermal – radiative transfer – stars: neutron – gamma-rays: bursts.

1 INTRODUCTION

The soft gamma repeaters (SGRs) are a small, enigmatic class of hard X-ray transient sources (Norris et al. 1991). The identification of these sources with neutron stars is suggested by the relative hardness and extreme luminosities of the bursts, and by the coincidence of all three known repeaters with young ($t \sim 10^4$ yr) supernova remnants (Cline et al. 1982; Kulkarni et al. 1994; Murakami et al. 1994; Vasisht et al. 1994), as well as by the detection of persistent X-ray emission from at least two sources (Rothschild et al. 1993; Rothschild, Kulkarni & Lingenfelter 1994; Murakami et al. 1994). SGR 0526 − 66 also emitted the famous and peculiar burst on 1979 March 5, which lasted a thousand times longer, and released $\sim 10^4$ times more energy, than the soft bursts that characterize all three sources. We will argue that the March 5 event, unique though it may be, provides a Rosetta stone for the SGR sources.

SGR bursts are much more luminous than ordinary X-ray bursts [$L \sim (10^3$–$10^4) L_{\rm edd}$ as compared with $L \sim L_{\rm edd}$] and have harder spectra (a blackbody temperature $T \sim 9$ keV for the bursts of SGR 1806 − 20: Fenimore, Laros & Ulmer 1994). They share with the Type II X-ray bursts (which are emitted by the Rapid Burster: Lewin, van Paradijs & Taam 1992) a tendency for the brightest bursts to have flat-topped profiles, and a marked degree of spectral uniformity within bursts. Besides showing only weak spectral evolution during single events (Kouveliotou et al. 1987; Golenetskii et al. 1987), SGR bursts of widely differing fluences emitted by the same source have similar spectra (Fenimore et al. 1994). The similarity between the spectra of the soft tail of the March 5 event and the ensuing short, soft bursts is especially remarkable, given the factor $\sim 10^4$ difference in total burst energy (Mazets et al. 1982). It has been suggested that SGR bursts have a characteristic luminosity (Paczyński 1992), but this may be an artefact of the coincidence that most of the repeat bursts detected from 0526 − 66 had peak fluxes within a factor of 2 of the instrumental detection threshold (Norris et al. 1991). Unlike Type I or Type II X-ray bursts, SGR bursts show absolutely no correlation between the burst energy and the time before the next (or since the previous) burst (Laros et al. 1987). This suggests that the trigger for SGR bursts is not accretion, but rather an instability of the stellar magnetic field (Duncan & Thompson 1992, hereafter DT92.

The hyper-Eddington radiative fluxes associated with SGR bursts strongly suggest some confinement mechanism for the radiating plasma. The simplest possibility is magnetic confinement (Thompson & Duncan 1993b, hereafter TD93b; Duncan & Thompson 1994, hereafter DT94; see also Lamb 1982, and references therein). The energies radiated in SGR bursts, if deposited in the magnetosphere of a neutron star, are sufficient to generate a thermal photon–electron–positron plasma with a very high optical depth to electron scattering. We will show that such a confined bubble of hot plasma loses energy by shrinking in volume, with radiative diffusion confined to a thin photospheric boundary layer. This model predicts weak spectral evolution as the radiative surface area decreases, and the luminosity of the escaping X-rays declines (DT94; Section 3). Both these features are consistent with the observed behaviour of the extended, soft-spectrum tail of the 1979 March 5 event. This tail was also modulated on an 8-s period, with pulse and interpulse features that decline with distinct time histories over many cycles (Mazets et al. 1979; Cline et al. 1980). Idealizing the emission as blackbody, one finds an *initial* emitting area of the first peak of the soft tail that is moderately larger than the surface area of a neutron star (Section 7), declining to moderately less than the surface area over the first ~ 10 s. At the same time, the X-ray spectrum hardly varied (Mazets et al. 1982). These observations suggest thermal emission zones that are physically tied to the surface of the neutron star (via a confining magnetic field), are periodically occulted as the star rotates, and that shrink gradually on a time-scale somewhat longer than the rotation period. This behaviour does not suggest

emission from a 'hotspot' on the star's surface, which must redden as the intensity declines.

Other, more direct, support for magnetic confinement also comes from the March 5 burst. The hard initial transient phase of this burst contained an energy $\sim 1\times10^{44}$ erg (if radiated isotropically: Mazets et al. 1979) and had a harder spectrum than the remainder of the burst (Fenimore et al. 1981). Whatever mechanism triggered the event evidently released a large amount of energy outside the neutron star, in a very pure form consisting almost entirely of photons and electron–positron pairs. Even a tiny contamination by ions and electrons would provide a large enough scattering depth to soften the observed photon spectrum (via adiabatic work done on the baryons) to an energy well below the electron rest mass (Section 2.1). Thus *sudden accretion is almost certainly not a viable mechanism for powering the March 5 event*, and one is limited to energy sources intrinsic to the star. A magnetic field is the cleanest plausible energy source, i.e. one that is not contaminated with baryonic matter.

Now, the total observed duration of the March 5 burst was ~ 200 s, more than ~ 1000 times the duration of the initial hard spike, even though the total energy detected from the burst was only ~ 5 times the energy detected from the hard spike. This suggests that essentially *all* the energy of the March 5 burst was released outside the neutron star during the initial ~ 0.15-s transient phase, with some of the energy escaping immediately and the rest remaining trapped in the stellar magnetosphere.

The hypothesis of magnetic confinement allows us to make a simple and reliable estimate of the dipole magnetic field strength of SGR 0526 − 66. The total energy radiated in the soft tail of the March 5 event was $E_{\rm tail}\approx 3.6\times10^{44}$ erg (Mazets et al. 1979). Confinement of this energy in the form of a photon-pair plasma by a closed magnetic flux loop of outer radius ΔR requires that the field pressure at the outer boundary of the loop exceed

$$\frac{[B(R_\star+\Delta R)]^2}{8\pi}\gtrsim\frac{E_{\rm tail}}{3\Delta R^3}. \qquad (1)$$

Here, $R_\star$ is the stellar radius. For a dipole field geometry $B(R)=B_\star(R/R_\star)^{-3}$, which will be a reasonable approximation at $\Delta R\gtrsim R_\star$, a polar field strength

$$B_\star>4\times10^{14}\left(\frac{\Delta R}{10\ {\rm km}}\right)^{-3/2}\left(\frac{1+\Delta R/R_\star}{2}\right)^3\ {\rm G} \qquad (2)$$

is implied. The presence of the hard-spectrum initial transient (which was probably due to a relativistic outflow) suggests that the confinement may have saturated, in which case equation (2) gives an *estimate* of the dipole field strength rather than a lower bound. We conclude that, *in order to confine the energy radiated in the soft tail of the March 5 event, the magnetic field of the neutron star must exceed that of a typical radio pulsar by a factor* $\gtrsim 10^2$. We have termed such an object a 'magnetar'.

A magnetar spins down very rapidly by the usual mechanism of a magnetized, relativistic wind. As a result, rotation plays no important dynamical role in this model of SGRs. The essential physical difference between pulsars($B_{\rm dipole}\sim 10^{12}$–$10^{13}$ G) and magnetars ($B_{\rm dipole}\sim 10^{14}$–$10^{15}$ G) is that, in the latter, the (external) magnetic energy begins to dominate the rotational energy at a very early age,

$$t_{\rm mag}\sim 200\left(\frac{B_{\rm dipole}}{10B_{\rm QED}}\right)^{-4}\ {\rm yr}, \qquad (3)$$

where[1]

$$B_{\rm QED}=\frac{m_{\rm e}^2}{e}=4.4\times10^{13}\ {\rm G} \qquad (4)$$

is the magnetic flux density at which the energy of the first electron Landau level becomes comparable to the electron rest mass. Thus *the predominant source of free energy in the star is magnetic, not rotational.* Although one cannot rule out the possibility that the cores of ordinary pulsars contain very strong magnetic fields, the dipole magnetic energy of a pulsar never exceeds its rotational energy even in a Hubble time, if $B_{\rm dipole}<5\times10^{12}$ G.

How was the March 5 event triggered? One possibility (Thompson & Duncan 1993a, hereafter TD93a) is that diffusion of the magnetic field through the stellar interior creates a configuration which is subject to a sudden, large-scale interchange instability (e.g. Flowers & Ruderman 1977). The resulting large-amplitude oscillations of the magnetosphere damp quickly (Blaes & Thompson, unpublished). The net result is a pair fireball, part of which expands away from the star, and part of which is trapped in regions of closed field lines (cf. Paczyński 1992). We identify the initial hard transient of the 1979 March 5 event with the escaping fireball. The energy trapped near the star was converted into an optically thick photon-pair plasma, which was also contaminated by a trace of baryonic matter blown off the surface. In this model, the long, soft-spectrum tail of the March 5 event was radiated by this confined plasma.

The repeat bursts from SGR 0526 − 66 which followed the March 5 event had spectra and peak fluxes comparable to those of the March 5 soft tail, but with much shorter durations and smaller total energies, $E_{\rm SGR}\sim 10^{41}$ erg (Golenetskii, Ilyinskii & Mazets 1984; Golenetskii et al. 1987). This is comparable to the maximum observed burst energies emitted by the other two SGRs (e.g. Norris et al. 1991). Because of their spectral similarities, we conjecture that these SGR bursts are radiated from a confined magnetospheric plasma via the same basic mechanism which operated in the March 5 soft tail. The trigger for SGR bursts is evidently much less energetic (by a factor $\lesssim 10^4$) and much more common than the March 5 trigger. A plausible candidate mechanism is cracking of the neutron star crust (DT94).

The above estimate (2) for the dipole field of SGR 0526 − 66 is a remarkable result. None the less, at least six other independent arguments point to magnetic fields of this strength in the SGR sources. (See DT94 for a preliminary discussion.)

(1) *A dipole field* $B_{dipole}\sim 6\times10^{14}$ *G is required to spin down an isolated neutron star to the observed period of 8.0 s in the* $\sim 10^4$*-yr age of the surrounding supernova remnant N49 (DT92).*

The suggested spin-down mechanism is the same one that is known to operate in radio pulsars. SGR 0526 − 66 was

[1]Throughout this paper we use units in which $\hbar=c=1$. Here $m_{\rm e}$ and e are the rest mass and charge of the electron.

probably *not* spun down by accretion, because the displacement of the burster from the centre of the supernova remnants indicates a recoil velocity $\gtrsim 1000$ km s^{-1}, large enough to disrupt even a tight binary (DT92). This constraint would perhaps be avoided if SGR 0526−66 were an old, spun-down neutron star which accreted a disc during the supernova explosion of its binary companion, but then the occurrence of the March 5 event would be difficult to understand (Section 7.3).

(2) *If the March 5 event was powered by a decaying magnetic field, then its total energy, $E_{tot} \sim 5\times 10^{44}$ erg (Mazets et al. 1979), must be no more than a fraction of the available magnetic free energy. Approximating the external field as a dipole with polar strength B_{dipole}, this suggests that $\frac{1}{12}B_{dipole}^2 R_\star^3 \gg E_{tot}$ or, equivalently,*

$$B_{\rm dipole} \gg 0.8\times 10^{14}\ {\rm G}. \qquad (5)$$

The total energy released could have been larger than 5×10^{44} erg if the initial hard transient were beamed, or if most of the energy of the trapped pairs were radiated to neutrinos (Section 5). Of course, a large fraction of the external magnetic energy becomes available for powering a burst only if the field lines are strongly sheared or twisted. This free magnetic energy can be released when the crust yields to the applied magnetic stress (TD93a), or when the field anchored in the core is subjected to a large-scale interchange instability, or when the external shear reaches such an amplitude that the connectedness of the field lines can be changed by reconnection. (See Mikić & Linker 1994 for a recent discussion in the context of solar magnetospheric eruptions.)

Typical SGR bursts have energies $E_{\rm SGR} \lesssim 10^{41}$ erg. Impulsive energy releases of this magnitude are expected when the Maxwell stresses in the crust grow strong enough to crack it. Although this kind of energy release is *gated* by the crustal lattice, most of the free energy is magnetic rather than elastic (as long as $B \lesssim 6\times 10^{15}$ G: Section 2). The required crustal field strength is

$$B_{\rm crust} \simeq 1\times 10^{15}\left(\frac{E_{\rm SGR}}{10^{41}\ {\rm erg}}\right)^{-1/2}\left(\frac{\ell}{1\ {\rm km}}\right)\left(\frac{\theta_{\rm max}}{10^{-3}}\right)\ {\rm G} \qquad (6)$$

(Section 2). Here ℓ is the length of the fracture and $\theta_{\rm max} \sim 10^{-3}$ is the limiting strain at which the crustal lattice cracks.

(3) *SGR sources are associated with young ($t \sim 10^4$ yr) neutron stars. The decaying magnetic field must be capable of triggering SGR activity on this time-scale. Diffusion of magnetic field lines through the crust by Hall drift and through the core by ambipolar diffusion (Goldreich & Reisenegger 1992) both occur on this time-scale if $B \gtrsim 3\times 10^{15}$ G (DT94). The decay rate is therefore controlled by the strength of the internal toroidal field.*

An age $t \sim 10^4$ yr is reasonably well established for the Large Magellanic Cloud supernova remnant (SNR) N49 which contains SGR 0526−66 (Vancura et al. 1992). A similar age is suggested for both SNR G10.0−0.3 which contains SGR 1806−66 (Kulkarni et al. 1994), and SNR G42.8+0.6 which may be associated with SGR 1900+14 (Vasisht et al. 1994). This implies a magnetar birthrate in our Galaxy of[2] $\sim(1\text{–}10)\times 10^{-4}$ yr^{-1} (DT92; Kulkarni et al. 1994). It is significant that no SGRs are observed with much larger ages, even though the inferred birthrate implies that many aged magnetars exist in the Galaxy. This indicates that $\sim 10^4$ yr is a *characteristic* age for the kind of magnetic activity manifested in SGRs.

An internal field of 3×10^{15} G, although higher than our estimates for the external dipole field, is plausible if the magnetic field is generated by an α–Ω dynamo during a short, vigorous convective phase after the birth of the neutron star (DT92; Thompson & Duncan 1994b, hereafter TD94b). The strongest toroidal field that could be generated in a rapidly rotating young neutron star with rotation period $P_{\rm rot}$ is $B_\phi \sim 3\times 10^{17}(P_{\rm rot}/1\ {\rm ms})^{-1}$ G. A toroidal magnetic field much stronger than the poloidal field is probably stable on a hydrodynamical time-scale and, therefore, over most of the SGR activity lifetime (Thompson & Duncan 1995, hereafter TD95).

Hall drift in the crust has different consequences when $B \gtrsim B_{\rm QED}$ from those when the field is weaker. In particular, most of the available magnetic energy is converted to *seismic* energy when $B \gtrsim B_{\rm QED}$ (TD95).

(4) *A very strong magnetic field suppresses the electron scattering cross-section of one photon polarization state, below the Thomson value σ_T, by a factor $\sigma_{es}/\sigma_T \sim (\omega m_e/eB)^2 = 4\times 10^{-4}(\omega/10\ keV)^2(B/B_{QED})^{-2}$ (e.g. Herold 1979). The consequent decrease in the scattering opacity allows a much higher radiative flux to escape from a magnetically confined photon-pair plasma (Section 3). This can lead to photon luminosities much higher than the standard Eddington value, $L_{SGR} \sim 10^4 L_{edd}$, as observed in SGRs, but only if these neutron stars have surface magnetic fields $B_\star \gtrsim 3\times 10^{14}$ G.*

The essential physics of this argument was invoked by Paczyński (1992), who showed that the limiting Eddington flux is amplified by a very strong magnetic field. Indeed, the cooling rate of the trapped photon plasma may be limited by ablation of ions and electrons from the neutron star surface, in which case the radiative flux is close to the magnetic Eddington limit (Section 3). None the less, there are several reasons why magnetospheric emission is to be preferred over surface emission in SGR models: in particular, the lack of spectral evolution is difficult to understand in surface emission models (Section 7.3.2).

The magnetic Compton opacity increases with radius in a dipole field as $\sigma_{\rm es}(R) \propto R^6$ (at constant temperature). This implies that *most of the radiative flux escapes near the neutron star surface, even if the confined photon-pair plasma fills a volume much larger than that of the neutron star* (Section 3). Thus the magnetic confinement model provides a simple explanation for the deep, periodic 8-s modulations of the soft tail of the March 5 event.

The strong similarities between Type II X-ray bursts (XRBs) and SGR bursts mentioned above lead us to suggest that these two types of bursts share the same radiative mechanism. The huge difference between the characteristic luminosities of SGRs ($L \sim 10^4 L_{\rm edd}$) and Type II XRBs ($L \sim L_{\rm edd}$) is then naturally ascribed to the much weaker magnetic

[2]The higher value of the birthrate applies if one identifies anomalous X-ray pulsars with some SGR-like properties (spin period ~ 10 s, association with SNRs, no detected companion, uniform spin-down history) as magnetars. The most notable of such sources is 1E 2269+586 (TD93a; TD93b; Corbet et al. 1994). Other possible magnetar candidates include 4U 0142+614, 1E 1048.1−5937 and RXJ 1838−03 (TD95).

field of the Rapid Burster (which is the best studied source of Type II XRBs). This field is constrained to be $B_{\rm dipole} \sim 10^{12}$ G, characteristic of X-ray pulsars (DT94; Section 7.4).

(5) *Persistent X-ray emission from SGR 0526−66 at the level $L_X = 7\times10^{35}$ erg s^{-1} has been detected by both* Einstein *(Rothschild et al. 1993) and* ROSAT *(Rothschild et al. 1994). The minimum crustal magnetic energy required to power this emission is*

$$\left(\frac{B^2_{\rm crust}}{8\pi}\right) 4\pi R_\star^2 \Delta R \gtrsim L_{\rm X} t_{\rm SGR}, \qquad (7)$$

where $\Delta R \sim 1$ km is the depth of the crust and $t_{SGR} \sim 0.5\times10^4$ yr is the age of the neutron star (inferred from SNR N49: Vancura et al. 1992). This implies that $B_{crust} \gtrsim 1\times10^{15}$ G.

A more realistic calculation indicates that $B_{\rm crust} \gtrsim 3\times10^{15}$ G is required (TD93b; TD95) to power the surface X-ray emission. A photon luminosity as high as $\sim10^{36}$ erg s^{-1} could also be powered by a slow, diffusive rearrangement of the core magnetic field. When the magnetic decay luminosity in the core is higher than $\sim10^{35}$ erg s^{-1}, most of the energy is converted to neutrinos (cf. Van Riper 1991). A large fraction of the magnetic energy released in the crust is converted to low-energy seismic waves, which then couple to magnetospheric Alfvén modes (e.g. Blaes et al. 1989). In this manner, a strong internal magnetic field could power the radio plerion discovered around SGR 1806−20 by Kulkarni et al. (1994) (Section 7.1.2). Note, however, that 1806−20 is the only SGR showing such radio emissions, and unlike SGR 0526−66 does not show strong evidence for a large transverse velocity. These differences might be explicable if the optical–infrared counterpart detected by Kulkarni et al. (1995) is a binary companion to a magnetar.

(6) *The initial hard spike of the March 5 event had a duration $\Delta t_{spike} \approx 0.15$ s (Mazets et al. 1979; Cline et al. 1980; Barat et al. 1983). This is comparable to the internal Alfvén crossing time of the star (or, equivalently, the growth time of an internal magnetic interchange instability) if*

$$B \sim 7\times10^{14}\left(\frac{\rho}{10^{15}\,{\rm g\,cm^{-3}}}\right)^{1/2}\left(\frac{\ell}{10\,{\rm km}}\right){\rm G}. \qquad (8)$$

An alternative possibility is that the energy was released abruptly (in much less than 0.1 s) and that the duration of the resulting fireball was broadened by matter loading. Unfortunately, this also implies a large amount of adiabatic cooling, and hence an implausibly large total burst energy (Section 2). Thus we conjecture that $\Delta t_{\rm spike}$ is the actual time-scale over which pairs and Poynting flux were ejected from the neutron star. This is consistent with the chaotic variability of the hard spike on short time-scales (Barat et al. 1983). The overall duration of the spike is then determined by the motion of the magnetic footpoints across the neutron star, and is essentially the Alfvén crossing time.

To summarize: we have given seven different estimates of the magnetic field of SGRs [including equation (2)], all of which indicate that $B \gtrsim 10 B_{\rm QED}$. Each of these estimates is easily questioned on its own, but when taken together they provide a self-consistent picture for the SGRs, in which *the decaying magnetic field itself is the agent which powers the bursts, confines the photons and pairs near the neutron star surface, and suppresses the scattering depth across the confined photon-pair plasma, allowing hyper-Eddington photon cooling.*

1.1 Magnetar formation and recoils

How is a magnetar formed? A hot, new-born neutron star undergoes vigorous entropy-driven convection with an overturn time of order ~1 ms (Burrows & Lattimer 1988; TD93a) as soon as the energy flux has settled to a quasi-steady state in the outermost layers of the star. As a result, a very strong dipole magnetic field is generated by a helical dynamo if the initial spin is in the millisecond range (DT92). Since the dynamo rapidly cuts off at longer spin periods, this mechanism operates only in a narrow range of initial conditions. Thus a bimodal distribution of dipole magnetic field strengths is expected in this scenario.

There are strong selection effects against observing strong-$B_{\rm dipole}$ neutron stars as radio pulsars, both because they spin down rapidly, and because the birthrate is low [see point (3) above]. By the same token, only those neutron stars with the strongest magnetic fields are detectable as sources of SGR bursts, since otherwise the diffusing field cannot generate sufficient stresses to crack the neutron star crust (which is the favoured mechanism for triggering SGR bursts: Section 2), and since bursts emitted by neutron stars with dipole fields of intermediate strengths generate subluminous bursts.

A millisecond spin period is the natural consequence of the accretion-induced collapse of a white dwarf (e.g. Narayan & Popham 1989), or possibly the merger of a white dwarf companion with the core of an evolved star. In the latter case, the dwarf will collapse immediately if its mass exceeds the Chandrasekhar mass evaluated at the central pressure of the star. Note that the convective instability is guaranteed to occur if the dwarf is able to collapse directly to nuclear density, which requires a pre-collapse dipole field stronger than 10^7 G in accretion spin-equilibrium (TD94b). A significant fraction of accreting white dwarfs in cataclysmic variables have fields this strong (Schmidt & Liebert 1987). When the dwarf has a dipole field less than 10^6 G, the star spins rapidly enough that its collapse becomes rotationally supported before the centre reaches nuclear density (cf. Tohline 1984). In this case the collapsing star will remain relatively cold, both because the bounce shock is substantially weakened, and because the lepton number leaks out before the electron neutrinos develop a large chemical potential (TD94b).

Although the strongest white dwarf magnetic fields, $B \sim 5\times10^8$ G (Schmidt 1989), correspond to a neutron star magnetic field of order 10^{14} G upon compression to nuclear matter density, stronger magnetic fields can be generated in a rapidly rotating, new-born neutron star. The ratio of convective kinetic energy to gravitational binding energy is larger during the transient phase of diffusive neutrino cooling than during any previous convective phase driven by nuclear burning. As a result, the magnetic field generated by an α–Ω dynamo in a new-born neutron star will be stronger than any field inherited from previous phases of stellar evolution (TD93a).

There is some evidence that SGRs are *high-velocity* neutron stars. The identification of SGR 0526−66 with a quiescent X-ray source (Rothschild et al. 1993, 1994) has

revealed that the star is displaced 25 arcsec from the SNR centre. The age of this SNR is $t_{N49} \simeq 5.1 \times 10^3 (E_{51}/n)^{-1/2}$ yr, where $n \sim 0.9$ cm^{-3} is the ambient hydrogen density inferred from the nebular X-ray emission and E_{51} is the energy of the formative explosion in units of 10^{51} erg (Vancura et al. 1992). (Although $E_{51} \approx 1$ for most Type II supernovae, a large remnant energy is expected if the neutron star is formed with a spin period less than ~ 3 ms: DT92; section 15.3 in TD93a.) The transverse velocity is therefore $V_\perp = (1200 \pm 300)(E_{51}/n)^{1/2}$ km s^{-1}, and the most likely three-dimensional proper motion is $(3/2)^{1/2} V_\perp = 1500 (E_{51}/n)^{1/2}$ km s^{-1}. The position of SGR 1806−20 in the SNR G10.0−0.3 also suggests a high transverse velocity, $V_\perp \gtrsim 500$ km s^{-1} (Kulkarni et al. 1994), although in this case the uncertainty is larger because of the irregular shape of the SNR. Finally, there is some tentative evidence that SGR 1900+14 has $V_\perp \gtrsim 10^3$ km s^{-1}, based on the displacement of the SGR error box (Hurley et al. 1994) from the centre of the SNR G42.8+0.6 (Vasisht et al. 1994). If this SNR is truly the birthplace of SGR 1900+14, then the SGR acquired a sufficient recoil velocity to escape from the remnant.

Proper motions of the order of 10^3 km s^{-1} are not unheard of in first-generation radio pulsars: in a recent interferometric survey, 8 per cent of the stars had $V_\perp > 800$ km s^{-1} (Lyne & Lorimer 1994). Although none of the pulsars with high velocities appears to have a particularly strong magnetic dipole field, the inferred proper motion of SGR 0526−66 lies in the high-end tail of the pulsar $V_\perp$ distribution. Thus it is possible that a significant fraction of the proper motion of SGR 0526−66 is a biproduct of the mechanism that generated the strong magnetic field. For example, a strong field will suppress convection in the new-born neutron star, and impart an anisotropy to the escaping neutrino radiation[3] (section 13 in TD93a; DT92). This mechanism clearly predicts a positive correlation between $B_{\rm dipole}$ and $V_\perp$, but it should be emphasized that the required strong field may sometimes be internal to the star. If the seed magnetic field inherited by the new-born neutron star from previous phases of stellar evolution is unusually strong, then a toroidal field $B_\phi \sim 3 \times 10^{15}$ $(B_{\rm seed}/3 \times 10^{12}\ {\rm G})$ $(P_{\rm rot}/10\ {\rm ms})^{-1}$ G will be generated during the first 10 s by linear winding (before the outer convective layer of the star reaches into the central core, e.g. Burrows 1987; Wilson & Mayle 1989). The seed field will not, in general, be symmetric about the equator, in which case the resulting toroidal field suppresses the convective energy flux preferentially in one hemisphere. A transient, small-scale magnetic field, amplified by the convective motions to $\sim 3 \times 10^{15}$ G, might have a similar effect (TD93a). Another mechanism for generating an anisotropic neutrino flux depends upon parity non-conservation in the weak interactions (Vilenkin 1979, unpublished; Dorofeev, Rodionov & Ternov 1985; Bisnovaty-Kogan 1993). This probably cannot generate kicks as large as $V_\perp \sim 1000$ km s^{-1}, however, unless some special assumptions are made about neutrino physics, e.g. that the neutrinos have intrinsic magnetic moments.

[3]It is also possible that the convective motions themselves impart the required anisotropy to the neutrino radiation (e.g. Janka & Müller 1994), with a correlation between $V_\perp$ and $B_{\rm dipole}$ arising as a secondary effect.

Given the large recoil of at least one SGR source, and the inferred birthrate of 10^{-4}–10^{-3} yr^{-1}, there should exist many old magnetars in the halo of our Galaxy. It is possible that these old magnetars emit classic gamma-ray bursts from locations in the halo (DT92; Duncan, Li & Thompson 1993; TD93b; Podsiadlowski, Rees & Ruderman 1995). Alternatively, new-born magnetars should emit relativistic winds of sufficient luminosity to power gamma-ray bursts from cosmological distances (Thompson 1994).

1.2 Plan of the paper

The plan of this paper is as follows. Sections 2, 3 and 4 treat the successive physical stages of an SGR burst.

In Section 2, we discuss how magnetic and crustal stresses in a magnetar can evolve to the point of a catastrophic energy release. We outline the various instabilities, and explain how the durations and energetics of the bursts can be used to choose between them. We suggest that the March 5 event was caused by a large-scale reconnection/interchange instability of the magnetic field, whereas the SGR bursts are initiated by magnetically induced fractures of the neutron star crust. In a companion paper (TD95) we calculate how the energy of a decaying magnetic field is continuously converted into persistent surface X-ray emission, magnetospheric Alfvén radiation, and neutrinos (see also TD93b).

In Section 3 we explain why a confined pair plasma is the inevitable consequence of a large and rapid energy release into the magnetosphere. We present a calculation of the 'magnetic' Eddington limit in Section 3.1 that corrects previous treatments (Paczyński 1992). The thermodynamics of a strongly magnetized photon-pair plasma is discussed in Section 3.3. We then show in Sections 3.4–3.6 that photon energy loss proceeds not by simple diffusion across the magnetosphere, but rather by the inward propagation of the plasma boundary, inside which lies a thin radiative layer. We find analytic approximations for these 'cooling waves' in several distinct physical regimes, applicable to typical SGR events, to the March 5 event soft tail, and to Type II X-ray bursts. Using these solutions, we consider SGR burst light curves in Section 3.7, and explain why in this model the spectral evolution is weak.

Section 4 concentrates on the final phase of an SGR event, the relatively faint photon afterglow, which is radiated by the crust after the magnetospheric pair plasma has dissipated. We show that only a small fraction of the energy of the hot pair plasma is conducted into the cold neutron star crust over the duration of an SGR burst. We compare the observational evidence for such faint, crustal emissions (Kouveliotou et al. 1987) with the expected luminosity of the crustal hotspot.

In Section 5 we calculate the neutrino cooling rate of the trapped pair plasma, and show that neutrino cooling is negligible for typical SGR bursts, but not for the March 5 event.

In Section 6 we return to the subject of radiative transfer in a very strong magnetic field, now considering the physics which may determine the emergent spectra of SGR bursts. We present the Boltzmann equation for stimulated photon splitting (and photon merging) in Section 6.1. The combined effects of photon splitting and magnetic Compton scattering are calculated in Section 6.3. Although energy transport

occurs primarily in the extraordinary polarization state, rapid scattering of the photons in the ordinary polarization state ensures convergence to a Bose–Einstein distribution. We develop a modified diffusion approximation for radiative transfer, in which the energy flux and photon-number flux are expressed as linear superpositions of gradients in temperature T and chemical potential μ. We show that bremsstrahlung and double Compton scattering are less important than photon splitting as photon emission processes in the magnetosphere.

We summarize our results in Section 7, and apply them to the three known SGR sources, 0526−66, 1806−20 and 1900+14. Section 7.3 gives a critical discussion of surface cooling as an alternative radiative mechanism for SGR bursts and the March 5 event, as well as a discussion of sudden accretion as an alternative triggering mechanism. We explain why we favour magnetic triggering and magnetospheric emission over these alternatives.

In Section 7.4 we suggest that Type II X-ray bursts, which share with the SGR bursts the property of weak spectral evolution, are also radiated by a pair plasma trapped in the magnetosphere of a neutron star. The much lower characteristic luminosity of these bursts [$L \sim L_{\rm edd}$ as compared to $L \sim (10^3\text{–}10^4) L_{\rm edd}$ for SGR bursts] is ascribed to the much weaker magnetic field of the Rapid Burster, which is constrained to be $B_{\rm dipole} \sim 10^{12}$ G. The concurrent emission of Type I and Type II X-ray bursts from the Rapid Burster leads us to suggest that patches of the stellar surface have a magnetic flux density much lower than $B_{\rm dipole}$, and that the Rapid Burster is an example of a neutron star the magnetic field of which is in the process of being buried.

Throughout this paper, we use natural units in which $\hbar = c = 1$. We always express the numerical values of expressions in c.g.s. units, except for temperatures which we normalize in units either of keV or MeV, e.g. $T_{\rm MeV}$. We frequently use a subscript to denote the relevant exponent, namely $R_\star = R_{\star 6} \times 10^6$ cm, $E = E_{41} \times 10^{41}$ erg, and so on.

2 ENERGETICS AND THE BURST TRIGGER

Any model for SGR 0526−66 must account for the huge difference between the energy emitted by the March 5 event ($E \sim 5 \times 10^{44}$ erg) and that of a typical repeat burst ($\sim 10^{41}$ erg). Our favoured explanation (DT94) is that the March 5 burst was caused by a large-scale readjustment of the stellar magnetic field, whereas the SGR bursts were triggered when magnetic stresses in a patch of the crust (perhaps a few kilometres in radius) built up sufficiently to crack it.

The internal field evolution of a magnetar differs from that of a pulsar in two important ways. First, the dipole field of a magnetar is strong enough to crack the neutron star crust as it diffuses through the stellar interior. Although the internal magnetic field will relax to magnetostatic equilibrium before the crust solidifies, ambipolar diffusion and Hall drift eventually cause departures from magnetostatic equilibrium, with the result that crustal stresses build up (section 14 in TD93a). Large-scale hydromagnetic rearrangements of the core are not suppressed by the rigidity of the crust. Secondly, the decay time is a strong function of the magnetic field strength. A stronger field is capable of triggering much more energetic bursts at much smaller ages.

The sudden displacement of the magnetic footpoints injects an Alfvén pulse into the magnetosphere with a characteristic frequency

$$\nu(\Delta\ell) \sim \frac{V}{\Delta\ell}. \tag{9}$$

Here, $\Delta\ell$ is the total horizontal displacement of the field lines, and V is the propagation velocity of the magnetic footpoints. In the case where the burst is triggered by a cracking of the crust, V is comparable to the shear wave velocity,

$$V \sim V_\mu = (\mu/\rho)^{1/2} = 1.4 \times 10^8 \ {\rm cm\ s^{-1}}, \tag{10}$$

where μ is the shear modulus of the crust,

$$\begin{aligned}\mu &= 0.3 Z^2 e^2 \left(\frac{\rho Y_{\rm e}}{Z m_{\rm n}}\right)^{4/3} \\ &= 1 \times 10^{31} \left(\frac{\rho}{\rho_{\rm nuc}}\right)^{4/3} \left(\frac{Z}{40}\right)^2 \left(\frac{A}{1000}\right)^{-4/3} {\rm erg\ cm^{-3}}\end{aligned} \tag{11}$$

(Baym & Pines 1971). The numerical value of V_μ in equation (10) refers to a density $\rho/\rho_{\rm nuc} \sim 0.5$, at which $A \sim 1000$ and $Z \sim 32$ are the characteristic nucleon number and charge per nucleus (Negele & Vautherin 1973). There is a characteristic magnetic field strength above which the dominant restoring force is magnetic rather than elastic,

$$B = B_\mu \equiv (4\pi\mu)^{1/2}, \tag{12}$$

which is $B_\mu \simeq 6 \times 10^{15}$ G near the base of the crust.

A key point is that any harmonic excitation of the magnetosphere with a frequency ν [equation (9)] has a minimum characteristic dimension (Fig. 1a)

$$R_\nu \sim \Delta\ell \left(\frac{c}{V_\mu}\right), \tag{13}$$

since the magnetospheric Alfvén velocity is very close to the speed of light. Thus an Alfvén pulse is released directly into the magnetosphere only if the field lines anchored at the position of the crustal fracture have a length greater than $\sim R_\nu$. Otherwise, such a direct injection of Alfvén waves is suppressed, and the seismic waves excited in the crust by the fracture propagate through the crust toward the magnetic poles, where they finally are converted to magnetospheric Alfvén waves (cf. Blaes et al. 1989).

The minimum Alfvén excitation radius will not be much larger than the radius of the neutron star in the case where a patch of the crust fractures and shifts a small distance $\Delta\ell$ in response to magnetic stresses: one finds $R_\nu \sim 20 \Delta\ell_4$ km. The case of a large-scale interchange instability is more complicated, since (1) the readjustment of the core magnetic field may proceed in a large number of discrete steps mediated by the build-up and release of crustal strains, and (2) the instability may be accompanied by reconnection (Section 2.1). The characteristic Alfvén excitation radius scales with the length of the crack. Notice that each successive fracture occurs on a time-scale much less than $R_\star/V_{\rm A}$, where

$$V_{\rm A} = 9 \times 10^6 B_{15} \rho_{15}^{-1/2} \ {\rm cm\ s^{-1}} \tag{14}$$

is the core Alfvén velocity and $B = B_{15} \times 10^{15}$ G is the magnetic field strength in the core.

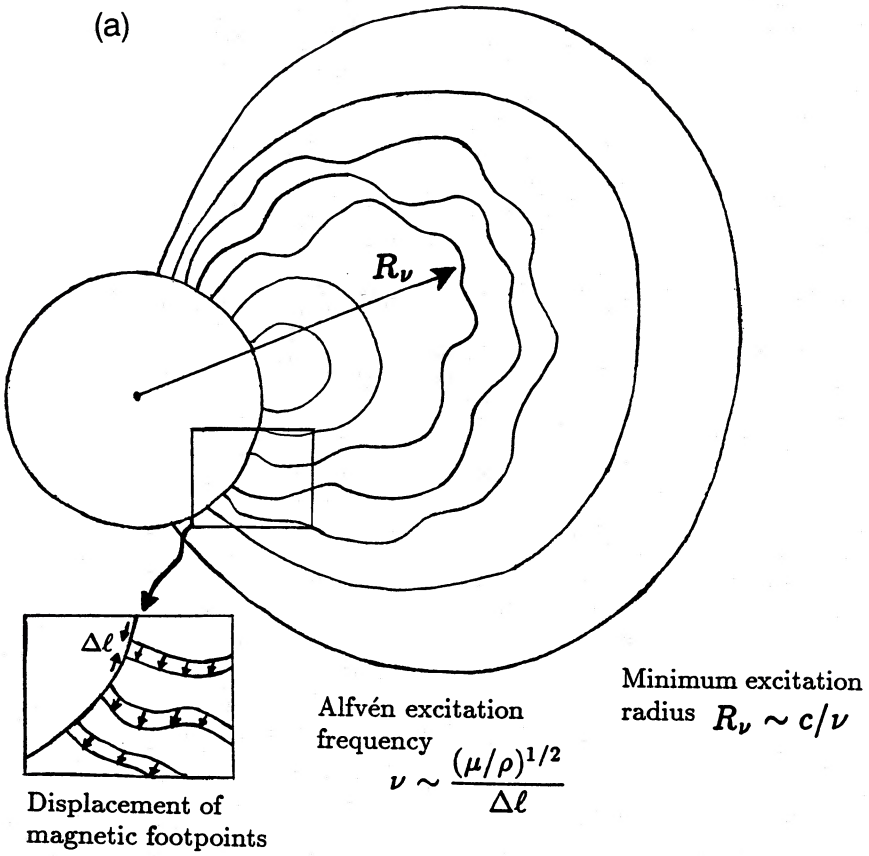

Figure 1. (a) A sudden shift in the magnetospheric footpoints (driven either by a large-scale interchange instability of the core magnetic field, or by a fracture of the neutron star crust) sends an Alfvén pulse of duration ν^{-1} [equation (9)] into the magnetosphere. The characteristic minimum radius of the resultant excitation is $R_\nu = c/\nu$ [equations (13) and (31)]. In this figure, we make the simplifying assumptions that the external field is roughly dipolar, and that the initial crustal shear motion (i.e. the fracture) is localized at high magnetic latitude. (To make the presence of the Alfvén waves clear, they are represented with shorter wavelengths than may be realistic. The modes that are initially excited in the magnetosphere would have wavelengths comparable to R_ν.)

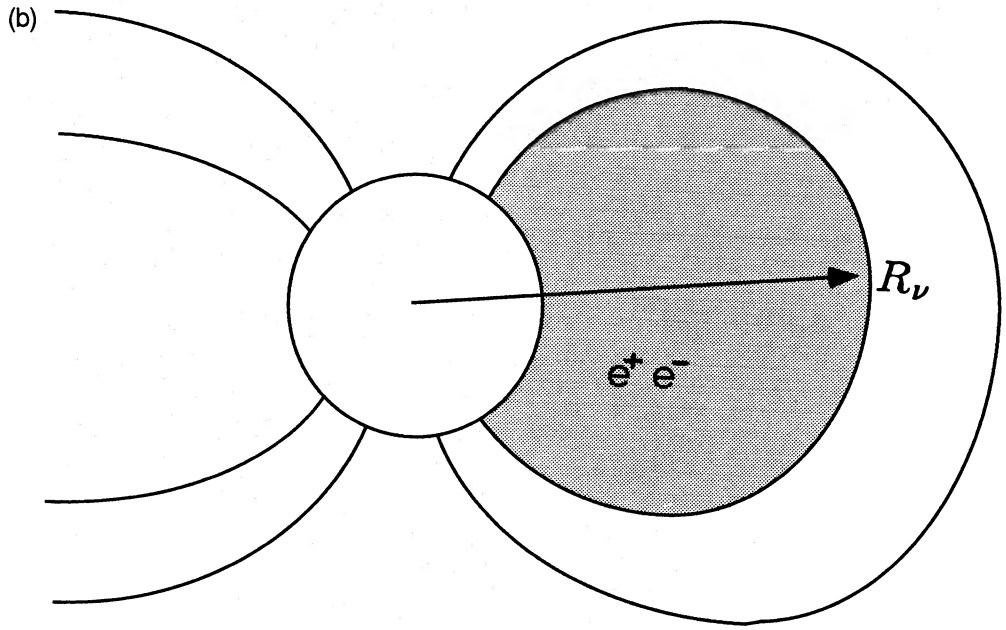

Figure 1. (b) Alfvén waves trapped on closed magnetic field lines cascade to small scales, creating a photon-pair plasma (Blaes & Thompson, unpublished). One possible geometry in which the plasma is confined in an arch is shown.

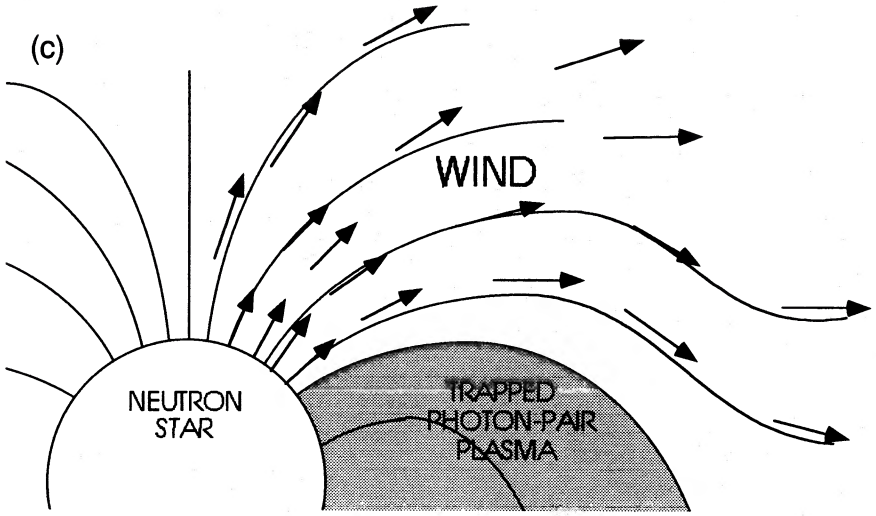

Figure 1. (c) Not all the energy can be contained by the magnetosphere at radius R_ν unless the total energy released is a very small fraction of the dipole magnetic energy of the star. As a result, the pressure of the photon-pair plasma drives a wind from the magnetosphere. This probably occurred in the 1979 March 5 event, but probably not in most ordinary SGR events.

The observational consequences of the Alfvén excitation depend upon the magnetic field strength at the outer radius $R_{\max} = R_\star + \Delta R_{\max}$ of the zone into which the waves are injected. If $B(R_{\max})$ is strong enough to contain the wave energy ΔE in a volume $\sim \Delta R_{\max}^3$,

$$\frac{B^2(R_{\max})}{8\pi} \gtrsim \frac{\Delta E}{3\Delta R_{\max}^3}, \tag{15}$$

then the Alfvén waves remain trapped on the closed field lines on the dynamical time-scale $\Delta R_{\max}/c$. The waves quickly undergo non-linear damping (Blaes & Thompson, unpublished) with Alfvén power cascading to higher wave-numbers, ultimately dissipating into a magnetically confined thermal pair plasma (Fig. 1b). If, instead, $B(R_{\max})$ is weaker than the bound (15), then the net result is a relativistic outflow the duration of which is $\sim R_\nu/c$ (Fig. 1c).

The pattern of Alfvén excitation in the magnetosphere depends upon the exterior field geometry and the location of triggering crustal motions on the star. Fig. 1(a) and (b) show the case where the fracture occurs in a small patch of the crust, and at a high enough magnetic latitude that the magnetospheric field lines can support an Alfvén pulse of frequency $V_\mu/\Delta\ell$. Notice that the resultant excitation and trapped pair plasma are highly asymmetrical, even if the exterior magnetic field is cylindrically symmetric. Other patterns of Alfvén excitation would result from different field geometries and crustal fracture patterns.

2.1 Trigger of the March 5 event

Experience with modelling of solar flares and coronal mass ejections (e.g. Sturrock et al. 1984) suggests that it should be very difficult to decide on a particular magnetospheric instability as the trigger for the March 5 event. None the less, the observed ~ 0.2-s duration of the initial hard transient of the March 5 event (Mazets et al. 1979; Cline et al. 1980; Barat et al. 1983) effectively eliminates some mechanisms: in particular, any magnetospheric instability that releases energy on the magnetospheric Alfvén crossing time of

$$\frac{R_\star}{c} \sim 3\times 10^{-5}\ \mathrm{s}. \tag{16}$$

For comparison, those characteristic time-scales observed in solar flares that are much longer than the magnetospheric Alfvén crossing time are probably the signature of physical processes occurring below the photosphere.

The diffusion of an internal magnetic field causes a displacement of the footpoints of the external magnetic field – in a manner roughly analogous to the turbulent convective motions in the Sun, except on a much longer time-scale. The basic magnetospheric instability which we have in mind is an interchange instability, which leads to an exchange in the positions of the magnetic footpoints (TD93a). This instability may be driven by a reduction in either the internal or the external magnetic energy.

In the case where the external magnetic field drives the instability, a change in the connectedness of the external field lines is required. Since reconnection typically occurs at a fraction of the Alfvén velocity, the growth time of the instability is estimated to be an order of magnitude larger than (16). This is, indeed, comparable to the $\sim 2\times 10^{-4}$ s rise time of the March 5 event (Mazets et al. 1979). In the case where the instability is driven by the internal field, the connectedness of the magnetic footpoints may or may not change. The growth time of the instability is

$$\Delta t \sim \frac{\Delta\ell}{V_{\mathrm{A}}} \sim 0.1 B_{15}^{-1}\rho_{15}^{1/2}\rho_{15}^{1/2}\left(\frac{\Delta\ell}{R_\star}\right)\mathrm{s}, \tag{17}$$

where V_{A} is the internal Alfvén velocity [equation (14)]. This is comfortably close to the observed duration of the intitial hard transient of the March 5 event, if we take $B \sim B_{\mathrm{dipole}} \sim 6\times 10^{14}$ G (DT92). (The internal magnetic field is probably somewhat stronger.)

In sum, the fast rise time of the March 5 event suggests that a reconnection front appeared in the magnetosphere at the beginning of this burst (Paczyński 1992); whereas the longer duration of the hard transient phase of the burst implies that the hard transient was powered mainly by a large-scale hydromagnetic rearrangement of the neutron star core.

What is the precise difficulty with a magnetospheric instability that proceeds on the very short time-scale (16)? If protons and pairs are ejected from the magnetosphere on this time-scale, then the observed gamma-ray flash has a similar duration. Contamination with ions and electrons would certainly lengthen the observed burst, but it would also significantly dilute and soften the gamma-ray flux by adiabatic expansion. Suppose that a mass ΔM_b of baryons is mixed in with an energy ΔE_0 of photons and pairs. If ΔM_b is large enough to lengthen the burst, then the scattering depth through the fireball remains large while the rest-frame temperature has dropped well below m_e and all but a tiny fraction of the positrons have annihilated. The observed burst duration is therefore determined by the radius where the fireball becomes optically thin. The bulk Lorentz factor of the fireball saturates at $\gamma_b = \Delta E/\Delta M_b$ at a radius $\sim \gamma_b R_\star$. If the baryon loading increases by a factor of order unity from the beginning to the end of the burst, then the fireball material is confined within a shell of radial thickness

$$\Delta r \sim \frac{r}{2\gamma_b^2}. \tag{18}$$

This expression holds outside a radius $r \gtrsim \gamma_b^2 (c\Delta t)$, where Δt is the duration of the outflow at the source. The Thomson scattering depth is

$$\tau_T = \frac{Y_e \Delta M_b \sigma_T}{4\pi r^2 m_n r}, \tag{19}$$

where Y_e is the electron number per baryon, and the photon energy is reduced by adiabatic expansion from ΔE_0 to

$$\Delta E \sim \Delta E_0 \left(\frac{r}{\gamma_b R_\star}\right)^{-1} \qquad (r > \gamma_b R_\star). \tag{20}$$

The observed duration of the gamma-ray flash is $\Delta t = \Delta r$ at the radius where $\tau_T \sim 1$. Normalizing Δt to 0.2 s, we infer that the fireball becomes optically thin only at a very large distance from the star,

$$r(\tau_T = 1) = 4 \times 10^{12} \Delta E_{44}^{1/2} Y_e^{-1/2} \left(\frac{\Delta t}{0.2\ \mathrm{s}}\right)^{1/2} \mathrm{cm}. \tag{21}$$

The required baryon loading is large,

$$\gamma_b = 28 \Delta E_{44}^{1/4} Y_e^{-1/4} \left(\frac{\Delta t}{0.2\ \mathrm{s}}\right)^{-1/4}. \tag{22}$$

The key difficulty is that the initial photon energy ΔE required is enormous compared with the observed burst energy of $\sim 1 \times 10^{44}$ erg,

$$\frac{\Delta E}{\Delta E_0} = 2 \times 10^5 \Delta E_{44}^{1/4} Y_e^{-1/4} \left(\frac{\Delta t}{0.2\ \mathrm{s}}\right)^{3/4}. \tag{23}$$

Indeed, ΔE is much larger than the external magnetic energy of the star. *We conclude that the observed ~ 0.2-s duration of the initial hard spike of the March 5 event must reflect the time-scale over which pairs and photons were ejected from the neutron star.* Note also that expression (23) extrapolates to $\Delta E/\Delta E_0 \sim 200 \Delta E_{44}^{1/4} Y_e^{-1/4}$, not to unity, at $\Delta t \sim 3 \times 10^{-5}$ s. There is a very large energetic cost to *any* lengthening of the burst beyond the time interval over which the photons and pairs are ejected from the star.

Thus the initial hard transient of the March 5 event appears to have been a relativistic outflow that continued for many times the external Alfvén time-scale (16). An interchange instability does indeed generate such an outflow. Shear Alfvén waves propagating along the dipole magnetic field cannot transmit energy at a rate higher than

$$L_A(R) \simeq 4\pi R^2 \frac{B^2(R)}{8\pi} c = 5 \times 10^{51} \left(\frac{B_{\mathrm{dipole}}}{6 \times 10^{14}\ \mathrm{G}}\right)^2 \left(\frac{R}{R_\star}\right)^{-4} \mathrm{erg\ s^{-1}} \tag{24}$$

at radius R. Equation of L_A with $\Delta E/\Delta t$, where ΔE is the total energy of the hard spike of the March 5 event, yields a maximum radius

$$\frac{R_A}{R_\star} = 130 \left(\frac{B_{\mathrm{dipole}}}{6 \times 10^{14}\ \mathrm{G}}\right)^{1/2} \left(\frac{\Delta E}{1 \times 10^{44}\ \mathrm{erg}}\right)^{-1/4} \left(\frac{\Delta t}{0.2\ \mathrm{s}}\right)^{1/4} \tag{25}$$

within which the Alfvén waves can be converted to a relativistic outflow. Such a large-scale rearrangement of the stellar magnetic field will proceed in a large number of discrete steps, mediated by the build-up and release of crustal stresses. We estimate the wavelength of the resulting Alfvén pulses in the next section, and show that it is comparable to R_A. As a result, the damping of Alfvén waves in the outer magnetosphere must generate sufficient pair plasma pressure that the magnetic field lines break open and the pairs escape. This model is probably consistent with the rapid variability of the X-ray flux during the initial ~ 0.2 s (Barat et al. 1983).

What fraction of the burst energy remains trapped in the magnetosphere after the neutron star core has relaxed to a new equilibrium? The magnetic field at radius R_A is so weak that only a tiny fraction

$$\sim (R_A/R_\star)^{-3} (\tfrac{1}{12} B_{\mathrm{dipole}}^2 R_\star^3 / \tfrac{1}{3} \Delta E) \sim 4 \times 10^{-4} (B_{\mathrm{dipole}}/6 \times 10^{14}\ \mathrm{G})^{1/2} \Delta E_{44}^{-1/4} (\Delta t/0.2\ \mathrm{s})^{-3/4}$$

of the energy ΔE remains trapped. However, a magnetospheric reconnection front (which, we have argued, initiated the March 5 event) would release energy in a relatively small volume $(\Delta R_{\mathrm{max}})^3 \sim R_\star^3$. As a result, a large fraction of the energy released by a reconnection front is trapped on closed field lines (until it is able to diffuse across the magnetic field lines, which we suggest was responsible for the extended, soft emissions of that burst).

If the magnetic dipole field of the March 5 source were as strong as $\sim 6 \times 10^{14}$ G, then the total energy released in the March 5 event could be even greater than the value derived from the total X-ray fluence. Most of the energy in the trapped pair plasma is lost to neutrino radiation if the energy

of this plasma exceeds $\sim 4\times10^{44}$ erg and the confinement radius is $\Delta R_{\rm max}\sim 10$ km (Section 5).

It should be emphasized that any large-scale interchange instability must be driven by diffusive motions of the magnetic field in the neutron star core. The most likely diffusive process on the short time-scales of interest ($\sim 10^4$ yr) is ambipolar diffusion (cf. Goldreich & Reisenegger 1992). An extremely strong field ($B\sim 10^{16}$ G) can heat the core sufficiently to allow significant radial transport of magnetic flux by the irrotational mode of ambipolar diffusion (TD93b). If the trigger is internal to the star, then the instability is suppressed by the finite tensile strength of the crust if

$$B_{\rm crust} < \theta_{\rm max}^{1/2} B_\mu \sim 2\times10^{14}\left(\frac{\theta_{\rm max}}{10^{-3}}\right)^{1/2}\ {\rm G}, \tag{26}$$

where B_μ is given by equation (12). An external reconnection event driven by shearing of the magnetic footpoints is not limited by the crustal tensile strength, since the instability does not involve any further displacements of the footpoints.

There is an important distinction between a magnetar and the Sun. The drift velocity of the magnetospheric footpoints across the solar surface is much larger relative to the internal Alfvén velocity than is the diffusive velocity of the footpoints across the neutron star surface. In the Sun these two velocities are comparable, whereas in a magnetar the diffusion velocity $\sim R_\star/t$ at age $t\sim 10^4$ yr is smaller than the core Alfvén velocity (14) by a factor

$$\sim 3\times10^{-13} B_{15}^{-1}\rho_{15}^{1/2} R_{\star 6}(t/10^4\ {\rm yr})^{-1}!$$

This suggests that the onset of reconnection in the neutron star magnetosphere is a subtle process. It is plausible that the final small displacement of the magnetospheric footpoints that is needed to trigger reconnection is provided by a sudden cracking of the crust. The estimate (26) is then more appropriate in equation (17), and the growth time of the instability is $\Delta t\sim 0.1$ s if $\Delta\ell\sim 2$ km. This is a reasonable displacement, since the $\sim 5\times10^{44}$ erg radiated in the March 5 event was ~ 60 times smaller than the energy in a 6×10^{14} G dipole field.

Let us discuss some possible triggering mechanisms in more detail.

(1) The relaxation of the internal field to magnetostatic equilibrium inevitably causes tangential discontinuities in the field (e.g. Moffatt 1986). However, reconnection at these discontinuities is (temporarily) impeded by the stable stratification of the neutron star (section 14 in TD93a). This statement holds, in particular, for reconnection between domains of magnetic flux with *opposing* vertical signs: this can take place only to the extent that *vertical* fluid motions are allowed. Diffusion of the internal field can eventually bring into contact two domains with the same vertical sign, thereby triggering a reconnection layer that may propagate upward into the magnetosphere.

(2) Alternatively, the diffusion of the magnetospheric footpoints can shear the external magnetic field. Simulations of this process (in the context of solar magnetospheric eruptions: Mikić & Linker 1994) show that the external field expands outward and becomes more strongly radial at a critical value of the shear. This leads to reconnection, expulsion of a closed magnetic plasmoid, and a reduction in the shear. A simple, cylindrically symmetric model of this process, which shows the same qualitative features, has been contructed by Lynden-Bell & Boily (1994). The ejection of a plasmoid of size $\sim R_\star$ provides a simple mechanism for releasing a large amount of energy in photons and pairs from the neutron star's magnetosphere, but the energy would be released on a very short time-scale compared with the initial hard transient of the March 5 event.

(3) Finally, the internal field may diffuse into a configuration where an interchange (Flowers–Ruderman) instability is no longer inhibited by topology. In this case, motions of the fluid core along equipotential surfaces rearrange both the internal and external fields. Although reconnection is not a necessary consequence of this instability, the very rapid $\sim 2\times10^{-4}$ s rise time of the March 5 event (Mazets et al. 1979) suggests that a reconnection front appeared at the beginning of this burst.

2.2 Trigger of SGR bursts

Now let us consider the brief, much less energetic repeat bursts, which we suggest are triggered by cracking of the neutron star crust (DT94). Blaes et al. (1989) and Ruderman (1991) have discussed the related possibility that classical gamma-ray bursts are powered by elastic energy in the crusts of old neutron stars. When a strong magnetic field is responsible for cracking the crust, however, the magnetic energy released dominates the crustal deformation energy if $B<B_\mu\equiv(4\pi\mu)^{1/2}=6\times10^{15}$ G at the base of the crust, To see this, let us assume that the field is deformed away from magnetostatic equilibrium by an amount δB, and that the resulting Maxwell stress is balanced by the crustal elastic stress. The maximum allowable deformation is

$$\frac{B\delta B}{4\pi} - \theta_{\rm max}\mu, \tag{27}$$

where $\theta_{\rm max}\sim 10^{-4}$–$10^{-2}$ is the yield strain of the crust. The available magnetic energy density is then

$$\frac{(\delta B)^2}{8\pi}\sim\frac{1}{2}\left(\frac{B_\mu}{B}\right)^2\theta_{\rm max}^2\mu, \tag{28}$$

which exceeds the crustal deformation energy by a factor $\sim(B_\mu/B)^2$. Equivalently, the angle by which the magnetic field is bent, $\theta_B\sim\delta B/B$, is *larger* than the compensating crustal strain by a factor[4]

$$\theta_B\sim\left(\frac{B_\mu}{B}\right)^2\theta_{\rm max}. \tag{29}$$

What fraction of the available magnetic energy is released when the crust fractures? Clearly, this depends on the amount of slippage. If the stressed patch of crust slips by a distance that is a fraction $\sim\delta B/B$ of its size, then a significant

[4]When $B>B_\mu$, no self-consistent equilibrium exists under a simple harmonic perturbation, since the crustal strain required to compensate the bent magnetic field induces an even larger bending of the field. An equilibrium can be found only when the crustal stress has a higher wavenumber in the direction $\hat{\boldsymbol{z}}\times(\delta\boldsymbol{B}/\delta B)$, where $\hat{\boldsymbol{z}}$ is a unit vector in the local vertical direction.

fraction of the available magnetic energy is converted directly into an Alfvén pulse and also into seismic waves that damp on a longer time-scale. The maximum amount of magnetic energy released in a patch of area ℓ^2 is, accordingly,

$$E_{\max} \sim 4\times 10^{40}\ell_5^2 B_{15}^{-2}\left(\frac{\theta_{\max}}{10^{-3}}\right)^2 \text{ G}.$$

Here B is the internal crustal magnetic field, which may very well be dominated by a toroidal component that is larger than the external dipole. If, however, the fractional slippage is comparable to the lattice strain θ, then the elastic energy released dominates the magnetic energy by a factor $\sim(B_\mu/B)^2$. We expect that the large estimate of the fractional slippage is more realistic, since the crust can shift a much larger horizontal distance than $\theta_{\max}\ell$ when it cracks over a length-scale ℓ. Then the magnetic footpoints undergo a total displacement

$$\Delta\ell \sim \theta_B\ell \sim 0.04 B_{15}^{-2}\left(\frac{\theta_{\max}}{10^{-3}}\right)\ell_5 \text{ km} \qquad (30)$$

when the crust cracks. The minimum excitation radius (13) of the resulting Alfvén pulse is, accordingly,

$$R_\nu \sim 10 B_{15}^{-2}\left(\frac{\theta_{\max}}{10^{-3}}\right)\ell_5 \text{ km}. \qquad (31)$$

We can make a similar estimate in the case where the poloidal field of the neutron star undergoes a large-scale interchange instability (which is the suggested mechanism powering the 1979 March 5 burst). In this case, stresses in the crust build up as the core fluid is displaced in the horizontal direction (along equipotential surfaces). The motion of the external magnetic footpoints is impeded until the crust is stressed to the point that it cracks. When this happens, the magnetic footpoints are displaced a distance $\sim(B_\mu/B)^2\theta_{\max}R_\star$ horizontally.[5] The resulting characteristic wavelength of the Alfvén pulse is larger than the normalization given in equation (31) by a factor ~ 10. This process is repeated a large number of times, until the core achieves a new magnetostatic equilibrium. Notice that R_ν is much smaller than the estimate $R_\nu \sim 3\times 10^4 R_{\star 6} B_{15}^{-1}\rho_{15}^{1/2}$ km obtained by substituting $\Delta\ell \sim R_\star$ and $V = V_A$ in equation (13).

To conclude, let us contrast the triggering mechanisms for the March 5 event and for the soft repeat bursts. We have suggested that the dominant energy source for both types of bursts is *magnetic*. In both cases, the tensile strength of the crust plausibly provides a gate for the release of the magnetic energy. However, the two types of bursts are distinguished by the *amplitude* of the displacement of the external magnetic footpoints. It appears that the March 5 event involved large-scale horizontal motions of the fluid core that continued until a new magnetostatic equilibrium was established. The Maxwell stresses driving this flow were strong enough that, when the point of instability had been reached, the flow was quasi-continuous. By contrast, the short bursts (emitted by all the SGR sources) involve only small horizontal displacements of the magnetic footpoints, of an amplitude required to relieve the crustal stresses.

One could imagine that the SGR events were caused by reconnection of very small-scale, high-multipole flux elements; or that the March 5 event was powered by the large-scale release of crustal energy.[6] It is difficult to understand, however, why more bursts of intermediate strength should not appear from the March 5 source if both the March 5 event and the repeat bursts were due to reconnection. The most energetic repeat bursts[7] (on 1979 March 6 and 1981 January 12) detected from SGR 0526−66 had fluences of less than 0.5 per cent of the March 5 event. In addition, the maximum amount of elastic energy that can be stored in the crust, assuming the largest reasonable value of the yield strain ($\theta_{\max} \sim 10^{-2}$), is barely sufficient to power the March 5 event (e.g. Blaes et al. 1989). Thus it seems to us (cf. DT94) that the large difference in burst energy is most naturally explained if the March 5 event was triggered by a large-scale interchange instability combined with reconnection, whereas most of the short repeat bursts are caused by cracking of a patch of the crust without reconnection.

3 COOLING OF A MAGNETIZED PAIR PLASMA: THE SOFT TAIL OF THE 1979 MARCH 5 BURST AND THE SOFT REPEAT BURSTS

After the onset of reconnection, or the injection of Alfvén waves into the magnetosphere, energetic charges are rapidly accelerated *throughout* the region of fluctuating fields. This leads to the creation of secondary charges by inverse Compton scattering of photons above the pair-production threshold, and very quickly to an optically thick photon-pair plasma (Fig. 1b).

Although reconnection of magnetic field lines may proceed via the creation of a thin, hot neutral sheet, particle acceleration is not confined to such a diffusive layer. Only a small fraction of the Alfvén wave energy needs to be dissipated in order to generate sufficient charges to support the fluctuating current density. None the less, non-linear couplings between Alfvén waves will generate very high-wavenumber turbulence which transfers its energy effectively to the particles (Blaes & Thompson, unpublished).

Thus our starting point for modelling SGR bursts is an optically thick electron–positron cloud, trapped in the magnetosphere of a neutron star (Fig. 2). Our main purpose in this section is to explain how the pair plasma cools by X-ray emission from its surface. Alternative cooling mechanisms, such as neutrino radiation and conduction into the cold neutron star crust, are treated in Sections 4 and 5.

3.1 Magnetic Compton scattering and enhanced Eddington flux

We consider Compton scattering in a very strong magnetic field, when the excitation energy of the first electron Landau level

$$\omega_{Be}(1) = (m_e^2 + 2eB)^{1/2} - m_e \qquad (32)$$

[5]Here B is the magnetic field strength near the base of the crust, not in the core.

[6]This possibility has also been noted by M. A. Ruderman (private communication).

[7]Detected by more than one spacecraft. The 1982 February 27 burst was detected only by *Konus* (Golenetskii et al. 1987).

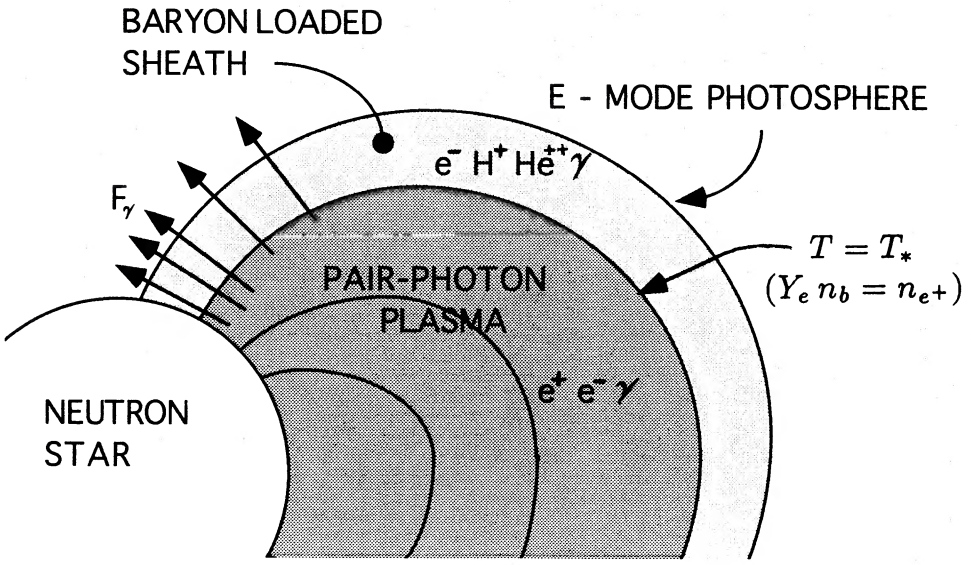

Figure 2. The deposition of $\gtrsim 10^{38}$–10^{41} erg in the magnetosphere of a neutron star is sufficient to generate an optically thick photon–electron–positron plasma. The surface of this plasma is congruent with the magnetic field lines. The surface layers lose heat by radiative diffusion, and the scattering opacity in these layers is dominated by a small contaminant of ions and electrons blown off the neutron star surface.

greatly exceeds the photon energy ω. The cross-section of a photon with electric vector perpendicular[8] to $\boldsymbol{B}$ (the extraordinary mode, or 'E-mode') is strongly suppressed (Mészáros 1992):

$$\frac{\sigma_{es}(\mathrm{E})}{\sigma_T} \simeq \frac{1}{\sin^2\theta_{kB}}\left(\frac{\omega m_e}{eB}\right)^2. \tag{33}$$

Here, θ_{kB} is the angle between $\boldsymbol{B}$ and the photon's wavevector. This holds when the dielectric tensor is dominated by the plasma, which is true in the case of surface emission from a neutron star. Alternatively, when the dielectric tensor is dominated by vacuum polarization corrections (which is true in the case of emission from the magnetosphere), $\sigma_{es}(\mathrm{E})$ is larger by a factor $\sin^2\theta_{kB}$ (Herold 1979). The orthogonal polarization state (the ordinary mode, or 'O-mode') has a much higher cross-section,

$$\frac{\sigma_{es}(\mathrm{O})}{\sigma_T} \simeq \sin^2\theta_{kB}. \tag{34}$$

At high scattering optical depth, diffusion of photons across the magnetic field occurs primarily in the E-mode. It is appropriate to work with Rosseland mean cross-sections rather than opacities when the scattering particles consist mainly of electron–positron pairs, because the total number density of scatterers is not related to the mass density by any simple proportionality. The Rosseland mean scattering cross-section for diffusion in the direction perpendicular to the field is reduced by a factor[9]

$$\frac{\sigma_{es}^{\perp}(B,T)}{\sigma_T} = 2\pi^2\left(\frac{m_e T}{eB}\right)^2 = 7.6\times10^{-5}\left(\frac{T}{10\ \mathrm{keV}}\right)^2\left(\frac{B}{10B_{\mathrm{QED}}}\right)^{-2} \tag{35a}$$

below the Thomson cross-section (Silant'ev & Yakovlev 1980). The cross-section in the direction parallel to the field is higher,

$$\sigma_{es}^{\parallel}(B,T) = 2\sigma_{es}^{\perp}(B,T) \tag{35b}$$

(Silant'ev & Yakovlev 1980). These expressions hold for surface emission. In the case of magnetospheric emission, one has instead

$$\frac{\sigma_{es}^{\perp}(B,T)}{\sigma_T} = \frac{\sigma_{es}^{\parallel}(B,T)}{\sigma_T} = 5\pi^2\left(\frac{m_e T}{eB}\right)^2. \tag{36}$$

Now, the E-mode scattering cross-section $\sigma_{es}(\mathrm{E})$ is the sum of two terms: the cross-section $\sigma_{es}(\mathrm{EE})$ for scattering into the same polarization state, and the cross-section $\sigma_{es}(\mathrm{EO})$ for switching into the O-mode:

$$\sigma_{es}(\mathrm{E}) = \sigma_{es}(\mathrm{EE}) + \sigma_{es}(\mathrm{EO}). \tag{37}$$

[8]When ω is much less than $\omega_{Be}(1)$, the polarization eigenmodes depend on the quantity $x = (1/2)(eB/m_e\omega)\sin^2\theta_{kB}$ (e.g. Mészáros 1992). The O- and E-eigenmodes are *linearly* polarized when $x \gg 1$, and *circularly* polarized when $x \ll 1$. That is, the eigenmodes are linearly polarized in all parts of k-space except for a small cone of angular width $\sim(\omega m_e/eB)^{1/2}$ centred on $\boldsymbol{B}$, where they are circularly polarized. Notice also that, when $B > B_{\mathrm{QED}}$, the condition $\omega \ll eB/m_e$ is not the same as the condition $\omega \ll \omega_{Be}(1)$. None the less, the polarization eigenmodes and the scattering cross-sections of these modes depend on B only through the ratio x, so long as $\omega \ll \omega_{Be}(1)$ (e.g. Herold 1979).

[9]The numerical coefficients in this and the following equation correct those appearing in equations (6) and (7) of Paczyński (1992). In particular, radiative diffusion is *slower* parallel to the field, because the E-mode cross-section peaks when $\boldsymbol{k}$ is aligned with $\boldsymbol{B}$ [equation (33)].

When $\omega m_e/eB \sim 10^{-2}$–$10^{-3}$ (as in the SGR model discussed in Sections 1–4), one has $\sigma_{es}(EO) \sim 3\sigma_{es}(EE)$ (see table 4 in the appendix of Mészáros 1992). This implies that efficient switching between the two modes occurs inside the E-mode photosphere. A similar equation holds for $\sigma_{es}(O)$, where one finds

$$\sigma_{es}(OO) \simeq \sigma_{es}(O), \tag{38}$$

but

$$\sigma_{es}(OE) \sim \sigma_{es}(EO) \ll \sigma_{es}(O). \tag{39}$$

One important feature of (35) and (36) is that the E-mode scattering cross-section is *independent of the electron mass.* Substitution of $\sigma_T = (8\pi/3)(\alpha/m_e)^2$ in equation (35) yields

$$\sigma_{es}^{\perp}(B, T) = \frac{16\pi^3}{3}\,\frac{\alpha T^2}{B^2}. \tag{40}$$

This suggests that expressions (35) and (36) are qualitatively correct in strong fields ($B > B_{QED}$) when $T \gtrsim m_e$. We will therefore use these expressions for both cases $T < m_e$ and $T > m_e$. Expression (40) will break down when T approaches $(2eB)^{1/2}$, the energy of the first Landau level. A calculation of the Rosseland mean scattering cross-sections in a magnetized, relativistic pair plasma would be useful.

This suppression of Thomson scattering leads to an enhancement of the limiting radiative flux where the radiation pressure force balances the force of gravity (e.g. Joss & Li 1980; Paczyński 1992). Assuming that the outward photon pressure gradient force against the electrons is precisely balanced by the downward force of gravity on the ions,

$$\frac{1}{\rho_b}\,\frac{dP}{dR} = -g(R), \tag{41}$$

one finds the magnetic Eddington flux,

$$F_{edd}(B) = \frac{g m_p}{(Y_{e^-} + Y_{e^+})\,\sigma_{es}(B, T_{max})}, \tag{42}$$

where Y_{e^+} (Y_{e^-}) is the electron (positron) number per baryon and T_{max} is the limiting temperature at the photosphere. Notice that, when both polarization states are optically thick, the pressure gradient force is the same for each polarization state. The energy flux $F(i)$ carried by polarization state i is inversely proportional to the opacity $\kappa(i)$ of that state, whereas the upward acceleration of matter is $\kappa(i)F(i)$. The dependence on $\kappa(i)$ cancels. Because the Rosseland mean opacity (35) is defined in terms of the energy density in *both* polarization modes, however, no additional factor of 2 appears in (42).

Writing $F_{edd}^B = (\pi^2/120)T_{max}^4$ (here T_{max} is the effective temperature for blackbody emission in one polarization state) and taking $\boldsymbol{B}$ *locally* to lie in the radial direction, this equation implies

$$\left[\frac{T_{max}(\parallel)}{m_e}\right]^6 = \frac{45}{4\alpha^2\pi^5}\,\frac{g_\star m_p}{(Y_{e^-} + Y_{e^+})m_e^2}\left[\frac{B(R)}{B_{QED}}\right]^2\left(\frac{R}{R_\star}\right)^{-2}, \tag{43}$$

for plasma-dominated polarization modes. Here, $g(R) = g_\star(R/R_\star)^{-2}$. The resulting effective temperature is

$$T_{max}(\parallel) = 7.6\,(Y_{e^-} + Y_{e^+})^{-1/6}\left[\frac{B(R)}{B_{QED}}\right]^{1/3}\left(\frac{R}{R_\star}\right)^{-1/3}\left(\frac{g_{\star,14}}{2}\right)^{1/6}\ \text{keV}. \tag{44}$$

The corresponding flux is

$$F_{edd}^B(R) = 1.7\times 10^{27}(Y_{e^-} + Y_{e^+})^{-2/3}\left[\frac{B(R)}{B_{QED}}\right]^{4/3}\left(\frac{R}{R_\star}\right)^{-4/3} \times \left(\frac{g_{\star,14}}{2}\right)^{2/3}\ \text{erg cm}^{-2}\,\text{s}^{-1}. \tag{45}$$

Hereafter, we call this limiting flux the 'magnetic Eddington flux'. The corresponding luminosity over an area of $4\pi R^2$ is

$$L_{edd}^B(R) = 2.1\times 10^{40}(Y_{e^-} + Y_{e^+})^{-2/3}\left[\frac{B(R)}{B_{QED}}\right]^{4/3} R_{\star 6}^2 \times \left(\frac{R}{R_\star}\right)^{2/3}\left(\frac{g_{\star,14}}{2}\right)^{2/3}\ \text{erg s}^{-1}. \tag{46}$$

The opacity is smaller by a factor of 2 in the case of radiative transport across $\boldsymbol{B}$; use of the same expression for ρ_b yields a slightly larger coefficient for $T_{max}(\perp)$ of 8.5 keV. The opacity is larger by a factor $\frac{5}{4}$ in the case of emission from the magnetosphere, which yields a slightly smaller coefficient for $T_{max}(\parallel)$ of 7.3 keV.

When $\boldsymbol{B}$ is entirely non-radial, or when the radiative flux is in the non-radial direction, magnetic stresses will enter into the force balance (41). None the less, we will argue (Sections 3.2 and 3.5) that the radiative flux across the magnetic field near the neutron star surface cannot greatly exceed the magnetic Eddington flux. This implies that the high burst luminosities of SGRs require magnetic fields stronger than B_{QED}.

3.2 The inevitability of an optically thick magnetospheric pair plasma

What is the immediate consequence of releasing $\sim 10^{41}$ erg into the magnetosphere of a neutron star? This energy could be deposited in the form of either relativistic particles or Alfvén waves.

Relativistic particles are rapidly thermalized, as a simple argument shows. Suppose that electrons and positrons with uniform Lorentz factors γ_e are deposited in a time $\Delta t \sim 0.1$ s and a volume $\sim \Delta R_{max}^3$. Here $\Delta R_{max} + R_\star$ is the maximum radial extent of the (closed) magnetic field lines on which the particles are created. Dissipation is slowest when the relativistic particles are injected in the lowest Landau level: that is, when their momenta are locally parallel to $\boldsymbol{B}$. It is not necessary to assume that the particles move in both directions along $\boldsymbol{B}$, although that may be the case. Suppose that, initially, no photons are present in the magnetosphere. In the absence of collisions, these particles then stream a total distance $\sim 2\Delta R_{max}$ along the magnetic field lines before colliding with the stellar surface. Given a constant injection

rate $\dot{n}_{e^\pm}$ over a time Δt and a total deposited energy ΔE, the *minimum* particle density is

$$n_{e^\pm} \simeq 2\Delta R_{\max}\dot{n}_{e^\pm} = \frac{2\Delta E}{\gamma_e m_e \Delta t \Delta R_{\max}^2}. \quad (47)$$

The total Thomson depth across a distance $\Delta R_{\max}$ is very high,

$$\tau_T(\Delta R_{\max}) \sim 5\times 10^7 \frac{\Delta E_{41}}{\gamma_e \Delta R_{\max 6}\Delta t_{-1}}. \quad (48)$$

Now let us suppose that some seed photons are present, which is guaranteed to be the case since the streaming charges emit curvature photons. The e-folding time of the photon energy density U_γ due to Comptonization is

$$\frac{U_\gamma}{\dot{U}_\gamma} \sim \frac{U_\gamma}{\frac{4}{3}\gamma_e^2 \sigma_T n_e U_\gamma}$$

$$\sim \gamma_e^{-2}[\tau_T(R_{\max})]^{-1}\Delta R_{\max} \ll \Delta R_{\max}. \quad (49)$$

This time-scale is much less than the streaming time $2\Delta R_{\max}$, and decreases as γ_e increases. The same effect will therefore occur if the particles are injected on field lines that open across the light-cylinder, although in that case the limiting energy density of the plasma is lower by a factor $\sim \Delta R_{\max}/\Delta t$.

Expression (49) holds[10] so long as the centre-of-mass energy of the Compton scattering events is less than m_e, which implies that $\gamma_e \lesssim (m_e \Delta R_{\max})^{1/4} \sim 1\times 10^4 \Delta R_{\max 6}^{1/4}$ if the photons are curvature photons with characteristic energy $\sim \gamma_e^3/\Delta R_{\max}$. Compton drag will rapidly reduce the particle energies below this value. In addition, if the charges stream in both directions along the magnetic field with $\gamma_e > \omega_{Be}(1)/m_e$, then they will lose energy at a similar rate by Compton scattering into higher Landau levels. The synchrotron photons emitted by these excited states create new charges by single-photon pair production. We conclude that the energy of the relativistic particles is rapidly converted to a thermal photon-pair plasma, even if the particles are injected steadily over the duration of the burst.

Energy deposited in the form of Alfvén waves is converted by non-linear couplings to higher wavenumbers. The thermalization time therefore depends on the strength of these non-linear couplings, but typically is shorter than the observed ~ 0.1-s duration of SGR bursts (Blaes & Thompson, unpublished).

The quasi-thermal spectra of SGR bursts suggest that the emission region is optically thick. For example, the brightest bursts from SGR 1806 − 20 have approximately blackbody spectra, with a temperature $T_{bb} \simeq 9$ keV which corresponds to an emitting surface of radius $\sim 12(D/8\ \mathrm{kpc})$ km at a distance D (Fenimore et al. 1994). Although other spectral models do give better fits to the data, the fact that the inferred radiative area is close to that of a neutron star strongly suggests that the radiation is, to a first approximation, blackbody. It is common practice to model the spectra as optically thin thermal bremsstrahlung emission, but *such an emission model is not physically consistent.* The free–free optical depth[11] across the emitting volume is $\tau_{ff} \sim F_X/F_{bb}(T_{ff})$, where F_X is the X-ray flux at the source, and $F_{bb}(T_{ff})$ is the blackbody flux at temperature T_{ff}. For $T_{ff} \sim 20$ keV (Fenimore et al. 1994), one has $\tau_{ff} \sim 0.04(D/8\ \mathrm{kpc})^2$. The corresponding magnetic Compton scattering depth is enormous [cf. equation (113)].

The injection of energy must of course be completed in less than the duration of the SGR burst. That is, the injection luminosity L_{inj} must be larger than or equal to the observed luminosity L_γ of the burst. It is natural to consider two cases: one where the injected energy is radiated at the photosphere as fast as it is released by the star, $L_{inj} \sim L_\gamma$ (cf. Melia & Fatuzzo 1993); and a second in which the energy is injected very quickly, $L_{inj} \gg L_\gamma$, and then reradiated on a longer time-scale.

An injection luminosity $L_{inj} \sim L_\gamma$, combined with the quasi-thermal spectra of the bursts, requires that the energy injection be precisely balanced by the radiative diffusion rate out of the magnetosphere. This is very difficult to achieve, for two reasons.

(1) If the scattering depth is dominated by electron–positron pairs, then such a balance is unstable. The thermal pair density grows exponentially with temperature for $T \ll m_e$, regardless of the magnetic field strength [see equations (52) and (54) below], so that an upward perturbation of the internal temperature T_c of the plasma causes the radiative flux to *decrease.* The temperature increases further as energy continues to be injected into the magnetosphere, leading to a rapid quenching of the radiative flux.

(2) Electrons and ions blown off the stellar surface, and suspended by the photon pressure, will provide a huge scattering depth across the magnetosphere, if the radiative flux is as high as that emitted by SGR bursts *and* if the magnetic field is weaker than B_{QED}.

Indeed, it is straightforward to show that *the scattering opacity at the photosphere must be dominated by the electron–baryon component.* We will demonstrate this in two different regimes. (A) When the Landau level excitation energy $\omega_{Be}(1) \ll T$ and also $T \ll m_e$ (which together imply that $B \ll B_{QED}$; this is probably unrealistic for SGRs but not for Type II XRBs), equation (54) for the pair density implies that the Thomson depth is $\tau_T = n_{e^\pm}\sigma_T \ell > 1$ across a distance $\ell \sim 10$ km only when $T_c > T_{pair} = 22$ keV. (B) Alternatively, when the magnetic field is much stronger than B_{QED}, the critical temperature T_{pair} is only slightly larger. For example, when $B = 10B_{QED}$, equations (33) and (52) together imply that $T_{pair} = 27$ keV. For comparison, the bursts of SGR 1806 − 20 have a best-fitting blackbody temperature $T_{bb} \sim 9$ keV (Fenimore et al. 1994), which is well below the temperature at which the pairs contribute significantly to the opacity.

Let us normalize the baryon density in the magnetosphere to the value that can be supported by photon pressure against gravity,

$$\rho_b(T) = \varepsilon_b \frac{P_\gamma(T)}{Rg(R)}, \quad (50)$$

[10]The curvature photons are beamed along $\boldsymbol{B}$ when $\gamma_e \gg 1$, but the bending of the field lines ensures that the photons Compton scatter at a rate comparable to (49).

[11]In a strong magnetic field, this is the optical depth of the E-mode.

where the parameter ε_b does not greatly exceed unity. Then, in the case $\omega_{Be}(1) \ll T$ ($B \ll B_{QED}$), we find a very large electron scattering depth at a temperature T_{eff},

$$\tau_{es} \sim \tau_T \sim 3 \times 10^3 \, Y_e \varepsilon_b \left(\frac{L_\gamma}{10^3 \, L_{edd}} \right). \tag{51}$$

Note that a luminosity of $10^3 L_{edd}$ emitted from a spherical surface of radius R corresponds to an effective temperature of $10 \, R_6^{-1/2}$ keV.

When the radiative flux out of the magnetosphere exceeds the (magnetic) Eddington rate, ions and electrons are easily ablated from the neutron star surface and the matter density in the magnetosphere approaches the limiting value $\varepsilon_b \sim 1$. However, the Rosseland mean scattering depth (35) through the electron–baryon component is suppressed by a strong magnetic field. This implies that, *in order to achieve an X-ray luminosity as high as* $\sim (10^3$–$10^4) L_{edd}$ *from a trapped pair plasma, the magnetic field of the neutron star must be very strong,* $B > B_{QED}$. As a result, the scattering optical depth through the ablated electrons at temperature T_{eff} drops from (51) to $\tau_{es} \sim 1$.

For both of these reasons, we expect that *the radiative flow out of the magnetosphere is determined not by the injection luminosity* L_{inj}, *but instead by the rate at which the photons can diffuse across the confining magnetic field.* This is consistent with Alfvén power estimates (Blaes & Thompson, unpublished) which show that, when $B \gg B_{QED}$, the seismic energy in the crust is injected into the magnetosphere very rapidly, $L_{inj} \gg L_\gamma$.

3.3 Thermodynamics of photon-pair plasmas in strong magnetic fields

When the higher Landau levels are unoccupied, $\omega_{Be}(1) \gg T$ [cf. equation (32)], the energy density of the one-dimensional thermal pair gas is[12]

$$U_{e^\pm} = m_e n_{e^\pm} = \frac{eBm_e^2}{(2\pi^3)^{1/2}} \left(\frac{T}{m_e} \right)^{1/2} \exp\left(-\frac{m_e}{T} \right) \quad \text{for } T \ll m_e, \tag{52}$$

and

$$U_{e^\pm} = \frac{1}{12} eBT^2 \qquad \text{for } T \gg m_e \, (B \gg B_{QED}). \tag{53}$$

In the non-magnetic limit, $\omega_{Be}(1) \ll T$, we have instead

$$U_{e^\pm} = m_e n_{e^\pm} = \frac{2^{1/2}}{\pi^{3/2}} m_e^4 \left(\frac{T}{m_e} \right)^{3/2} \exp\left(-\frac{m_e}{T} \right) \quad \text{for } T \ll m_e \, (B \ll B_{QED}), \tag{54}$$

and

$$U_{e^\pm} = \frac{7}{4} \frac{\pi^2}{15} T^4 \qquad \text{for } T \gg m_e. \tag{55}$$

In magnetic fields weaker than B_{QED}, $\omega_{Be}(1) \simeq eB/m_e = m_e (B/B_{QED})$, whereas, in magnetic fields stronger than B_{QED}, $\omega_{Be}(1) \simeq (2eB)^{1/2} = m_e (2B/B_{QED})^{1/2}$. Thus equation (54) is applicable only when $B \ll B_{QED}$, and equation (53) is applicable only when $B \gg B_{QED}$. The total energy density of a thermal photon-pair plasma is

$$U_{tot} = U_{e^\pm} + U_\gamma = U_{e^\pm} + \frac{\pi^2}{15} T^4. \tag{56}$$

When all the electrons sit in the lowest Landau level [$\omega_{Be}(1) \gg T$], $U_{e^\pm}$ is proportional to B. At a fixed temperature, the pair density increases with the magnetic flux density, on account of the larger density of states ($eB/2\pi$) in the two dimensions orthogonal to the field. This amplification of phase space has an interesting result: the pair (rest mass) energy density *dominates* the photon energy density when $B \gg B_{QED}$ for wide range of T, including $T < m_e$. In the case $B = 10 B_{QED}$, for example, the ratio $\eta = U_{e^\pm}/U_\gamma$ exceeds unity for $T > 60$ keV, reaching a peak of $\eta = 5.8$ at $T = 160$ keV, before asymptotically approaching the ultrarelativistic value of $\eta = 7/4$. This is in marked contrast to the behaviour of $\eta(T)$ for $B < B_{QED}$, which monotonically increases, approaching $\eta = 7/4$ from below as T increases past m_e. Thus pairs can dominate the *energy density* in a non-relativistic, $B \gg B_{QED}$ gas; but note that the *pressure* transverse to the field remains dominated by photons.

If an energy $E = E_{41} \times 10^{41}$ erg is thermalized within a 'magnetic bottle' of size ΔR_{max}^3, the total energy density (56) within the confined plasma is

$$U_{tot} = 10^{23} E_{41} \Delta R_{max\,6}^{-3} \text{ erg cm}^{-3}. \tag{57}$$

Equations (56) and (57) together provide an implicit relation for T. For $B = 10 B_{QED}$ (idealized as uniform throughout the plasma volume), a typical SGR burst with $E_{41} \Delta R_{max\,6}^{-3} = 1$ is in the regime of equation (52) and pair-dominated, with $T = 100$ keV and $\eta = 4.6$. The temperature is an insensitive function of the energy density in this regime, as a result of the exponential in equation (52). In particular, if U increases by factor 10 (or 10^2), the temperature increases by only a factor 1.6 (or 3.7).

In the case of the 1979 March 5 event, the confined energy was $E_{tail} \simeq 3.6 \times 10^{44}$ erg (if isotropic, and neglecting neutrino losses: Mazets et al. 1979). For $R_{max\,6} = 1$ and $B(R_{max}) \sim B_{QED}$, one finds that $T \sim \omega_{Be}(1) \sim m_e$, and that the photons and pairs give comparable contributions to the energy density:

$$U_{tot} \simeq \left(\frac{11}{4} \right) \frac{\pi^2}{15} T^4. \tag{58}$$

One finds a temperature

$$T_{MeV} = 1.0 \left(\frac{E_{tail}}{4 \times 10^{44} \text{ erg}} \right)^{1/4} \Delta R_{max\,6}^{-3/4} \tag{59}$$

within the photon-pair plasma that, we hypothesize, emitted the soft tail of the March 5 event.

3.4 The cooling wave

When the opacity is provided by electron–positron pairs, plasma on closed magnetic field lines is self-trapping. In thermal equilibrium, there is no way of separating the

[12] We use the notation $U_{e^\pm} = U_{e^+} + U_{e^-}$ and $n_{e^\pm} + n_{e^+} + n_{e^-}$.

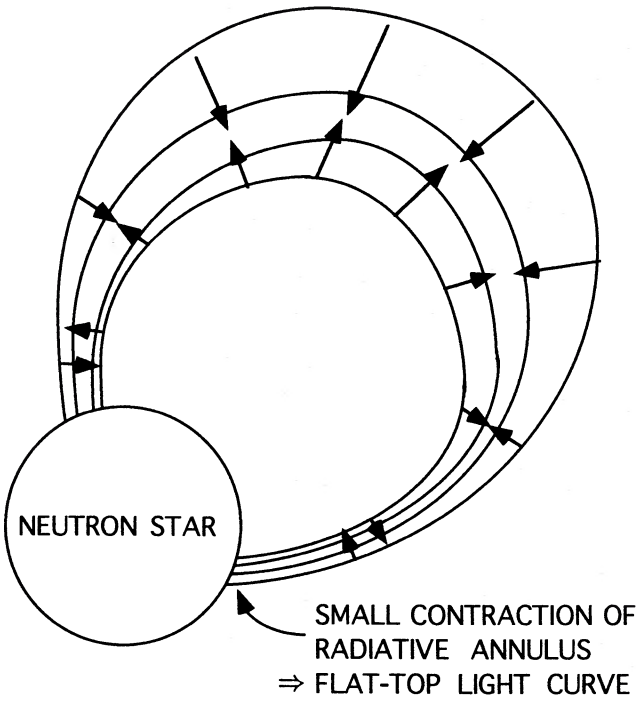

Figure 3. A photon-pair plasma, trapped in a loop of magnetic flux, loses energy as its cool photosphere propagates inward. The scattering opacity at the photosphere is dominated by the electron–ion contaminant.

photons from the source of opacity. The outermost layers of the plasma will be much cooler, however, and the opacity is dominated by electrons ablated from the neutron star surface (Fig. 3).

The boundary between the inner, pair-dominated bubble and the outer, baryon-loaded sheath may be estimated as follows. We take the maximum baryon density (50) that can be supported against gravity by the photon pressure, and equate the corresponding electron density $Y_e\rho_b/m_n$ with the density $n_{e^\pm}$ of the one-dimensional positron gas [equation (52)]. This yields a characteristic temperature T_* which is a weak function of B, $(\varepsilon_b Y_e)$ and R. One finds, in particular,

$$T_* = 30 \text{ keV} \tag{60}$$

for $B = 10B_{QED}$ G, $R = 10$ km and $\varepsilon_b Y_e = 1$. The dependence of T_* on B for various values of $\varepsilon_b Y_e$ is shown in Fig. 4.

Precisely how does the trapped pair plasma cool? The photons will diffuse across the magnetic field lines, but the scattering depth through the pair plasma is enormous (even when the magnetic suppression of the E-mode cross-section is included). The resulting diffusion time across the plasma at a distance R from the neutron star,

$$t_{diff}(R) \sim \frac{\tau_{es}(E)R}{c}, \tag{61}$$

is much longer than a typical SGR burst.

We have already seen (Section 3.3) that most of the energy of the pair plasma is stored in the rest mass of the pairs, $U \simeq m_e n_{e^\pm}$, if the magnetic field is stronger than B_{QED} and the thermal energy of the plasma is in the range expected for SGR bursts. It is possible to avoid the complicated relation (54) between $n_{e^\pm}$ and T by parametrizing the photon energy density as $U_\gamma = (\pi^2/15)T^4 = \varepsilon_\gamma U$. One finds that ε_γ is minimized at $\varepsilon_\gamma \simeq (1 + B/B_{QED})^{-1}$ at a temperature ~ 100 keV.

We assume that the pairs are confined within a volume $\sim \Delta R_{max}^3$. The Rosseland mean scattering depth across the plasma[13] at radius R is obtained from equation (36),

$$\tau_{es}(R) \simeq 5\pi^2 \left[\frac{Tm_e}{eB(R)}\right]^2 \sigma_T n_{e^\pm} R$$
$$= 4.3 \times 10^9 \varepsilon_\gamma^{1/2} E_{41}^{3/2} R_{\star 6} \Delta R_{max6}^{-9/2} \left(\frac{B_\star}{10B_{QED}}\right)^{-2} \left(\frac{R}{R_\star}\right)^7. \tag{62}$$

Here, $B_\star$ is the field strength at radius $R_\star$, and a dipolar geometry is assumed. The Rosseland mean depth through the electron–ion component at the photosphere is somewhat smaller,

$$\tau_{es}(R) = 5\pi^2 \left(\frac{Tm_e}{eB}\right)^2 \tau_T$$
$$= 3.5 \times 10^6 \varepsilon_b \varepsilon_\gamma^{3/2} E_{41}^{3/2} \Delta R_{max6}^{-9/2} \left(\frac{B_\star}{10B_{QED}}\right)^{-2} \left(\frac{R}{R_\star}\right)^7. \tag{63}$$

The parameter ε_b is defined in equation (50). We can now evaluate the diffusion time (61) across the pair plasma. We find

$$t_{diff}(R) = 6 \times 10^4 \varepsilon_\gamma^{1/2} E_{41}^{3/2} R_{\star 6}^2 \Delta R_{max6}^{-9/2} \left(\frac{B_\star}{10B_{QED}}\right)^{-2} \left(\frac{R}{R_\star}\right)^8 \text{ s}. \tag{64}$$

As the confinement radius ΔR_{max} grows, the diffusion at radius $R \sim R_\star$ becomes smaller (the pair density declines). This diffusion time is longer than the ~ 0.1-s duration of an SGR burst unless the surface field is extremely strong, or the confinement volume is extremely large: $B(R_\star) > 3 \times 10^{17} \Delta R_{max6}^{-9/4}$ G. By contrast, the diffusion time at radius R_{max} becomes *longer* as R_{max} increases, as a result of the rapid weakening of B with distance from the neutron star. One finds $t_{diff}(R_{max}) \propto R_{max}^{7/2}$ for a dipole field.

The cooling time is far shorter than equation (64) indicates, for the following reason. The outer boundary of the pair plasma bubble is not, in fact, static. A sharp temperature gradient forms in a thin layer just inside the boundary, and the radiative flux $F_\perp$ perpendicular to the magnetic field lines is enhanced. This thin shell cools rapidly, and moves inward. We now determine its speed of propagation, and the resulting radiative flux.

Free streaming keeps the plasma almost isothermal along the magnetic field lines. When the radiative shell is thin, the temperature gradient ∇T is almost perpendicular to $\boldsymbol{B}$. The temperature increases[14] rapidly from the photospheric value T_{eff} up to the interior value T_c.

Almost all the energy is transported by the E-mode when $T \ll eB/m_e$. Local thermodynamic equilibrium (LTE) is

[13] Along a line intersecting the plasma in the non-radial direction.

[14] This neglects spatial gradients in T on the confinement scale R_{max}. The temperature at the centre of the plasma may therefore be somewhat higher than T_c (the temperature at the inner boundary of the radiative shell).

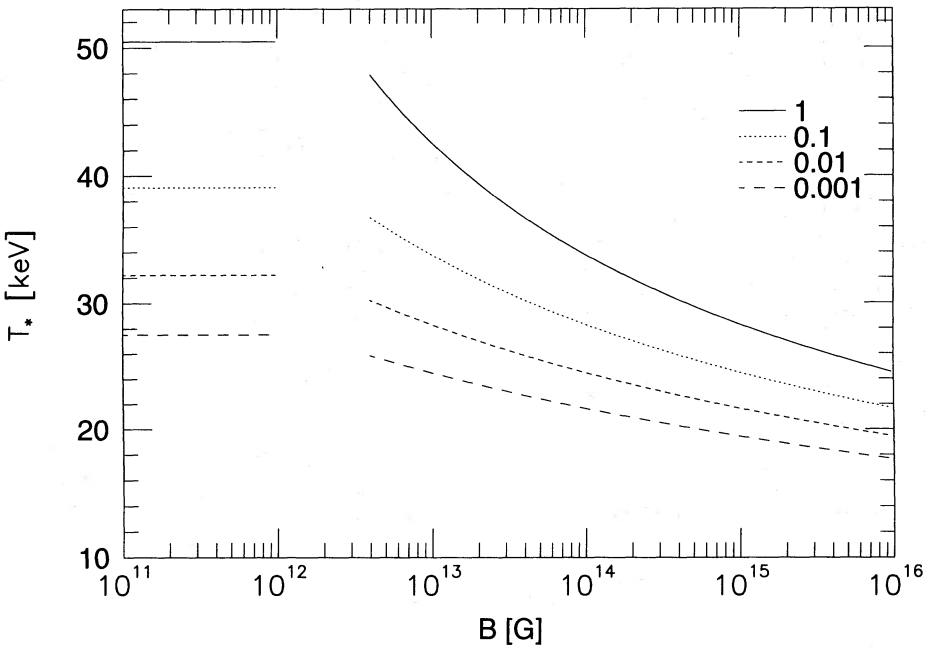

Figure 4. The temperature T_* at which the density of positrons in thermal equilibrium [equation (52) or (54)] is equal to the electron density that can be supported against gravity by the photon pressure [equation (50)]. The various curves are labelled by the free parameter $\varepsilon_b Y_e/R_6$.

established by photon splitting inside the E-mode photosphere down to a temperature ~ 10 keV (Section 6). The radiative flux is[15]

$$F_\perp = \frac{4\pi^2}{45} \frac{T^4}{n_e(B,T)\sigma_{es}^{\perp}(B,T)\ell_T} \tag{65}$$

in the diffusion approximation. Here, $\sigma_{es}^{\perp}(B,T)$ is the Rosseland mean opacity as altered by the magnetic field [equation (36)]. In the magnetosphere of a neutron star, the separation between two magnetic field lines diverges above the surface in proportion to $B^{-1/2}$, and so the temperature scalelength increases with height as

$$\ell_T \equiv \left| \frac{\nabla_\perp T}{T} \right|^{-1} \propto B^{-1/2}. \tag{66}$$

The radiative flux is therefore strongest near the neutron star surface. This conclusion is strengthened when the magnetic suppression of $\sigma_{es}^{\perp}(B,T)$ [equation (36)] is included.

There are two distinct physical processes that can limit the propagation velocity of the cool boundary. Which effect is dominant depends on the energy density of the pair plasma and the strength of the magnetic field.

(1) The radiative flux across the magnetic field lines is strongest near the neutron star surface, and indeed most of the pair plasma energy is lost through a narrow annulus just above the surface when the E-mode scattering cross-section is suppressed well below σ_T. The photosphere cannot propagate inward any faster than thermal energy can be advected along the magnetic field lines *toward* the neutron star (Fig. 5) from the upper regions of the pair bubble (where most of the thermal energy is stored). In general, the maximum advective velocity is reached at the inner boundary of the thin radiative shell, where the temperature reaches T_c.

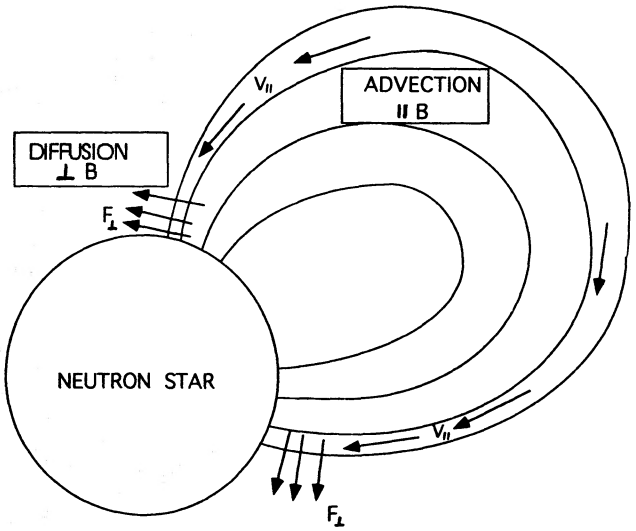

Figure 5. The Rosseland mean scattering opacity is suppressed in a strong magnetic field, $\sigma_{es}(B) \propto B^{-2}$ [equation (35)]. The opacity grows rapidly with radius in a dipolar magnetic field, $\sigma_{es} \propto R^6$, so long as T_{eff} remains less than the energy of the first Landau level. As a result, the radiative flux is highest near the neutron star surface. Most of the energy of the photon-pair plasma is stored near the maximum radius R_{max} of the confining magnetic field lines, and so the thermal energy is *advected* along the magnetic field lines toward the neutron star surface.

[15]Throughout Section 3, we assume that the photon distribution function is Planckian. Deviations from a blackbody spectrum are considered in Section 6.3.

(2) The electron–ion contaminant is the dominant source of opacity at the photosphere, in most instances. This component settles to the stellar surface as the photons diffuse outward and the supporting photon pressure is removed (DT94). This instability is related to the thermal–diffusive 'photon bubble' instability which occurs in neutron star accretion columns (Arons 1992). However, the ions and electrons will not settle out if the radiative flux exceeds the (magnetic) Eddington flux. In a very strong ($B > B_{QED}$) magnetic field, photons streaming away from the E-mode photosphere can ablate material from the neutron star surface. This effect is enhanced by the tendency of E-mode photons to split, thereby creating O-mode photons with a much higher scattering depth. As a result, the radiative flux cannot exceed a numerical multiple of the *magnetic Eddington flux* (45). The advection of ions and electrons from the stellar surface provides the scattering particles at the photosphere in a self-consistent manner.

Even in a simplified field geometry such as a pure dipole, an exact solution of the radiative transfer problem is not possible analytically. We can make progress, however, by separating out the effects of diffusive and advective energy transport. The photosphere propagates inward locally at a velocity $V_\perp$. In the absence of advective motions along the magnetic field lines, the photospheric energy flux is related to the thermal energy density U_c at the base of the radiative boundary layer by

$$F_\perp = V_\perp U_c. \tag{67}$$

The energy flux approaches this limiting value when $T \ll T_c$. Time derivatives are converted to spatial derivatives by substituting

$$\frac{\partial}{\partial t} \rightarrow V_\perp \nabla_\perp, \tag{68}$$

where $\nabla_\perp$ is the spatial gradient in the direction perpendicular to $\boldsymbol{B}$. When one allows for advection and diffusion along the magnetic field lines, the energy equation becomes[16]

$$V_\perp \nabla_\perp U + \nabla_\parallel (H V_\parallel) = -\nabla_\perp F_\perp - \nabla_\parallel F_\parallel. \tag{69}$$

Here, H is the enthalpy density, and $\nabla_\parallel$ and $V_\parallel$ are the spatial gradient and the advective velocity in the direction parallel to $\boldsymbol{B}$.

The radiative flux perpendicular to $\boldsymbol{B}$ is established at the inner boundary of the radiative layer; it receives only a small contribution at temperatures $T \ll T_c$, since $V_\perp \nabla_\perp U \times \ell_T \sim F_\perp (V_\perp / c)(n_e \sigma_{es}^\perp \ell_T)$. Radiative diffusion parallel to the magnetic field can generally be neglected inside the photosphere, where $\ell_T \ll R_\star$. In the absence of radiative gains or losses across the field lines, the vertical gradient is $\nabla_\parallel (H V_\parallel) = (3/R)(H V_\parallel)$ in a dipolar magnetic field. At the inner edge of the radiative layer, the two terms on the left-hand side of (69) are comparable in magnitude to each other, and to the term $-\nabla_\perp F_\perp$. This leads to the estimate

$$\frac{V_\perp}{\ell_T} \sim \frac{|V_\parallel|}{R}. \tag{70}$$

[16]The dynamical pressure of the advective motions can be neglected to a first approximation.

More exact expressions for $V_\perp$ are derived below.

In general, the magnitude of this advective velocity *increases* inward from the photosphere (in the direction normal to $\boldsymbol{B}$). To show this, we must estimate the baryon density at $T < T_*$. We assume that momentum balance along the field lines is solved by

$$\nabla_\parallel \left(\frac{1}{2} V_\parallel^2 \right) \simeq \frac{1}{\rho_b} \nabla_\parallel P_\gamma \simeq -\frac{1}{2} g, \tag{71}$$

which integrates to

$$V_\parallel^2 \simeq R g(R), \tag{72}$$

and yields an estimate for the baryon density,

$$\rho_b \simeq \frac{2 P_\gamma}{R g(R)}. \tag{73}$$

This is slightly larger than the maximum density that can be supported by the photon pressure against gravity at a distance $\sim R$ above the neutron star surface, and the ions and electrons collapse toward the surface at a velocity (72) which is a substantial fraction of the free-fall velocity.

In the case where the radiative flux is limited by advection, we must work out how the advective velocity scales with depth (temperature) in the plasma. One can combine equations (65), (67) and (70) to obtain

$$\frac{|V_\parallel|}{c} \sim \frac{F_\perp^2 n_e \sigma_{es}^\perp (B, T) R}{T^4 U_c}. \tag{74}$$

Assuming that $F_\perp$ is effectively constant in the radiative boundary layer, one finds the scalings

$$\frac{|V_\perp|}{c} \propto T^2 \qquad (T < eB/m_e, T < T_*), \tag{75}$$

and

$$\frac{|V_\parallel|}{c} \sim \text{constant} \qquad (T > eB/m_e, T < T_*), \tag{76}$$

at a temperature $T < T_*$. When the pairs dominate the opacity, one has instead

$$\frac{|V_\parallel|}{c} \propto T^{-3/2} \exp\left(-\frac{m_e}{T} \right) \qquad (T < eB/m_e, T > T_*). \tag{77}$$

We conclude that, for a given surface heat flux $F_\perp$, the largest advective velocity is achieved at $T \sim T_c$.

The assumption of constant $F_\perp$ is accurate when the opacity is dominated by the pairs, since the radial dependence of $F_\perp$ is fixed in local thermodynamic equilibrium. The situation is more complicated in the baryon-loaded sheath, where the electron density is not a unique function of temperature. None the less, we argue in Section 3.6 that little redistribution of the heat flux along $\boldsymbol{B}$ will occur in the baryon-loaded sheath when $B \gg B_{QED}$.

We are now in a position to derive the radiative flux $F_\perp$. We consider three cases in turn.

3.4.1 Case A: SGR burst cooling wave

We assume that the inward propagation of the photosphere is limited by the advection of heat at the base of the photosphere (at temperature T_c) *and* $T_c \ll eB/m_e$. We conjecture that this case applies to bright SGR bursts.

In order to solve for $F_\perp$, we must determine where most of the radiative losses from the bubble occur. These losses can be either localized near the stellar surface or distributed over most of the surface area of the bubble. For parameters appropriate to SGR bursts ($B > B_{QED}$ but $T < m_e$), one finds that the thermal energy is dominated by the pairs, not the photons (Section 3.3), so that $U \simeq H \simeq m_e n_{e^\pm}$. The temperature is low enough that all the pairs are in the lowest Landau level, and $n_{e^\pm} \propto B$ [equation (52)]. Since $\sigma_{es}^{\perp}(B, T) \propto B^{-2}$, the radiative flux integrated across a single flux tube of width $a \propto B^{-1/2}$ (i.e. the luminosity per unit length of the tube) scales as

$$aF_\perp \propto \frac{a}{\ell_T n_e \sigma_{es}^{\perp}(B, T)} \propto B^{-1/2+1/2-1+2} \propto (R_\star + \Delta R)^{-3}, \qquad (78)$$

assuming that T is constant along the tube. Integration of this expression over R shows that the radiative luminosity transported across the tube is equal to $a(R_\star)F_\perp(R_\star)\Delta R$, where ΔR, the height of the effective radiative zone, is given by

$$\frac{\Delta R}{R_\star} \simeq \frac{1}{2}. \qquad (79)$$

This applies for a flux tube with true height $\Delta R_{max} \gtrsim R_\star$, and for idealization of the external field as dipolar, which is reasonable for such a tall magnetic bottle. {More generally, for $B(r) \propto r^{-n}$, the height of the effective radiative zone is $\Delta R/R_\star \simeq (n-1)^{-1}[1-(R_{max}/R_\star)^{-(n-1)}]$.} Now,

$$\int_{R_\star}^{R_\star + \Delta R_{max}} F_\perp \, dR \simeq F_\perp(R_\star)\Delta R \simeq V_\perp n_e(T_c) m_e \Delta R_{max}. \qquad (80)$$

The right-hand side of this equation arises as follows. Consider a flux tube of width ℓ_T at the inner boundary of the cooling layer. The total thermal energy per unit length of the tube is proportional to the enclosed flux,

$$U\ell_T^2 \simeq m_e n_{e^\pm} \ell_T^2 \propto B\ell_T^2, \qquad (81)$$

and is therefore constant along the tube when $\nabla_\parallel T_c = 0$.

At the inner boundary of the cooling layer, one has $\nabla_\parallel(HV_\parallel) \simeq -V_\perp \nabla_\perp U$, which implies that

$$\frac{3|V_\parallel|}{R_\star} \sim \frac{V_\perp \nabla_\perp n_e}{n_e} \simeq \frac{m_e}{T\ell_T} V_\perp. \qquad (82)$$

Since the magnetic field lines converge monotonically toward the stellar surface without forming a nozzle, $|V_\parallel|$ is bounded above by the sound speed c_s. We estimate that

$$|V_\parallel| \simeq c_s \qquad (83)$$

at $T \simeq T_c$.

To see the general form of the solution for $F_\perp$, note that the heat flux at the base of the pair bubble is, to order of magnitude,

$$F_\perp \sim \frac{T_c^4/\ell_T}{\sigma_{es}^{\perp}(B, T_c) n_e(T_c)} \sim \frac{T_c^4 (n_e T_c V_\parallel / F_\perp)}{\sigma_{es}^{\perp}(B, T_c) n_e(T_c) R_\star} \left(\frac{\Delta R_{max}}{\Delta R}\right). \qquad (84)$$

Neglecting the distinction between the photon energy density and the pair energy density, we see that $F_\perp$ scales with the electron scattering depth τ_{es} across the confinement volume as

$$F_\perp \sim \frac{U}{\tau_{es}^{1/2}}, \qquad (85)$$

as opposed to the naïve estimate $F_\perp \sim U/\tau_{es}$.

A more precise expression for $F_\perp$ is obtained by combining equations (36), (65), (79), (82) and (80):

$$F_\perp[\mathrm{A}] \simeq \left[\frac{8}{75} \frac{T_c^3 (eB)^2}{m_e^2 \sigma_T R_\star}\right]^{1/2} \left(\frac{|V_\parallel|}{c}\right)^{1/2} \left(\frac{\Delta R_{max}}{R_\star}\right)^{1/2}. \qquad (86)$$

The corresponding effective temperature (in one polarization state) is

$$T_{eff}[\mathrm{A}] = 15.1 R_{\star 6}^{-1/8} \left(\frac{T_c}{100\ \mathrm{keV}}\right)^{3/8} \left(\frac{B}{10\ B_{QED}}\right)^{1/4} \left(\frac{|V_\parallel|}{c/\sqrt{3}}\right)^{1/8} \times \left(\frac{\Delta R_{max}}{R_\star}\right)^{1/8} \mathrm{keV}. \qquad (87)$$

For a burst energy $E = 10^{41}$ erg and confinement radius $\Delta R_{max} = 30$ km ($T_c = 70$ keV), this corresponds to $T_{eff}[\mathrm{A}] = 15.2(B/10\ B_{QED})^{1/4}$ keV.

3.4.2 Case B: March 5 burst cooling wave

Consider a magnetospheric pair-photon plasma in which the thermal pressure is close to the maximum value that the magnetic field can contain, and $B > B_{QED}$. The inward propagation of the photosphere is limited by the settling of the baryon component. We conjecture that this case applies to the soft tail of the March 5 event.

The electron scattering opacity is no longer suppressed by the strong magnetic field, since $T_c \sim (eB)^{1/2} > m_e$ (cf. equation 59). The thermal energy density is now approximately independent of B: $U \simeq (11\pi^2/60)T^4$. The relation between $|V_\parallel|$ and $V_\perp$ becomes

$$\frac{|V_\parallel|}{R_\star} = \frac{V_\perp}{\ell_T}, \qquad (88)$$

since $H = \frac{4}{3}U$ and $\nabla_\perp U = 4U/\ell_T$. If the cooling rate were limited by advection at temperature T_c, then one would find, by an argument similar to case A, that

$$F_\perp[\mathrm{B}] \sim \left(\frac{T_c^5}{\sigma_T R_\star}\right)^{1/2} \left(\frac{|V_\parallel|}{c}\right)^{1/2} \left(\frac{\Delta R_{max}}{R_\star}\right)^{1/2}. \qquad (89)$$

However, this radiative flux turns out to be much higher than the magnetic Eddington flux (45), which means that ablation from the stellar surface is likely to modify the observable result (Section 3.5).

3.4.3 Case C: Type II X-ray burst cooling wave

Consider a photon-pair plasma confined by a magnetic field weaker than B_{QED}, with central temperature $T_c \gg eB/m_e$. The inward propagation of the photosphere is limited by the settling of the baryon component. We conjecture that this case applies to Type II X-ray bursts (Section 7.4).

The Rosseland mean scattering cross-section depends weakly on B: $\sigma_{es}^{\perp}(B, T) \sim \sigma_T$. The heat flux integrated across a flux tube of width a scales as $aF_\perp \propto a/\ell_T \sim$ constant, implying that the luminosity per unit length along the tube is independent of R. The relation between $F_\perp$ and $V_\perp$ becomes

$$F_\perp \simeq \frac{\pi^2}{15} T_c^4 V_\perp . \tag{90}$$

The radiative flux is still highest close to the neutron star surface, since $\ell_T \propto B^{-1/2}$ is smallest there. Let us calculate $F_\perp$ under the assumption that the cooling flux is limited by the rate at which pressure gradients parallel to $\boldsymbol{B}$ are smoothed out.

The relation between $|V_\parallel|$ and $V_\perp$ reduces to (88), since $H_\gamma = \frac{4}{3} U_\gamma$ and $\nabla_\perp U_\gamma = 4U_\gamma/\ell_T$. Substituting equations (88) and (90) into (65), together with the pair density (54), we find that

$$F_\perp[\mathrm{C}] \simeq \frac{0.15}{\alpha} m_c^4 (m_e \Delta R_{max})^{-1/2} \exp\left(\frac{m_e}{2T}\right)\left(\frac{T}{m_e}\right)^{13/4}\left(\frac{|V_\parallel|}{c}\right)^{1/2}. \tag{91}$$

The corresponding effective temperature is

$$T_{eff}[\mathrm{C}] = 8.5 \Delta R_{max\,6}^{-1/8} \exp\left[0.64\left(\frac{T}{100\ \mathrm{keV}} - 1\right)\right]\left(\frac{T}{100\ \mathrm{keV}}\right)^{13/16} \times \left(\frac{|V_\parallel|}{c/\sqrt{3}}\right)^{1/8} \mathrm{keV}. \tag{92}$$

Just as in case B, this radiative flux turns out to be much higher than the (non-magnetic) Eddington flux, for which $T_{eff} \simeq 1.9\, Y_e^{-1/4} R_6^{-1/2} (M/1.4\ M_\odot)^{1/4}$ keV. Once again we argue that $F_\perp$ is limited by ablation from the neutron star surface (Section 3.5).

In any of the three cases treated above, energy is not actually injected instantaneously into the magnetosphere, but is injected at a finite rate $\dot{U}$. A cool boundary layer develops immediately, but at the beginning the effective temperature is lower than our cooling solution would suggest. At a small time Δt after the injection begins, the surface radiative flux is limited to $F \sim \Delta t \dot{U}$. After a certain elapsed time (which is small compared to the total duration of the SGR burst), the flux reaches its limiting value.

3.5 Cooling rate as limited by ablation from the stellar surface

A basic assumption made in deriving these cooling models is that the photons are able to stream freely from the surface of the magnetic bottle to the observer. There is strong reason to suspect, however, that this assumption breaks down when the radiative flux from the base of the pair bubble [as given by equation (86), or (89) or (91)] exceeds the magnetic Eddington flux (42). This energy flux is far too high to be absorbed by the crust (Section 4). If its magnitude exceeds (4.2), then photons obliquely incident on the star will undergo scatterings in the stellar surface layers and inevitably ablate material from the surface. The photons that diffuse across the photosphere of the magnetospheric cooling wave are in the E-mode, with a Rosseland mean scattering cross-section that is suppressed below σ_T by the large factor (35). Photon splitting in a magnetic field stronger than B_{QED}, however, will create a comparable number of O-mode photons so long as the effective temperature is greater than ~10 keV (Section 6). These O-mode photons will then scatter many more times, and provide a strong radiative force even while the scattering depth of the E-mode remains small. The density of baryonic plasma will build up until the outward pressure of the photons is counterbalanced by gravity. The resulting plasma cloud is optically thick to electron scattering (Fig. 6).

What is the largest radiative flux that can be transmitted through this cold baryon-loaded sheath? The flux perpendicular to the magnetic field lines is $F_\perp \sim P_\gamma/\rho\kappa_{es}(B)\ell_T$, where ℓ_T is the temperature gradient scale. The narrower the sheath, the higher the limiting flux and the faster baryons are ablated from the surface. One therefore expects that ablation will widen the baryon-loaded sheath until either $F_\perp$ drops below the magnetic Eddington limit, or ℓ_T approaches its maximum possible value $R_\star$. In fact, both of these conditions are satisfied simultaneously. While $F_\perp$ still exceeds (42), the baryon density in the sheath is $\rho_b(R_\star) \sim P_\gamma(R_\star)/g_\star h$, where $h \sim R_\star$ is the vertical scaleheight. This yields a limiting radiative flux,

$$F_\perp \sim \left(\frac{h}{\ell_T}\right)\frac{g_\star}{\kappa_{es}(B_\star)} \sim F_{edd}^{B}(B_\star), \tag{93}$$

where we estimate $\ell_T \sim R_\star$.

The maximum radiative flux *perpendicular to* $\boldsymbol{B}$ is, to order of magnitude, equal to the magnetic Eddington limit (42) for *vertical diffusion. This suggests that the interaction of the radiative flux with the neutron star surface provides a value that forces this flux below (42).* The true value of the effective temperature just above the neutron star surface is then given by the minimum of equation (44) and the appropriate cooling wave solution for the trapped pair plasma. That is,

$$F_\perp = \min\{F_{edd}^{B}, F_\perp[i]\}, \tag{94}$$

where i = A [equation (86)], B [equation (89)] or C [equation (91)], as appropriate. One immediate consequence of (94) is that SGR burst sources ($T_{eff} \sim 10$–20 keV) necessarily have magnetic fields much stronger than B_{QED}.

3.6 Inhomogeneity of the photospheric heat flux

A more detailed justification of equation (93) requires an understanding of how the ion–electron component is distributed across the photosphere, which may span a large range of radii and magnetic field strengths. A key point is that the photosphere must remain congruent with the magnetic field lines as the plasma cools. Pressure balance along the radiative surface requires that T_{eff} *decrease* with distance

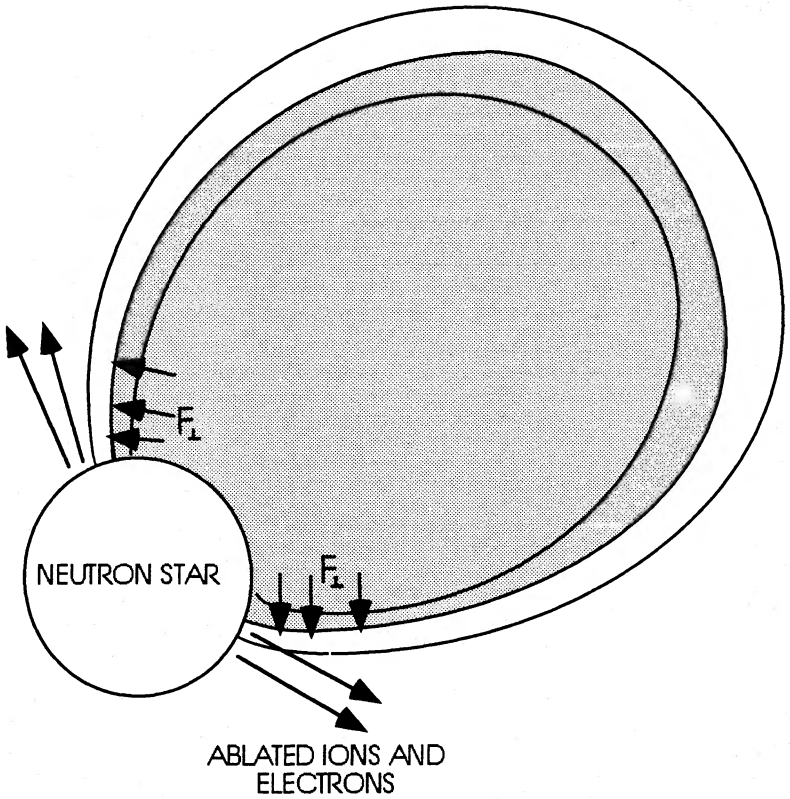

Figure 6. When the radiative flux out of the trapped pair plasma (as given by the cooling wave solution A–C) exceeds the magnetic Eddington flux $F^{B}_{\rm edd}$ [equation (45)], ions and electrons are ablated from the surface of the neutron star, and the radiative flux across the magnetic field lines is reduced to a value comparable to $F^{B}_{\rm edd}$.

from the neutron star. We first treat the case where B is much stronger than $B_{\rm QED}$. The case $B < B_{\rm QED}$ is somewhat subtler.

If the photosphere were to eat into the plasma faster at one point along a magnetic flux tube than at other points, large pressure gradients would develop along the field, and would be smoothed out rapidly, on a time-scale $\sim \Delta R_{\rm max}/c_{\rm s}$. However, $F_\perp$ is a strong function of position $x_\parallel$ along any closed field line. Indeed, the dependence of $F_\perp$ on $x_\parallel$ can be determined straightforwardly in the interior regions of the bubble where $T > T_*$: when the scattering opacity is dominated by the pairs, local thermodynamic equilibrium combined with pressure equilibrium along the field lines fixes the dependence of the charge density on $x_\parallel$. Most of the energy that diffuses out of the pair-dominated region and into the baryon-loaded sheath does so through a layer of height (79). Baryon ablation at the surface of the bubble only affects the size of the temperature gradient at the base of the radiative layer, and thence the overall normalization of $F_\perp$.

Note also that the photon bubble instability discussed by Arons (1992) does not operate when pairs are the dominant source of opacity: in thermal equilibrium, the photons cannot be separated from the scattering particles. This instability may occur in the baryon-loaded sheath, but it only transports energy *along* the field lines (as in the accretion column of a neutron star) at high scattering depth. Outward transport of thermal energy along the magnetic field lines by photon bubbles will not raise the cooling rate significantly, because the bubbles move into a region with a much higher magnetic scattering opacity, and a much longer diffusion time [which increases with radius as $\tau_{\rm diff}(R) \propto R^8$: equation (64)].

The distribution of the *surface* radiative flux is much more difficult to determine, because $n_{\rm e}$ is no longer a simple function of temperature. None the less, there is strong reason to believe that most of the emergent radiation escapes through a layer of height comparable to (79). If the surface flux $F_\perp$ were instead independent of $x_\parallel$, then the baryon density $\rho_{\rm b}$ would necessarily drop off very quickly with distance above the neutron star surface. To see this, suppose that $T_{\rm eff}$ is independent of $x_\parallel$. Then $\rho_{\rm b}\kappa_{\rm es}(B, T_{\rm eff})\ell_T \sim$ constant, which together with $\ell_T \propto B^{-1/2}$ implies that

$$\rho_{\rm b} \propto B^{5/2} \propto R^{-15/2}. \qquad (95)$$

Now, the radiative flux which emerges from the pair-dominated region at $R \lesssim \frac{3}{2}R_\star$ must be redistributed by advection along the magnetic field lines in order to smooth out $T_{\rm eff}$. The problem with a radial density profile as steep as (95) is that the same advective transport which smooths out the heat flow will also smooth out $\rho_{\rm b}$. A significant decrease in the photospheric heat flux with radius R is consistent with pressure equilibrium along the magnetic field lines only if the baryon density is high enough to induce a significant pressure stratification along the radiative surface. This leads, by the argument preceding equation (93), to the conclusion that $F_\perp \lesssim F^{B}_{\rm edd}$.

Now let us consider the effects of ablation from the stellar surface when the confining magnetic field is much weaker than B_{QED}. In this case, the magnetic field does not suppress the E-mode scattering cross-section, and most of the energy that leaks out of the pair-dominated bubble does so at $R \sim R_{max}$, rather than near the stellar surface (see case C of Section 3.4.3). The value of $F_\perp$ near the surface is bounded above by the (ordinary) Eddington value, and so pressure balance along the magnetic field lines then requires that $F_\perp < F_{edd}$ even where the radiation has no direct contact with the surface.

In the pair-dominated interior of the plasma, heat is always advected *toward* the stellar surface, where ℓ_T is smallest and $F_\perp$ is largest. Let us now estimate the outward advective velocity required to smooth out $F_\perp$ at temperatures $T < T_*$, where the opacity becomes dominated by the electron–baryon component. The requirement that the outward advective velocity be less than the sound speed limits $F_\perp$. Imagine that radiation that enters a magnetic flux tube (along a segment of length $\sim R$) is advected along the tube at a velocity $V_\parallel$. Balancing of inward diffusion with advection implies that

$$F_\perp R \sim U_\gamma \ell_T V_\parallel. \tag{96}$$

Taking $\rho_b \sim P_\gamma / gR$ and requiring $V_\parallel < c_s$ [equation (83)], we obtain

$$F_\perp^2 < P_\gamma(T) \frac{g}{\kappa_{es}(T)} \left(\frac{c_s}{c}\right) \qquad (T_{eff} < T < T_*). \tag{97}$$

We see that the limiting flux is highest if the advection occurs at $T = T_*$. Substitution of $T = T_*$ in (97) yields the expression for $F_\perp$ presented in DT94. That expression almost certainly overestimates $F_\perp$, however, for the reasons that we already described.

We conclude that only a mild, subsonic advective motion is required to redistribute the radiative flux along the magnetic field lines, when $F_\perp \sim F_{edd}^B$. None the less, one must still consider the baryon density profile across the photosphere. Assuming that T_{eff} is constant, one finds

$$\rho_b(R) \propto \ell_T^{-1} \propto R^{-3/2}, \tag{98}$$

since κ_{es} is also approximately constant. This baryon density profile is much shallower than that required to produce a uniform photospheric flux when $B \gg B_{QED}$ [equation (95)], and suggests that more smoothing of the flux will occur when $B \ll B_{QED}$.

These arguments also imply that the outer radius of the baryon sheath lies at most a factor ~ 2 beyond the outer radius R_{max} of the pair bubble. The limiting flux (93) corresponds to an E-mode scattering depth $\tau_{es}(E) \sim 1$ across the thickness ℓ_T of the baryon sheath at its base. An extension of the baryon sheath to a much larger outer radius $\sim NR_{max}$ corresponds to a small thickening $\delta\ell_T \sim N^{-1/2} R_\star$ of the base of the sheath (assuming a dipolar magnetic field). The additional scattering depth across the base of the sheath is $\delta\tau_{es}(E) \sim N^{-1/2}$, which suggests that the radiation supporting the bloated baryon sheath will escape in the horizontal direction, and the baryons will collapse toward a radius $R \lesssim 2\Delta R_{max}$.

3.7 SGR light curves and spectral evolution

How does the total X-ray luminosity L_X emitted by the cooling plasma vary with time? One has

$$L_X(t) \simeq A F_\perp, \tag{99}$$

where A is the effective radiating area. When $T > \omega_{Be}(1)$ ($B_\star < B_{QED}$), the radiating surface encompasses most of the area of the pair bubble. When $T < \omega_{Be}(1)$ ($B_\star > B_{QED}$), the radiating surface is an annulus of height $\Delta R / R_\star \sim 1/2$ that lies just above the neutron star surface [equation (79)]. That is, $A = C_{bubble} \Delta R$, where C_{bubble} is the circumference of the base of the pair bubble. This is the regime of interest for SGR bursts.

The photospheric flux $F_\perp$ depends only on B in the case where it is limited by ablation, $F_\perp = F_{edd}^B$. Thus $F_\perp$ is constant during a burst only to the extent that B is constant over the stellar surface. However, when the confinement volume is large, $\Delta R_{max} \gg R_\star$, a large contraction of the volume corresponds to a small displacement of the photosphere across the neutron star surface, and constant B should be a good first approximation. If instead $F_\perp$ is not limited by ablation from the stellar surface (which is the case if the appropriate cooling wave solution gives $F_\perp < F_{edd}^B$), then $F_\perp$ also depends on the internal temperature T_c of the pair bubble. The emergent flux density will, none the less, depend weakly on the thermal energy density in the bubble, e.g. $T_{eff} \propto U_c^{3/32}$ for cooling wave solution (A).

The constancy of $F_\perp$ leads to the prediction that *the effective temperature should vary weakly during the burst* (DT94). In this model, the radiative flux density varies much more slowly during a burst than the flux density emitted by a cooling neutron star surface (Paczyński 1992), which is probably accompanied by mass outflow if the radiative flux is close to the limiting Eddington value. For example, the spectra of Type I X-ray bursts (thermonuclear flashes) are seen to redden conspicuously with time (e.g. Lewin et al. 1992). A crustal cooling model also has difficulty explaining the lack of spectral softening observed during the soft tail phase of the 1979 March 5 event (Mazets et al. 1982), in which the temperature was observed hardly to change even while the total flux dropped by a factor ~ 5.

Notice also that, if the pair bubble is much larger than the neutron star ($\Delta R_{max} \gg R_\star$), and if the stellar field has a quasi-dipolar geometry all the way down to the stellar surface, then most of the outer regions of the pair bubble are confined by a relatively small amount of flux that is anchored at a small angular distance $\theta \sim (\Delta R_{max}/R_\star)^{-1/2}$ from the magnetic poles. In the case where the radiative flux is ablation-limited, the temperature gradient scale behind the photosphere is $\ell_T \sim \theta R_\star$, and $F_\perp$ is larger than (93) by a factor of $\sim \theta^{-2/3}$. If the bubble is cylindrically symmetric, which is probably the case in Type II X-ray bursts (Section 7.4) but not for SGR bursts or for the March 5 event, then $C_{bubble} \simeq 4\pi\theta R_\star$ (there is a contribution from each magnetic pole). The total luminosity scales weakly with θ and is very weakly dependent on the remaining plasma energy E:

$$L_X(t) \propto \theta^{1/3} \propto E^{-1/18}. \tag{100}$$

The light curve will be approximately *flat-topped*.

When the pair bubble is not much larger than the neutron star then the shape of the light curve will depend on the

geometry of the bubble. A bubble with a planar symmetry is produced when the crustal fracture propagates linearly over a distance $\sim R_\star$. In this case, the confining bundle of flux has a very flattened, elliptical cross-section: $A \simeq$ constant and the burst is flat-topped. By contrast, if the bubble has a cylindrical symmetry then both A and L_X decrease linearly with time:

$$L_X(t) = \left[1 - \frac{2F_\perp(R_\star)}{U_c}\left(\frac{\Delta R_{max}}{R_\star}\right)^{-4} t\right] L_X(t=0). \quad (101)$$

The light curve will have a triangular shape. Both types of light curves have been observed (see Kouveliotou et al. 1993 for SGR 1900+14; Mazets et al. 1982 and Golenetski et al. 1982 for SGR 0526−66; Kouveliotou et al. 1987 and Atteia et al. 1987 for SGR 1806−20).

The cooling magnetosphere does not radiate isotropically. Most of the emission will occur near the stellar surface if the field is stronger than B_{QED}, which is consistent with the large-amplitude, periodic modulation of the March 5 soft tail (Mazets et al. 1979). (In Section 6.3, we consider the effects of photon splitting outside the E-mode photosphere on the directionality of the radiation.) Of course, one does not expect to see any rotational modulation of the SGR bursts from SGR 0526−66, since their duration is typically ~ 10–100 times less than the 8-s rotation period. The same is true for the bursts of SGR 1806−20 if this object is also a slowly rotating magnetar.

4 HEAT CONDUCTION INTO THE NEUTRON STAR CRUST AND PHOTON AFTERGLOW

We now calculate the heat absorbed by the crust during the time it takes the pair plasma to leak out of the magnetosphere (Fig. 7a). Most of this absorbed heat is reradiated by surface photon emission after the pair plasma has dissipated (Fig. 7c). There is evidence for such 'photon afterglow' from SGR 1806−20 (Kouveliotou et al. 1987).

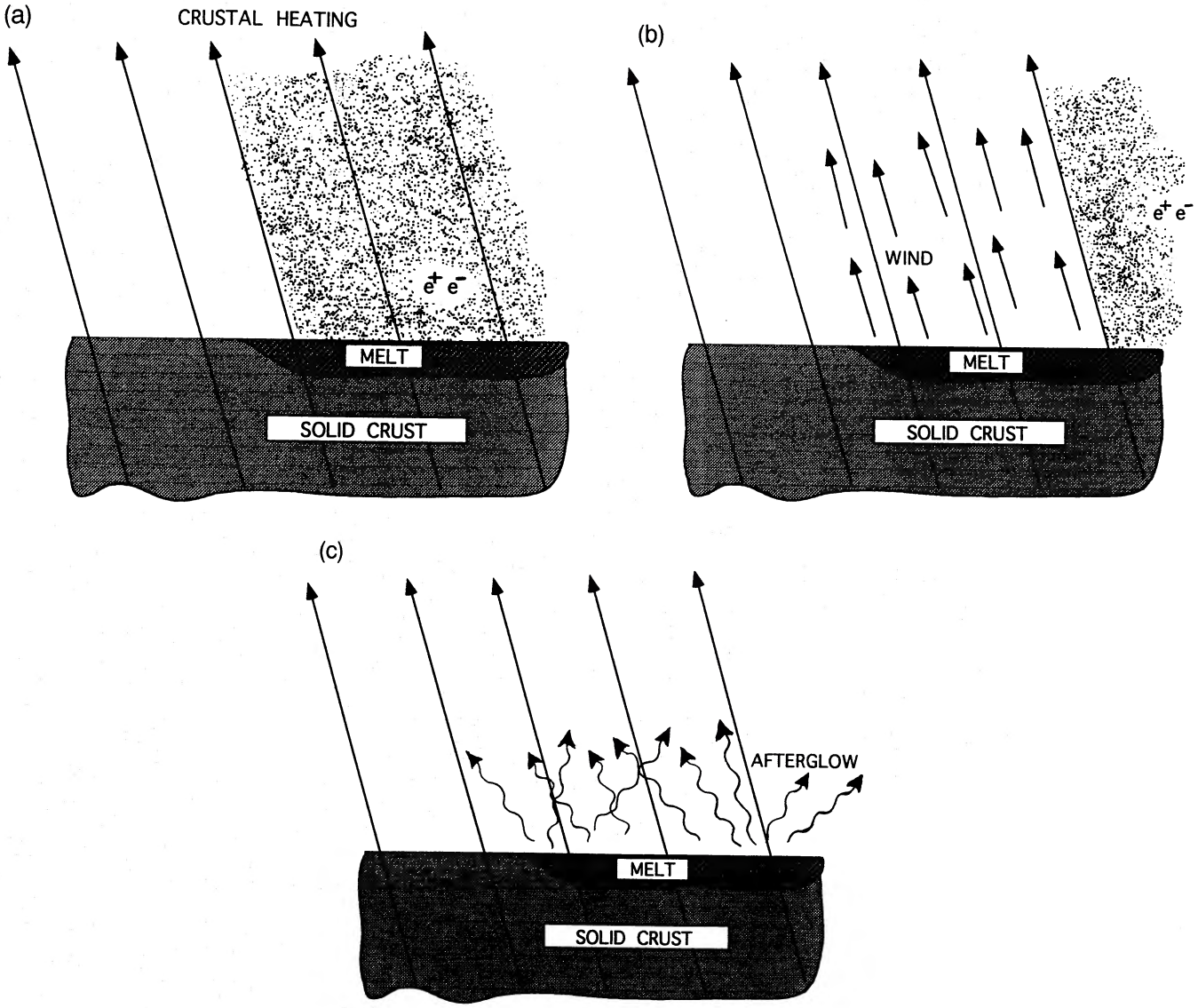

Figure 7. (a) Energy is conducted from the trapped pair plasma into the cold neutron star crust. (b) As the photon-pair bubble contracts in volume, the heated crust becomes exposed and a wind is driven off its surface. (c) After the ion–electron wind abates, the heated crust continues to glow for a time comparable to the exposure time, that is, for a time comparable to the duration of the SGR burst.

4.1 Total heat conducted into the crust during a soft burst

Heat transport in the outermost layers of the crust occurs primarily by radiative diffusion. Deeper in the crust, conduction by degenerate electrons dominates. The problem that we consider is the inverse of the usual neutron star cooling problem: the surface of the star, which is exposed to a mildly relativistic photon-pair plasma, is much hotter than the interior. We first calculate the rate at which photons diffuse downward from the hot bubble, through a layer of mildly relativistic electrons and heavy ions. Then we check the consistency of this calculation, by showing that electron conduction into the deep crust can be neglected.

The vertical radiative heat flux is

$$F_z = \frac{1}{\kappa_{es}^{\parallel}(B,T)\rho}\frac{\partial}{\partial z}\left(\frac{\pi^2}{45}T^4\right) \equiv -\lambda\frac{\partial T}{\partial z}, \tag{102}$$

where

$$\lambda = \frac{4\pi^2 T^3 m_n}{45 Y_e \sigma_{es}^{\parallel}(B,T)\rho}. \tag{103}$$

For simplicity, we assume that the magnetic field is aligned with the vertical, and assume a pure Fe composition, with $Z=26$, $A=56$ and $Y_e=0.464$. The electrons (which are much more numerous than the ions) are heated sufficiently to become non-degenerate; we demonstrate this in Appendix A. We consider two cases, depending on whether the electrons or the photons dominate the specific heat C_p. In the first case,

$$C_p = \frac{5}{2}\frac{Y_e\rho}{m_n}, \tag{104}$$

and the thermal diffusivity is

$$\chi = \frac{\lambda}{C_p} = \frac{T(eB)^2 m_n^2}{300\pi\alpha^2 Y_e^2\rho^2} = 1.7\times10^7 (B/10B_{QED})^2 T_{MeV}\rho_6^{-2}\ \mathrm{cm^2\ s^{-1}}; \tag{105}$$

whereas, in the second case,

$$C_p = \frac{16}{3}\frac{U_\gamma}{T} = \frac{16\pi^2}{45}T^3, \tag{106}$$

and

$$\chi = \frac{3}{128\pi^3\alpha^2}\frac{(eB)^2 m_n}{Y_e T^2\rho} = 2.7\times10^4 (B/10B_{QED})^2 T_{MeV}^{-2}\rho_6^{-1}\ \mathrm{cm^2\ s^{-1}}. \tag{107}$$

We will show, a posteriori, that the electrons make the largest contribution to C_p at the relatively low temperatures $T_{MeV}\sim0.1$ appropriate for SGR bursts, whereas the photons dominate C_p at the temperature $T_{MeV}\sim1$ appropriate for the March 5 event. We treat the first case here in detail (since it is slightly simpler), and discuss the second case in Appendix A.

The photons diffuse a depth

$$(\chi\Delta t)^{1/2} = 1.3\times10^3 \Delta t_{-1}^{1/2}(B/10B_{QED})\,T_{MeV}^{1/2}\rho_6^{-1}\ \mathrm{cm} \tag{108}$$

into the crust in the lifetime $\Delta t = \Delta t_{-1}\times10^{-1}$ s of the hot bubble. The density at the base of the heated layer is typically $\rho_6 = 1$–10. The mass of the heated crust is

$$M_{heat} = A\int_0^{(\chi\Delta t)^{1/2}}\rho(z)\,dz = \frac{1}{2}\rho(\chi\Delta t)^{1/2}, \tag{109}$$

where we use the $\rho(\Delta z)$ relation (A1).

The total heat absorbed into the section of the crust, of area A, covered by the hot bubble is

$$E_{th} = A\int_0^{(\chi\Delta t)^{1/2}}\int_0^T C_p(z,T)\,dz\,dT = \frac{5Y_e\rho(\chi\Delta t)^{1/2}TA}{4m_n} = 6.8\times10^{38}\Delta t_{-1}^{1/2}(B/10B_{QED})\,T_{MeV}^{3/2}A_{12}\ \mathrm{erg}. \tag{110}$$

Notice that the density scales out of this result. One may express this result in terms of an absorption luminosity,

$$L_{absorb} = 6.8\times10^{39}\Delta t_{-1}^{-1/2}(B/10B_{QED})\,T_{MeV}^{3/2}A_{12}\ \mathrm{erg\ s^{-1}}. \tag{111}$$

Parameters appropriate for SGR bursts ($T_{MeV}\sim0.1$, $\Delta t_{-1}\sim1$) yield an absorbed energy $E_{th}\sim2\times10^{38}(B/10B_{QED})A_{12}$ erg, which is small compared with the typical energy radiated in an SGR burst. This absorbed heat is easily sufficient to melt the crust to a depth somewhat greater than $(\chi\Delta t)^{1/2}$.

Direct neutrino radiation from the hot bubble (Section 5) is supplemented by neutrino radiation from the hot crust. Given that the temperature in the heated crust is equal to that in the interior of the hot magnetospheric bubble, the neutrino losses from the crust are dominated by pair annihilation, as in the bubble. The much smaller volume of the heated crust implies that the neutrino losses come almost entirely from the bubble itself. Bremsstrahlung neutrino radiation is tiny compared with annihilation radiation: from Pethick & Thorsson (1994), the emissivity per unit mass is $dL_{brem,\nu}/dM = 5.6\times10^{11}Y_e Z T_{MeV}^6$ erg g^{-1} s^{-1}. The total bremsstrahlung luminosity is only

$$L_{brem,\nu} = \frac{dL_{brem,\nu}}{dM}M_{heat} = 6\times10^{34}\Delta t_{-1}^{1/2}(B/10B_{QED})\,T_{MeV}^{13/2}\ \mathrm{erg\ s^{-1}}. \tag{112}$$

Now let us check the self-consistency of this calculation. Free–free absorption makes only a small contribution to the radiative opacity. The ratio of the Rosseland mean opacities is (Silant'ev & Yakovlev 1980)

$$\frac{\alpha_{ff}(B,T)}{\alpha_{es}(B,T)} = 1.58\times10^{-2}\left(\frac{T}{m_e}\right)^{-7/2}\frac{Z\alpha\rho_b}{m_e^3 m_n} = 1.0\times10^{-5}T_{MeV}^{-7/2}\rho_6(Z/26). \tag{113}$$

This shows that free–free absorption can be neglected in calculating the absorption of heat into the crust.

Thermal conduction by non-relativistic electrons into the deep crust is straightforward to estimate, because scattering of electrons by phonons and impurities can be neglected in the melted layer [which extends somewhat below a depth $(\chi\Delta t)^{1/2}$]. The thermal conductivity parallel to $\boldsymbol{B}$ will be comparable to the conductivity in an unmagnetized liquid

metal, which is

$$\kappa = \frac{\pi^3}{4\alpha^2 Z \ln\Lambda}\,\frac{n_e T}{\mu_e^2}$$

(e.g. Urpin & Yakovlev 1980). Here, $\mu_e = m_e[1+(\rho_6 Y_e)^{2/3}]^{1/2}$ is the effective mass of the electrons. For parameters of interest, the Coulomb logarithm is $\ln\Lambda \simeq 2$. The electron thermal diffusivity parallel to $\boldsymbol{B}$ is therefore

$$\chi_e(\|) \simeq \frac{\kappa}{C_p} = 1.2\times 10^3 \frac{T_{MeV}}{1+(\rho_6 Y_e)^{2/3}}\ \mathrm{cm\ s^{-1}}, \qquad (114)$$

which manifestly is much smaller than the radiative diffusivity (105) evaluated at a density $\rho \sim 10^6\ \mathrm{g\ cm^{-3}}$.

4.2 Baryon wind

After the hot magnetospheric plasma dissipates, the energy absorbed by the crust is released (Figs 7b and c). The surface X-ray flux resulting from energy injection *inside* the crust has been estimated by Eichler & Cheng (1989) and calculated in detail by Van Riper, Epstein & Miller (1991). The case that we are treating is somewhat different, in that the heat is absorbed from the exterior of the star. Moreover, the magnitude of the *downward* radiative flux during the heating phase can exceed the local 'Eddington' rate, at which the radiation pressure force balances the force of gravity. This means that significant mass ablation can occur as the heated layer cools. The absorbed heat is sufficient to drive off a baryon layer with mass as large as

$$\Delta M \sim \frac{E_{th}}{gR_\star} \qquad (115)$$

into the magnetosphere. To estimate the amount of mass actually lost, we must compare the radiation pressure force with the force of gravity at an appropriate depth in the heated layer.

Suppose that, at a certain spot on the neutron star surface, the external hot pair plasma dissipates in a time $\Delta t'$, which is much less than the total exposure time Δt and represents the time of passage of the cool photospheric boundary. The absorbed heat will escape from a depth $(\chi'\Delta t')^{1/2}$ in the interval $\Delta t'$ (where χ' is the radiative diffusivity at this depth). The total matter column density in this cooling layer is smaller than the total column density through the heated layer by a factor $(\Delta t'/\Delta t)^{1/2}$ (since $\chi^{1/2} \propto \rho^{-1}$).

The photon pressure is somewhat higher than the (non-degenerate) electron pressure at depth $(\chi\Delta t)^{1/2}$, and is much higher further up in the heated layer. At the moment that cooling begins, the vertical pressure gradient in the hydrostatically supported layer is then

$$-\rho g \sim -\frac{P_\gamma}{(\chi\Delta t)^{1/2}}\,. \qquad (116)$$

The escape of photons from depth $(\chi'\Delta t')^{1/2}$ will generate a steeper vertical pressure gradient

$$\frac{dP_\gamma}{dz} \sim -\frac{P_\gamma}{(\chi'\Delta t')^{1/2}} \qquad (117)$$

and an upward radiative heat flux $F_z \sim P_\gamma/\rho\kappa(\chi'\Delta t')^{1/2}$. The upward radiation pressure force is, compared with the force of gravity,

$$\frac{F_z\kappa}{g} = -\frac{1}{\rho g}\frac{dP_\gamma}{dz} \simeq \left(\frac{\chi'\Delta t'}{\chi\Delta t}\right)^{-1/2} \simeq \left(\frac{\Delta t'}{\Delta t}\right)^{-1/4}, \qquad (118)$$

where we use equation (A1) for the diffusion depth. The upward radiation force clearly wins out when $\Delta t' \ll \Delta t$. The entire cooling layer can be lifted only a short distance $\sim(\Delta t'/\Delta t)^{-1/4}\times(\chi\Delta t)^{1/2}$. A thin surface layer can be lifted a much larger distance, however, and we expect that the strong upward radiative momentum flux will blow a thin layer of material off the surface of the star and into the magnetosphere. As the cooled layer grows in thickness, the radiative flux at the surface becomes less strongly super-Eddington; ablation ceases when the depth of the cooled layer reaches $\sim(\chi\Delta t)^{1/2}$.

We conclude that equation (15) is a reasonable estimate of the ablated mass. The ratio of the ablated mass to the total mass of the heated crust is

$$\frac{\Delta M}{M_{heat}} \sim \frac{E_{th}}{M_{heat}gR_\star} \sim \frac{3Y_e T}{2m_n gR_\star} = 3\times 10^{-4}(T_{MeV}/0.1). \qquad (119)$$

4.3 Photon afterglow

When the baryon wind has abated, the crust will continue to cool, at a luminosity comparable to the rate (111) at which heat was absorbed into the crust (Fig. 7c). The corresponding luminosity is

$$L_{absorb} \simeq 2\times 10^{39}(B/10B_{QED})A_{12}\Delta R_{max\,6}^{-9/8}\ \mathrm{erg\ s^{-1}} \qquad (120)$$

for the March 5 event. (We assume that the magnetospheric pair plasma was trapped inside a volume of $\sim\Delta R_{max}^3$.) The afterglow luminosity is a factor of ~ 5 smaller for SGR bursts. This corresponds to a radiative flux which is ~ 30 times the ordinary Eddington flux but is much smaller than the magnetic surface Eddington flux (Paczyński 1992; Section 3.1).

In this model, the duration of the afterglow is predicted to be *comparable* to the duration of the burst. This was, indeed, observed for the 1983 November 16 and December 14 bursts of SGR 1806−20 (Kouveliotou et al. 1987). In both bursts, low-level emission before the main SGR burst was also detected at low statistical confidence. Such pre-glow is more difficult to understand in this model.

A direct connection between the durations of the burst and of the afterglow is *not* expected if the afterglow is due to some secondary energy release mechanism deep inside the crust. In such a case, the conduction time to the surface would be much longer and the afterglow luminosity much lower. Extrapolating the results of Van Riper et al. (1991) to the surface temperatures characteristic of the surface

emission of SGR 1806−20 [$L_X = 3\times10^{34}(D/8\ \mathrm{kpc})^2$ erg s^{-1}: Murakami et al. 1994] and SGR 0526−66 ($L_X = 7\times10^{35}$ erg s^{-1}: Rothschild et al. 1994),

$$T_{\rm eff} = (2\text{–}5)\times10^6 R_{\star 6}^{-1/2}\ \mathrm{K}, \tag{121}$$

one deduces extremely long afterglow time-scales of $\sim10^7$ s for energy deposition at a density of $\sim10^{12}$–10^{14} g cm^{-3} in a neutron star of radius 10 km. As a result, the excess afterglow luminosity is a miniscule fraction of the quiescent X-ray luminosity.

5 NEUTRINO COOLING

Our treatment of the cooling of a magnetospheric pair plasma has proceeded under the assumption that leakage across the confining magnetic field is the dominant energy loss mechanism. In this section, we show that direct neutrino losses from the pair plasma are negligible for SGR events, although they could play a role in determining the light curve of the soft tail of the March 5 event.

A first estimate of neutrino pair emission $e^+ + e^- \rightarrow \nu + \bar{\nu}$ from an electron–positron plasma in thermal equilibrium neglects magnetic effects. This estimate is accurate when $B > B_{\rm QED}$ *and* when the plasma pressure is not much less than the pressure of the confining field. The emissivity into three species of massless neutrinos is $\Lambda_{\nu\bar{\nu}} = 1.35\times10^{25} T_{\rm MeV}^9$ erg cm^{-3} s^{-1} (Dicus 1972; Soyeur & Brown 1979), which gives a characteristic time-scale for cooling due to neutrino radiation,

$$t_\nu(\mathrm{bubble}) = \frac{U_{e^\pm} + U_\gamma}{\Lambda_{\nu\bar{\nu}}} = 28\, T_{\rm MeV}^{-5}\ \mathrm{s}. \tag{122}$$

We have inferred a temperature close to 1 MeV [equation (59)] for the pair plasma that radiated the soft tail of the March 5 event. Neutrino cooling may therefore help to determine the light curve of the soft tail of the March 5 event, in which the flux decreased by a factor ~2 over the first 10 s. Using the estimate (59) for T, we find

$$t_\nu(\mathrm{bubble}) = 26\left(\frac{E}{4\times10^{44}\ \mathrm{erg}}\right)^{-5/4} V_{18}^{5/4}\ \mathrm{s}.$$

This suggests that the energy ($\sim 4\times10^{44}$ erg) radiated in the soft tail is in fact only a lower limit to the total energy of the pairs trapped in the stellar magnetosphere.

The neutrino emissivity is *suppressed* when $B > B_{\rm QED}$ and the pairs all reside in the lowest Landau level. One finds that

$$\Lambda_\nu = \frac{4G_{\rm F}^2}{3\pi}\left[\sum_i (C_V^2 + C_A^2)_i\right]\frac{m_{\rm e}^5 n_{\rm e^-} n_{\rm e^+}}{eB}$$

when $T \ll m_{\rm e}$ (Loskutov & Skobelev 1986). Here, $G_{\rm F}$ is Fermi's constant, C_{Vi} and C_{Ai} are the vector and axial vector coupling constants, and the sum is over neutrino flavours. This may be re-expressed as

$$\Lambda_\nu = \frac{G_{\rm F}^2}{3\pi}\left[\sum_i (C_V^2 + C_A^2)_i\right]\frac{U_{\rm th}^2 m_{\rm e}^3}{eB}, \tag{123}$$

since the total thermal energy density $U_{\rm th} = E_{\rm th}/\ell^3 \simeq m_{\rm e} n_{e^\pm}$ is dominated by the rest mass of the pairs (Section 3.3). The resulting neutrino cooling time is

$$t_\nu(\mathrm{bubble}) = \frac{U_{\rm th}}{\Lambda_\nu} = 2.6\times10^6 E_{41}^{-1}\ell_6^3 B_{15}\ \mathrm{s}. \tag{124}$$

In the case of SGR bursts, neutrino cooling can be entirely neglected unless the confining volume is very small, $\ell \lesssim 4\times10^3$ cm.

A similar expression can be derived for higher temperatures, $m_{\rm e} \ll T \ll (eB)^{1/2}$. From equation (9) of Loskutov & Skobelev (1986), one deduces

$$\begin{aligned}\Lambda_\nu &= \frac{G_{\rm F}^2 m_{\rm e}^2 eB}{12(2\pi)^5}\left[\sum_i (C_V^2 + C_A^2)_i\right]\int_{-\infty}^{\infty}\frac{dp}{E} f(p) \\ &\quad\times\int_{-\infty}^{\infty}\frac{dp'}{E'}(E+E')\,Q^4 \\ &= \frac{\zeta(3) G_{\rm F}^2}{24\pi^3}\left[\sum_i (C_V^2 + C_A^2)_i\right] m_{\rm e}^2 T^5 eB.\end{aligned} \tag{125}$$

Here, (E, E') and (p, p') are the energy and (longitudinal) momentum of the electron and positron, $Q^2 = (E+E')^2 - (p+p')^2$, and $f = [\exp(E/T)+1]^{-1}$. When $eB \gg T^2$, the photon energy density is small compared with the energy density of the one-dimensional pair gas, and the total thermal energy density is $U_{\rm th} \simeq \frac{1}{12} eBT^2$. Expression (125) can be rewritten as

$$\Lambda_\nu = \frac{6\zeta(3)}{\pi^3}\left[\sum_i (C_V^2 + C_A^2)_i\right]\frac{G_{\rm F}^2 U_{\rm th}^2 m_{\rm e}^2 T}{eB}. \tag{126}$$

The heated crust will also radiate neutrinos; we show in Section 4 that the resulting energy loss is very small.

6 THE EMERGENT SPECTRUM

We now discuss, in more depth, the physics of radiation transport in a very hot ($T > 10$ keV), optically thick, low mass-density ($\rho_{\rm b} \lesssim P_\gamma / gR_\star$) plasma which is confined by a very strong magnetic field ($B > B_{\rm QED}$). We defer a detailed calculation of the emergent X-ray spectrum to a later paper.

In this regime, the dominant scattering process is Compton scattering, for which the Rosseland mean cross-section is given by equations (35) and (36). Diffusion of photons through a plasma occurs almost completely in the E-mode. In an inhomogeneous magnetic field, the polarization basis states will vary from point to point; but this variation occurs slowly enough that the polarization of an individual photon adiabatically tracks the eigenmode. The indices of refraction of the two eigenmodes are

$$\begin{aligned} n_{\rm O} &= 1 + \frac{\alpha}{6\pi}\sin^2\theta_{kB}\left(\frac{B}{B_{\rm QED}}\right); \\ n_{\rm E} &= 1 + \frac{\alpha}{6\pi}\sin^2\theta_{kB}, \end{aligned} \tag{127}$$

when $B > B_{\rm QED}$. Here θ_{kB} is the angle between the photon wavevector and $\boldsymbol{B}$. [This compares with the usual vacuum

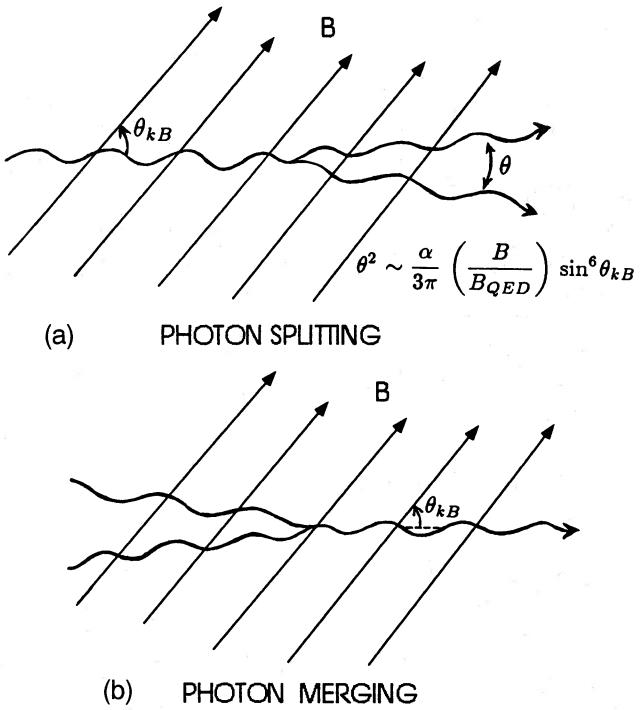

Figure 8. (a) Photon splitting in a strong magnetic field, $B > B_{\rm QED}$. (b) The inverse process of photon merging. In thermal equilibrium, the photon splitting and merging rates precisely cancel.

polarization correction $n-1 \propto \alpha\ \sin^2\theta_{kB}(B/B_{\rm QED})^2$ when $B < B_{\rm QED}$ (e.g. Berestetskii, Lifshitz & Pitaevskii 1982).] Mode tracking occurs so long as the difference between the indices of refraction of the two eigenstates satisfies

$$n_{\rm O} - n_{\rm E} \gtrsim (k\ell_B)^{-1}, \tag{128}$$

where k is the photon wavevector and ℓ_B is the gradient scale of the magnetic field. This condition is easily satisfied for a dipole field with $\ell_B \sim \frac{1}{3}R_\star$. Note also that the photon frequency is much higher than the electron plasma frequency near the photosphere, and so collective effects are negligible.

The dominant photon number-changing process is photon splitting (Fig. 8a),

$$\gamma \leftrightarrow \gamma + \gamma. \tag{129}$$

At finite photon density, the inverse process of photon merging also occurs (Fig. 8b), and in thermal equilibrium the splitting rates and merging rates are related by detailed balance (TD93b).

The photon splitting rate is given essentially by the value at zero plasma density. Splitting occurs in only two polarization channels, E↔O+O and E↔E+O (e.g. Berestetskii et al. 1982). Thus only the polarization state with the *low* scattering cross-section is able to split into two photons. The first polarization channel has the higher spontaneous rate, which is[17]

$$\Gamma_{\rm sp}({\rm E}\rightarrow{\rm O}+{\rm O}) = \frac{\alpha^3}{2160\pi^2}\sin^6\theta_{kB}\left(\frac{\omega}{m_{\rm e}}\right)^5 m_{\rm e}$$
$$(B > B_{\rm QED}\ \text{and}\ \omega < m_{\rm e}) \tag{130}$$

[17]This expression may be easily derived by taking the limit $B\sin\theta_{kB} \gg B_{\rm QED}$ of equation (23) of Adler (1971).

in a magnetic field stronger than $\sin\theta_{kB}B_{\rm QED}$. This expression is valid only for $\omega < m_{\rm e}$; a more general expression can be found in Adler (1971). The differential rate for a photon of energy ω to split into daughter photons 1 and 2 with energies ω_1 and $\omega - \omega_1$ is

$$\frac{{\rm d}\Gamma_{\rm sp}(\omega,\omega_1)}{{\rm d}\omega_1} = \frac{30\Gamma_{\rm sp}(\omega)}{\omega}\left(\frac{\omega_1}{\omega}\right)^2\left(1-\frac{\omega_1}{\omega}\right)^2. \tag{131}$$

Thus the splitting probability is maximized for $\omega_1 = \frac{1}{2}\omega$. The splitting rate in the second channel is smaller by the factor $(\Delta\theta)^2 \sim (\alpha/3\pi)\ \sin^2\theta_{kB}(B/B_{\rm QED})$. Here $(\Delta\theta)^2$ is the mean square angular separation between the two photons in the final state. Henceforth, we consider only the channel E→O+O.

Note that $\Gamma_{\rm sp}$ is *independent* of B, which contrasts sharply with the behaviour for $B < B_{\rm QED}$, where $\Gamma_{\rm sp} \propto (B/B_{\rm QED})^6$ (Adler et al. 1970). This means that a photon propagating radially in the equatorial plane ($\theta_{kB} = \pi/2$) of a dipole magnetic field experiences a spontaneous splitting rate that is *independent* of radius while $B > B_{\rm QED}$, but decays as $\Gamma_{\rm sp} \propto R^{-18}$ when $B < B_{\rm QED}$. One may define a *splitting photosphere* where the net splitting rate

$$\int_{R_\star}^{R} {\rm d}r\,\Gamma_{\rm sp}(r) = 1.$$

At high photon energies, this photosphere lies close to the radius $R_{\rm QED}$ where $B = B_{\rm QED}$. At low photon energies, the magnetosphere is entirely transparent to splitting. One may therefore define a characteristic photon energy for which the splitting probability out to radius $R_{\rm QED}$ is unity,

$$\omega_{\rm sp} = 37.5\left(\frac{R_{\rm QED}-R_\star}{10\ {\rm km}}\right)^{-1/5}\ {\rm keV}. \tag{132}$$

The equivalent blackbody temperature (at which the photon splitting rate is sufficient to maintain LTE) is

$$T_{\rm sp} = 0.28\,\omega_{\rm sp} = 11\left(\frac{R_{\rm QED}-R_\star}{10\ {\rm km}}\right)^{-1/5}\ {\rm keV}; \tag{133}$$

see equation (151) below.

The radiation transfer problem that must be solved is qualitatively different from the usual scattering problem. Let us compare with Compton scattering, including the double Compton process $e+\gamma \rightarrow e+\gamma+\gamma$ (Lightman 1981). At energies $\omega \ll m_{\rm e}$, a typical Compton scattering event involves a small change in photon frequency but a large change in momentum. The second photon emitted in the double Compton process typically is soft compared to the incident photon. By contrast, in a splitting event the energy of the incident photon is usually shared almost equally between the two daughter photons. In addition, the splitting process is almost collinear, in the sense that the momenta of the two emergent photons are directed almost parallel to the momentum of the seed photon. Thus a beam of photons incident on a magnetic field is broadened only over many splitting lengths. In a splitting process where the energy ω of the incident photon is distributed between daughter photons 1 and 2 as ω_1 and $\omega - \omega_1$, the angle between the incident

wavevector $\boldsymbol{k}$ and $\boldsymbol{k}_1$ is given by

$$\theta_1^2=\frac{\omega-\omega_1}{\omega_1}\,\frac{\alpha}{3\pi}\sin^2\theta_{kB}\left(\frac{B}{B_{\rm QED}}\right) \tag{134}$$

[analogous expressions for $B<B_{\rm QED}$ can be found in, e.g., Berestetskii et al. (1982)]. Only very low-energy daughter photons have momenta directed at a large angle with respect to the incident photon. The relative rate for such a process is small [see equation (131)], and the fraction of the beam energy lost is even smaller.

What is the effective mean free path $\lambda(T)$ for thermal photons undergoing rapid splitting and merging? In the absence of Compton scattering, the angular dispersion of a beam of photons undergoing N repeated splittings and mergings is $\theta^2(N)\sim N\theta_1^2$, and so

$$\frac{1}{\lambda(T)}\sim\frac{\alpha}{3\pi}\sin^2\theta_{kB}\left(\frac{B}{B_{\rm QED}}\right)\Gamma_{\rm sp}(T) \tag{135}$$

for a photon of energy $\omega\sim T$. However, the effective mean free path can be reduced to a value far below (135) if the photons Compton scatter while they are in the O-mode. The mean free path then becomes

$$\frac{1}{\lambda(T)}\sim\Gamma_{\rm sp}(T). \tag{136}$$

This expression is valid when

$$n_{\rm e}\sigma_{\rm es}({\rm E})<\Gamma_{\rm sp}(T)<n_{\rm e}\sigma_{\rm es}({\rm O}), \tag{137}$$

that is, when the splitting rate is small compared with the Compton scattering rate of the O-mode, but large compared with the Compton scattering rate of the E-mode. When are the inequalities (137) satisfied? For parameters T, B and $n_{\rm e}$ appropriate to SGR bursts, one always finds that $\Gamma_{\rm sp}(T)\ll n_{\rm e}\sigma_{\rm es}({\rm O})$. In order to compare the Compton scattering rate of the E-mode with the splitting rate, consider a mildly relativistic photon-pair plasma ($T\lesssim m_{\rm e}$) in a magnetic field stronger than $B_{\rm QED}$.

For the applications of interest here, the Rosseland mean scattering opacity is not modified significantly by photon splitting. The mean energy of the diffusing E-mode photons varies from $[\pi^2/3\,\ln(T/\mu)]T$ when the chemical potential $\mu\ll T$ to $\sim T$ when $\mu\gg T$ (Section 6.3). A typical photon energy is therefore $\omega\sim T$. Taking the equilibrium pair density at temperature T [equation (52)], we find

$$\frac{\Gamma_{\rm sp}(T)}{\sigma_{\rm es}^{\perp}(B,T)n_{\rm e^{\pm}}}=7\times10^{-9}\left(\frac{T}{m_{\rm e}}\right)^{5/2}\exp\left(\frac{m_{\rm e}}{T}\right)\left(\frac{B}{B_{\rm QED}}\right). \tag{138}$$

This shows that photon splitting has a negligible effect on radiative transfer in the interior of the electron–positron plasma, and is most important at the lowest temperatures, where the Compton depth is dominated by the electron–ion contaminant. Normalizing the electron density to (50), we find

$$\frac{\Gamma_{\rm sp}(T)}{\sigma_{\rm es}^{\perp}(B,T)n_{\rm e}}=9\times10^{-3}\varepsilon_{\rm b}^{-1}Y_{\rm e}^{-1}\left(\frac{T}{10\,{\rm keV}}\right)^{-1}\left(\frac{B}{10B_{\rm QED}}\right)^{2}. \tag{139}$$

Photon splitting is unimportant inside the E-mode photosphere even at the low temperatures characteristic of SGR emissions ($T\sim10$–20 keV), unless the ion density is less than a fraction $\varepsilon_{\rm b}\sim10^{-2}$ of the amount that the photon pressure can support against gravity. Photon splitting may be important *outside* the E-mode photosphere, however, where the splitting rate evaluated at the mean energy of the streaming E-mode photons is larger than (139) by a factor[18] $\sim(2.7)^5=140$. We discuss the effects of photon splitting on radiative transfer outside the E-mode photosphere in Section 6.3.

6.1 Stimulated photon splitting and photon merging

We now write down the Boltzmann equation for the photon occupation number, taking into account photon splitting and merging in the dominant E ↔ O + O mode. When the splitting process is almost collinear [which is a good approximation for $\sin^2\theta_{kB}(B/B_{\rm QED})\lesssim3\pi/\alpha$], this equation can be reduced to a one-dimensional integral over the energy of one of the daughter photons. Since energy and momentum are conserved exactly in each splitting and merging event, we have

$$\dot{n}_{\omega}^{\rm E}=\int_0^{\omega}{\rm d}\omega_1[n_{\omega_1}^{\rm O}n_{\omega-\omega_1}^{\rm O}-n_{\omega}^{\rm E}(1+n_{\omega_1}^{\rm O}+n_{\omega-\omega_1}^{\rm O})]\times\frac{{\rm d}\Gamma_{\rm sp}(\omega,\omega_1)}{{\rm d}\omega_1} \tag{140}$$

for the E-mode, and

$$\dot{n}_{\omega}^{\rm O}=\int_0^{\infty}{\rm d}\omega_2[n_{\omega+\omega_2}^{\rm E}(1+n_{\omega}^{\rm O}+n_{\omega_2}^{\rm O})-n_{\omega}^{\rm O}n_{\omega_2}^{\rm O}]\times\left(\frac{\omega+\omega_2}{\omega}\right)^2\frac{{\rm d}\Gamma_{\rm sp}(\omega,\omega_2)}{{\rm d}\omega_2} \tag{141}$$

for the O-mode. It is straightforward to show, starting from equation (141), that the rates of change in the photon number density due to splittings and mergings satisfy

$$\dot{N}_{\rm sp}^{\rm O}=-2\dot{N}_{\rm sp}^{\rm E} \tag{142}$$

for arbitrary $n_{\omega}^{\rm O,E}$. Here,

$$\dot{N}^{\rm O,E}=\int_0^{\infty}\dot{n}_{\omega}^{\rm O,E}\,\frac{4\pi\omega^2\,{\rm d}\omega}{(2\pi)^3}. \tag{143}$$

The angle between the photon momentum and $\boldsymbol{B}$ is suppressed in these expressions; one has $\Gamma_{\rm sp}(\theta_{kB})\propto\sin^6\theta_{kB}$. The net splitting rate vanishes in thermal equilibrium, as can be seen by substituting $n_{\omega}^{\rm E,O}=[\exp(\omega/T)-1]^{-1}$ in each of these expressions.

When the splitting/merging rates are not sufficient for the photon occupation numbers to relax to a Planck distribution, they will none the less be able to relax to a Bose–Einstein

[18]This assumes a Planckian spectrum, which slightly overestimates the mean energy because $\sigma_{\rm es}$ grows with frequency (Paczyński 1992).

distribution

$$n^{\rm O,E}=\left[\exp\left(\frac{\omega+\mu^{\rm O,E}}{T}\right)-1\right]^{-1} \tag{144}$$

as the result of rapid scattering in the O-mode, which ensures energy equipartition (Section 6.3). The net splitting rate does not vanish in this case. For example, the combination of occupation numbers in equation (140) reduces to

$$n^{\rm O}_{\omega_1}n^{\rm O}_{\omega-\omega_1}-n^{\rm E}_{\omega}(1+n^{\rm O}_{\omega_1}+n^{\rm O}_{\omega-\omega_1})= \frac{\exp\left(\frac{\omega+\mu^{\rm E}}{T}\right)-\exp\left(\frac{\omega+2\mu^{\rm O}}{T}\right)}{\left[\exp\left(\frac{\omega_1+\mu^{\rm O}}{T}\right)-1\right]\left[\exp\left(\frac{\omega-\omega_1+\mu^{\rm O}}{T}\right)-1\right]\left[\exp\left(\frac{\omega+\mu^{\rm E}}{T}\right)-1\right]}. \tag{145}$$

Rapid conversions between the O-mode and the E-mode at high optical depth [cf. equations (37)–(39)] also ensure that[19]

$$\mu^{\rm E}=\mu^{\rm O}=\mu. \tag{146}$$

Substituting (145) into (140) and (143), and noting that the main contribution to the integral over frequencies comes from $\omega\gg T$, we can write

$$\dot{N}^{\rm E}_{\rm sp}\simeq-\frac{7!}{2\pi^2}[1-\exp(-\mu/T)]\exp(-\mu/T)\langle\sin^6\theta\rangle\Gamma_{\rm sp}(T)\,T^3. \tag{147}$$

The average over angles yields

$$\langle\sin^6\theta\rangle=\frac{1}{2}\int_{-1}^{1}{\rm d}(\cos\theta)(1-\cos^2\theta)^3=\frac{16}{35}.$$

When $\mu\ll T$, the total number density of E-mode photons is $N^{\rm E}\simeq[\zeta(3)/\pi^2]T^3$, and one has

$$\frac{\dot{N}^{\rm E}_{\rm sp}}{N^{\rm E}}\simeq-\frac{7!}{2\,\zeta(3)}\left(\frac{\mu}{T}\right)\langle\sin^6\theta\rangle\Gamma_{\rm sp}(T). \tag{148}$$

In the opposite limit where $\mu^{\rm O,E}\gg T$, one has $N^{\rm E}\simeq\pi^{-2}\exp(-\mu/T)\,T^3$, and the net splitting rate is

$$\frac{\dot{N}^{\rm E}_{\rm sp}}{N^{\rm E}}\simeq-\frac{7!}{2}[1-\exp(-\mu/T)]\langle\sin^6\theta\rangle\Gamma_{\rm sp}(T). \tag{149}$$

The net change in the photon number density ($N=N^{\rm O}+N^{\rm E}$) at high optical depth is then, from equation (142),

$$\frac{\dot{N}_{\rm sp}}{N}=\frac{\dot{N}^{\rm O}_{\rm sp}+\dot{N}^{\rm E}_{\rm sp}}{N^{\rm O}+N^{\rm E}}=-\frac{1}{2}\,\frac{\dot{N}^{\rm E}_{\rm sp}}{N^{\rm E}}, \tag{150}$$

since ordinary Compton scattering preserves photon number (but not mode).

The fractional splitting rate $\dot{N}_{\rm sp}/N$ saturates when $\mu\gg T$. One may define a characteristic temperature $T_{\rm sp}$ at which the net change in the photon number along a length ℓ is $\Delta N/N\sim 1$. Expressed in terms of the energy $\omega_{\rm sp}$ of a photon with unit splitting probability along the path ℓ [as given by equation (132)], this temperature is

$$\frac{T_{\rm sp}}{\omega_{\rm sp}}\simeq\left(\frac{4}{7!\langle\sin^6\theta\rangle}\right)^{1/5}=0.28. \tag{151}$$

6.2 Alternative photon number changing processes

Bremsstrahlung is not an important source of photons near the photosphere, if the X-rays are emitted from the magnetosphere rather than from the neutron star surface. The bremsstrahlung opacity is comparable to the scattering opacity only at relatively high plasma densities and optical depths. To check this, we normalize the baryon density to the value at which the E-mode has unit optical depth across a distance $R_\star$. The resulting density is

$$Y_{\rm e}n_{\rm b}=2.0\times10^{20}\left(\frac{T}{10\ {\rm keV}}\right)^{-2}\left(\frac{B}{10B_{\rm QED}}\right)^{-2}\left(\frac{R_\star}{10\ {\rm km}}\right)^{-1}{\rm cm}^{-3}. \tag{152}$$

Most of the depth to free–free absorption is accumulated while a photon is in the ordinary polarization state, for which the absorption coefficient is larger than in the extraordinary state by a factor $\alpha_{\rm ff}({\rm O})/\alpha_{\rm ff}({\rm E})\sim(5\pi^2)^{-1}(eB/m_{\rm e}T)^2$. The ratio of the free–free opacity in the O-mode to the Compton opacity in the E-mode is, then [from equation (113)],

$$\frac{\alpha_{\rm ff}({\rm O})}{\alpha_{\rm es}({\rm E})}=\frac{\alpha_{\rm ff}({\rm O})}{\alpha_{\rm ff}({\rm E})}\,\frac{\alpha_{\rm ff}({\rm E})}{\alpha_{\rm es}({\rm E})} =7\times10^{-4}Z\left(\frac{T}{10\ {\rm keV}}\right)^{-15/2}\left(\frac{B}{10B_{\rm QED}}\right)^{4}\left(\frac{R_\star}{10\ {\rm km}}\right)^{-1}. \tag{153}$$

This approaches unity only in very strong magnetic fields, or over very short distances. In the case of *surface* X-ray cooling, however, as considered by Paczyński (1992), the electron density at the photosphere is high enough to ensure that $\alpha_{\rm ff}({\rm O})>\alpha_{\rm es}({\rm E})$, and the photon spectrum relaxes locally to a Planck distribution.

Double Compton scattering is a more effective source of photons than bremsstrahlung (in the case of magnetospheric emission), but once again it is a source which needs to be considered only in extremely strong magnetic fields. Given a small chemical potential μ, the O-mode states are filled at the rate[20]

$$\frac{1}{N^{\rm O}(T)}\,\frac{\partial}{\partial t}\left(\frac{{\rm d}N^{\rm O}}{{\rm d}\ln\omega}\right)\simeq\frac{4\alpha}{3\pi}\,\frac{\langle\omega^2\rangle}{m_{\rm e}^2}\left(\frac{\mu}{T}\right) \times\left[1+\frac{1}{\exp[(\omega+\mu)/T]-1}\right]n_{\rm e}\sigma_{\rm T}, \tag{154}$$

where we approximate the O-mode double-Compton cross-section by the value at $B=0$ (Lightman 1981). Here, ${\rm d}N^{\rm O}/$

[19]For applications of interest, the chemical potential is positive.

[20]Ulmer (1994) has independently considered double-Compton scattering in the case of *surface* X-ray cooling of a very strong magnetized neutron star, but does not include the frequency dependence of $\sigma(2\gamma)$. Free–free emission is the dominant source of photons in this case, and is effective since the crustal electron density is much higher than in magnetospheric emission models.

$d\omega$ is the total number of O-mode photons per unit energy interval and $\langle\omega^2\rangle \simeq 12[\zeta(5)/\zeta(3)]T^2$ for $\mu \ll T$. The expression in brackets is approximately T/μ for $\omega \ll \mu$. Thus the fractional rate of change in the photon number density (in both polarization modes) on the E-mode diffusion time-scale $t_{\rm diff} \simeq [\tau_{\rm es}(\mathrm{E})]^2[n_{\rm e}\sigma_{\rm es}(T)]^{-1}$ is

$$\frac{t_{\rm diff}}{N(T)}\frac{\partial N}{\partial t} \simeq \left[\frac{4\zeta(5)}{\pi^3\zeta(3)}\right]\alpha[\tau_{\rm es}(\mathrm{E})]^2\left(\frac{B}{B_{\rm QED}}\right)^2 \ln\left(\frac{\mu}{\omega_{\rm min}}\right) = 0.5[\tau_{\rm es}(\mathrm{E})]^2\left(\frac{B}{10B_{\rm QED}}\right)^2(1+0.18\ln\Lambda), \tag{155}$$

where

$$\Lambda = \left(\frac{T}{10\ \mathrm{keV}}\right)^{-1}[\tau_{\rm es}(\mathrm{E})]^2\left(\frac{B}{10B_{\rm QED}}\right)^2\left(\frac{\mu}{T}\right). \tag{156}$$

Only O-mode photons more energetic than $\omega_{\rm min} \sim m_{\rm e}/\tau_{\rm es}(\mathrm{E})\,\tau_{\rm es}(\mathrm{O})$ are upscattered to an energy $\sim T$. Inspection of (155) shows that double-Compton scattering can be neglected at the E-mode photosphere [$\tau_{\rm es}(\mathrm{E}) \simeq \frac{2}{3}$] for the SGR sources of interest in this paper. For example, the surface magnetic field strength of SGR 1806 − 20 is estimated to be $\lesssim 10B_{\rm QED}$ (Section 7.1), whereas the bursts of SGR 0526 − 66 have high enough effective temperatures ($T_{\rm eff}/T_{\rm sp} \sim 1.8$: Section 7.2) that the photon splitting is the dominant photon number-changing process.

Note that magnetic resonances will enhance the double-Compton scattering rate only if the scattering electron resides in an excited Landau level (Alexander & Mészáros 1991), which is not the case of the low values of $T/(eB)^{1/2}$ considered here. Virtual excited Landau states do not contribute significantly to the cross-section when $B \gg B_{\rm QED}$.

A fourth photon number-changing process is cyclotron emission from electrons in excited Landau levels. This process is not effective in the SGR model, in which $T_{\rm eff}$ is much less than the energy of the first Landau level, but it should be effective in the model for Type II X-ray bursts discussed in Section 7.4, in which $T_{\rm eff}/\omega_{Be}(1) = 0.1$–$0.2$.

6.3 Radiative transfer equations

Diffusion of photons through a plasma in a very strong magnetic field (with $Tm_{\rm e}/eB \ll 1$) occurs primarily in the E-mode. The relation $\sigma_{\rm es}(\mathrm{EO}) \sim 3\sigma_{\rm es}(\mathrm{EE})$ (cf. table 4 of Mészáros 1992) implies that efficient mode switching occurs inside the scattering photosphere of the E-mode. While in the O-mode, each photon scatters a large number of times (e.g. Mészáros, Nagel & Ventura 1980). The corresponding Compton parameter is

$$y = \tau_{\rm es}(\mathrm{O})\,\tau_{\rm es}(\mathrm{E})\frac{T}{m_{\rm e}} \simeq 5\times10^3[\tau_{\rm es}(\mathrm{E})]^2\left(\frac{T}{10\ \mathrm{keV}}\right)^{-1}\left(\frac{B}{10B_{\rm QED}}\right)^2 \tag{157}$$

inside the E-mode photosphere. So long as $B/B_{\rm QED} \gtrsim 0.3(T/10\ \mathrm{keV})^{1/2}$, this parameter is greater than unity everywhere inside the photosphere, which ensures that the photon distribution function will relax to a Bose–Einstein form.

The radiative transfer problem therefore has the following novel features.[21] First, the photon distribution function is a function of two parameters, T and μ, rather than just T. The energy flux $\boldsymbol{F}$ and photon number flux $\boldsymbol{F}_{\rm n}$ are independent variables, both of which can be calculated in the diffusion approximation as linear combinations of gradients of T and μ. This system of equations is closed by the relation

$$\nabla\cdot\boldsymbol{F}_{\rm n} = \dot{N}_{\rm sp} \tag{158}$$

between the divergence of the photon number flux and the rate of change of the photon number density N due to photon splitting.

The energy flux in the E-mode per unit frequency ν can be written as

$$F_\nu = -\frac{4\pi}{3}\frac{1}{\alpha_\nu(B)\rho}\frac{\partial B_\nu(T,\mu)}{\partial x}, \tag{159}$$

where the absorption coefficient is expressed in terms of the angle-averaged E-mode scattering cross-section as

$$\frac{1}{\alpha_\nu^{\parallel,\perp}(B)} = \left(\frac{n_{\rm e^\pm}}{\rho_{\rm b}} + \frac{Y_{\rm e}}{m_{\rm n}}\right)^{-1}\frac{3}{4}\int_{-1}^{+1}\mathrm{d}(\cos\theta)\begin{Bmatrix}2\cos^2\theta\\ \sin^2\theta\end{Bmatrix} \times \frac{1}{\sigma_{\rm es}(\mathrm{E})(\nu,\theta)} \tag{160}$$

(cf. Silant'ev & Yakovlev 1980), and the Planck function is generalized to

$$B_\nu(T,\mu) = \frac{4\pi\nu^3}{\exp[(2\pi\nu+\mu)/T]-1}. \tag{161}$$

The photon number flux is given similarly by

$$(F_{\rm n})_\nu = -\frac{4\pi}{3}\frac{1}{\alpha_\nu(B)\rho}\frac{\partial(B_{\rm n})_\nu(T,\mu)}{\partial x}, \tag{162}$$

where

$$(B_{\rm n})_\nu(T,\mu) = \frac{1}{2\pi\nu}B_\nu(T,\mu). \tag{163}$$

Our next step is to integrate the diffusion equations (159) and (162) over frequency. This leads to our main result in this section, the following expressions for the energy flux and photon number flux:

$$F = -\frac{1}{3}\left[\frac{1}{\alpha_T(B,T,\mu)\rho}\frac{\partial U(T,\mu)}{\partial T}\frac{\partial T}{\partial x} + \frac{1}{\alpha_\mu(B,T,\mu)\rho}\frac{\partial U(T,\mu)}{\partial\mu}\frac{\partial\mu}{\partial x}\right] = -\lambda_0(T,\rho)\left[I_1(\mu/T)\frac{\partial T}{\partial x} - I_2(\mu/T)T\frac{\partial(\mu/T)}{\partial x}\right] \tag{164}$$

[21] In this section we assume steady-state radiative transfer, as is appropriate to the outermost layers of the cooling wave (Section 3). We also assume a plane-parallel geometry, and neglect the complicated geometrical effects associated with radiative transfer in a neutron star magnetosphere.

and

$$F_{\rm n} = -\frac{1}{3}\left[\frac{1}{\beta_T(B,T,\mu)\rho}\frac{\partial n(T,\mu)}{\partial T}\frac{\partial T}{\partial x} + \frac{1}{\beta_\mu(B,T,\mu)\rho}\frac{\partial n(T,\mu)}{\partial \mu}\frac{\partial \mu}{\partial x}\right] \tag{165}$$
$$= -\frac{\lambda_0(T,\rho)}{T}\left[I_3(\mu/T)\frac{\partial T}{\partial x} - I_4(\mu/T)\,T\frac{\partial(\mu/T)}{\partial x}\right].$$

Here, $U(T,\mu)[n(T,\mu)]$ is the photon energy (number) density.

The first expression given in equations (164) and (165) directly parallels the standard LTE radiative transfer formalism. Expressions for the Rosseland mean coefficients $\alpha_{T,\mu}$ and $\beta_{T,\mu}$ are given in Appendix B. However, it is more convenient to normalize F and $F_{\rm n}$ to the photon energy flux at $\mu = 0$:

$$F = -\lambda_0\frac{\partial T}{\partial x}, \tag{166}$$

where

$$\lambda_0(T,\rho) = \frac{1}{3\alpha_T(B,T,0)\rho}\frac{\partial U(T,0)}{\partial T} \tag{167}$$
$$= \frac{1}{3\sigma_{\rm es}(B,T)\rho}\left(\frac{n_{e^\pm}}{\rho} + \frac{Y_{\rm e}}{m_{\rm n}}\right)^{-1}\frac{\partial U(T,0)}{\partial T}$$

is the radiative conductivity at $\mu = 0$, expressed in terms of the energy density $U(T,0) = (\pi^2/15)T^4$ in both polarization modes. The numerical coefficients I_1–I_4 in equations (164) and (165) can be written down in terms of simple integrals of the Bose–Einstein distribution over frequency:

$$I_1(\mu/T) = \frac{3}{\pi^2}\int_0^\infty {\rm d}x\,\frac{2x}{\exp(x+\mu/T)-1}; \tag{168}$$
$$I_2(\mu/T) = I_3(\mu/T) = \frac{3}{\pi^2}\int_0^\infty {\rm d}x\,\frac{1}{\exp(x+\mu/T)-1};$$
$$I_4(\mu/T) = \frac{3}{\pi^2}\,\frac{1}{\exp(\mu/T)-1}.$$

The photon number flux (165) becomes, at small μ/T,

$$F_{\rm n} = -\frac{3}{\pi^2}\,\frac{\lambda_0}{T}\ln\left(\frac{T}{\mu}\right)\frac{\partial T}{\partial x}. \tag{169}$$

The radiant energy is carried by photons with characteristic energy

$$\frac{F}{F_{\rm n}} = \frac{\pi^2}{3\ln(T/\mu)}\,T. \tag{170}$$

The logarithmic singularity is a benign infrared divergence. It occurs because E-mode photons of very small energy are nearly free-streaming, with $\sigma_{\rm es}(\nu) \propto \nu^2$. This divergence is cut off, in practice, by a finite chemical potential.

The opposite limit where $\mu \gg T$ is also interesting. The photon number flux freezes out at a constant value, and both F and $F_{\rm n}$ are proportional to $\partial(\mu/T)/\partial x$, with $\partial T/\partial x \to 0$. In this limit, equations (164) and (165) become

$$T \simeq \text{constant}, \tag{171}$$

and

$$F \simeq \frac{-1}{3\alpha_T(B,T,0)\rho}\frac{\partial U(T,\mu)}{\partial x}\times\left(\frac{2\pi^2}{15}\right); \tag{172}$$
$$TF_{\rm n} \simeq \frac{-1}{3\alpha_T(B,T,0)\rho}\frac{\partial U(T,\mu)}{\partial x}\times\left(\frac{2\pi^2}{15}\right),$$

where

$$U(T,\mu) \simeq \frac{6}{\pi^2}\,T^4\exp\left(-\frac{\mu}{T}\right) \qquad (\mu \gg T). \tag{173}$$

The mean photon energy is

$$\frac{F}{F_{\rm n}} \simeq T \qquad (\mu \gg T). \tag{174}$$

The final set of closed, second-order equations for T and μ/T is obtained as follows. Taking the x-derivative of equation (164) and invoking the constancy of the energy flux, $\partial F/\partial x = 0$, we obtain

$$0 = \frac{\partial^2 T}{\partial x^2} - \frac{TI_2}{I_1}\frac{\partial^2(\mu/T)}{\partial x^2} + \frac{\partial(\ln\lambda_0)}{\partial T}\left(\frac{\partial T}{\partial x}\right)^2 - \frac{TI_2'}{I_1}\left[\frac{\partial(\mu/T)}{\partial x}\right]^2 \tag{175}$$
$$-\frac{I_2}{I_1}\left[1 - \frac{I_1'}{I_2} + \frac{\partial(\ln\lambda_0)}{\partial(\ln T)}\right]\frac{\partial T}{\partial x}\frac{\partial(\mu/T)}{\partial x}$$

and

$$-\left(\frac{T}{\lambda_0 I_3}\right)\frac{\partial F_{\rm n}}{\partial x} = \frac{\partial^2 T}{\partial x^2} - \frac{TI_4}{I_3}\frac{\partial^2(\mu/T)}{\partial x^2}$$
$$+\frac{\partial[\ln(\lambda_0/T)]}{\partial T}\left(\frac{\partial T}{\partial x}\right)^2 - \frac{TI_4'}{I_3}\left[\frac{\partial(\mu/T)}{\partial x}\right]^2 \tag{176}$$
$$+\frac{I_4}{I_3}\left[\frac{I_3'}{I_4} - \frac{\partial(\ln\lambda_0)}{\partial(\ln T)}\right]\frac{\partial T}{\partial x}\frac{\partial(\mu/T)}{\partial x}$$
$$= \left(\frac{T}{\lambda_0 I_3}\right)\frac{7!}{2\pi^2}\left[1 - \exp\left(-\frac{\mu}{T}\right)\right]\exp\left(-\frac{\mu}{T}\right)\Gamma_{\rm sp}(T)\,T^3.$$

These two equations can be combined to yield equations for $\partial^2 T/\partial x^2$ and $\partial^2(\mu/T)/\partial x^2$ alone, which can then be expressed via equation (164) in terms of $\partial T/\partial x$ or $\partial(\mu/T)/\partial x$ alone.

We will not attempt a solution of these equations here. However, the temperature $T_{\rm sp}$ at which photon splitting and merging freeze out can be estimated quite simply, as a result of the very strong temperature dependence of the splitting/

merging rate. Equation (169) implies that

$$\frac{\partial F_n}{\partial x} \simeq \frac{3}{4\pi^2} \ln\left(\frac{T}{\mu}\right) \frac{F}{T\ell} = \dot{N}^{E}_{sp}, \tag{177}$$

where we substitute $\partial T/\partial x = -F/\lambda_0$ and write the radiative diffusivity λ_0 in terms of the thickness of the atmosphere at temperature T,

$$\ell = \frac{1}{\alpha_T(\mu=0)\rho} \int \alpha_T(\mu=0)\rho \, dx. \tag{178}$$

Substituting equation (148) for $\dot{N}^{E}_{sp}$ and writing F in terms of the effective temperature, $T_{eff} = (60/\pi^2)^{1/4} F^{1/4}$, we obtain

$$T^9_{sp} = \frac{3\pi^4}{64\alpha^3} \frac{T^4_{eff} m^4_e}{\ell} \frac{T_{sp}}{\mu(T_{sp})} \ln\left[\frac{T_{sp}}{\mu(T_{sp})}\right]. \tag{179}$$

One must have $\mu \sim T$ at the transition between the LTE regime and the constant-number-flux, constant-T regime. We estimate $\mu/T = e^{-1}$, and find

$$T_{sp} = 11.8 \left(\frac{T_{eff}}{10\ \text{keV}}\right)^{4/9} \left(\frac{\ell}{1\ \text{km}}\right)^{-1/9} \text{keV}. \tag{180}$$

This is the minimum spectral (colour) temperature for radiation emerging from the photosphere of a magnetically confined plasma with $T_{eff} \ll \omega_{Be}(1)$. Although the precise value of ℓ must be calculated from a detailed hydrostatic model for the plasma, the resulting freeze-out temperature T_{sp} is very insensitive to ℓ as well as to the value of μ/T at the transition.

6.4 Spectral evolution outside the E-mode scattering photosphere

As we have already discussed, diffusive radiative transport occurs almost entirely in the extraordinary polarization mode. Our attention in this section turns to radiative transfer outside the E-mode scattering photosphere. We have not, until now, made any attempt to distinguish this photosphere from the true photosphere, which is the surface at which the emergent spectrum is established. However, the E-mode spectrum can evolve by photon splitting and merging even outside the E-mode scattering photosphere. Significant evolution of the E-mode spectrum occurs only where $B > B_{QED}$; the strong dependence of the spontaneous splitting rate on B in weaker fields [$\Gamma_{sp}(B) \propto B^6$] ensures that splitting rapidly freezes out when B drops below B_{QED}. In what follows, we use the shorthand 'E-mode photosphere' for the E-mode scattering photosphere, 'O-mode photosphere' for the O-mode scattering photosphere, and 'splitting photosphere' for the surface surrounding the neutron star on which $|\boldsymbol{B}| = B_{QED}$. We sometimes make the simplifying assumption of a spherical geometry, in which the positions of the three photospheres are labelled as R_E, R_O and R_{QED}.

Although the O-mode photons do not diffuse across the E-mode photosphere, some fraction of the streaming E-mode photons are converted locally to the O-mode, by Compton scattering and (if T_{eff} is high enough) by photon splitting. An important point is that the scattering depth of the O-mode remains very large outside the E-mode photosphere: from equation (35) we have $\tau_{es}(O) \simeq \tau_T \sim 10^4 \tau_{es}(E)$ for $T_{eff} = 10$ keV and $B = 10 B_{QED}$.

Rapid Compton scattering of the O-mode has two important effects.

(1) The O-mode spectrum will remain close to Bose–Einstein (or Planckian, in the case of rapid photon splitting) in a region *outside* the E-mode photosphere where the y-parameter of the O-mode,

$$y(O) \simeq t_{res} n_e \sigma_T \left(\frac{T}{m_e}\right), \tag{181}$$

is greater than unity. The residency time t_{res} of the O-mode photons at electron density n_e may be limited by diffusion, by conversion to E-mode photons, or by advection along the magnetic field lines:

$$t_{res} = \ell_{n_e} \min\{[\tau_{es}(O)]^2, [\tau_{es}(OE)]^{-1}, (V_{stream}/c)^{-1}\}. \tag{182}$$

Here, ℓ_{n_e} is the electron density scalelength, $\tau_{es}(O)$ and $\tau_{es}(OE)$ are the associated scattering depths, and V_{stream} is the bulk streaming velocity of the photons together with the entrained baryons and electrons. One sees from equation (157) that $y(O)$ is much greater than unity at the E-mode photosphere, but is much less than unity at the O-mode photosphere. The value of $y(O)$ at the *splitting* photosphere is crucial in determining the shape of the emergent spectrum as we discuss in more detail below.

This Bose–Einstein spectrum is fully established only down to a minimum frequency $\omega_{min} = m_e/(n_e \sigma_T t_{res})$. The low-energy spectral cut-off is the maximum of ω_{min} and μ so long as photon splitting (instead of free–free emission) is the dominant photon number-changing process.

(2) A single E-mode photon splits (a large fraction of the time) into two O-mode photons. This, by itself, will not inhibit the streaming motion of the E-mode photons, since the two daughter photons are almost collinear with the original E-mode photon, and the E-mode is regenerated when pairs of O-mode photons merge. However, photon splitting combined with Compton scattering of the O-mode photons effectively randomizes the direction of the E-mode photons and prevents streaming. This suggests that, if photon splitting remains rapid outside the E-mode photosphere, then *both* E-mode and O-mode photons are *advected* along the magnetic field lines out to a radius where B drops below B_{QED} and the two modes are uncoupled. *This bulk streaming motion allows E-mode and O-mode photons to be emitted (and detected) in comparable quantities.*

Only a very small contaminant of electrons and ions is needed to generate a large scattering depth in the O-mode, and so the streaming motion can easily be *relativistic*. For example, if the electron density generates an O-mode scattering depth $\tau_{es}(O)$ at radius R, then the rest energy density in the associated ions is

$$\frac{\rho_b}{U^O(T)} \simeq 3 \times 10^{-3} \frac{\tau_{es}(O)}{Y_e R_6} \left(\frac{T}{10\ \text{keV}}\right)^{-4} = 40 \frac{\tau_{es}(E)}{Y_e R_6} \left(\frac{T}{10\ \text{keV}}\right)^{-6} \left(\frac{B}{10 B_{QED}}\right)^2. \tag{183}$$

Here, T is the temperature of the O-mode photons and we estimate $U^{O}(T)=(\pi^2/30)T^4$. One sees that the ρ_b remains tiny compared with U^{O} well inside the O-mode photosphere, but is much larger than U^{O} at the E-mode photosphere.

If O-mode photons were entirely absent outside the E-mode photosphere, how fast would the O-mode states be filled? A fraction $\tau_{es}(E)$ of the streaming E-mode photons are converted to the O-mode by Compton scattering. The highest energy O-mode states are filled first by photon splitting, and so it is sufficient to consider the lower energy states. We can simplify equation (141) by noting that the dominant contribution to $\dot{n}^{O}_{\omega}$ comes from $\omega_2 \sim 4T$, which allows us to approximate $n^{E}_{\omega+\omega_2} \simeq \exp[-(\omega+\omega_2)/T]$ and $n^{O}_{\omega_2} \simeq \exp(-\omega_2/T)$. We obtain

$$\dot{n}^{O}_{\omega} \simeq 1400\, e^{-\omega/T}[1-n^{O}_{\omega}(e^{\omega/T}-1)] \times\left[1+\frac{1}{2}\left(\frac{\omega}{T}\right)+\frac{1}{12}\left(\frac{\omega}{T}\right)^2\right]\Gamma_{sp}(T), \tag{184}$$

where it is convenient to express

$$1440\,\Gamma_{sp}(T)=\Gamma_{sp}(4.28T). \tag{185}$$

Although the energy of a split photon usually is divided almost equally between the two daughter photons, there is much less phase-space volume at low frequencies, and so the time to fill the low-energy O-mode states scales as

$$\frac{n^{O}_{\omega}}{\dot{n}^{O}_{\omega}} \propto \left(\frac{\omega}{T}\right)^{-1}. \tag{186}$$

The strong dependence of the splitting rate on ω implies that there is a minimum photon energy ω_{sp} below which splitting is ineffective. One can show that, for T_{eff} in the range 10–20 keV, this minimum frequency is always greater than T_{eff}, and to a first approximation simulated effects can be neglected in calculating the net splitting rate,

$$\dot{n}^{E}_{\omega}(\text{split}) = -n^{E}_{\omega}\int_0^{\omega} d\omega_1 (1+n^{O}_{\omega_1})(1+n^{O}_{\omega-\omega_1})\frac{d\Gamma_{sp}(\omega,\omega_1)}{d\omega_1} \simeq -n^{E}_{\omega}\Gamma_{sp}(\omega). \tag{187}$$

[Of course, $\dot{n}^{E}_{\omega}(\text{split}) = -\dot{n}^{E}_{\omega}(\text{merge})$ in thermal equilibrium.] The value of ω_{sp} is therefore given by equation (132). The temperature at which the *mean* photon energy is equal to ω_{sp} is

$$T'_{sp}=\frac{\omega_{sp}}{2.70}=14\ \text{keV}. \tag{188}$$

This slightly exceeds the critical temperature (180) where, at high scattering depth, the photon spectrum begins to depart from a Planckian distribution. The best-fitting blackbody temperatures of the bursts emitted by SGR 1806−20 (Fenimore et al. 1994) lie slightly below this bound, whereas for SGR 0526−66 we estimate (Section 7.2) that the best-fitting blackbody temperature is $T \simeq 16$ keV.

E-mode photons with energies less than ω_{sp} stream freely across the magnetic field lines. Higher energy E-mode photons are entrained with the O-mode photons and electrons on a time-scale $\sim R_E/c$. In the regime where $T_{eff} > T_{sp}$, the E-mode spectral distribution is close to Planckian at the E-mode photosphere,

$$n^{E}_{\omega} \simeq n^{O}_{\omega} \simeq [\exp(\omega/T)-1]^{-1} \qquad (T > T_{sp}). \tag{189}$$

In this regime, only the low-energy E-mode photons stream freely from the E-mode photosphere to the observer. The bulk of the radiant energy is released fastest from the magnetosphere if both the O-mode and high-energy ($\omega > \omega_{sp}$) E-mode photons stream along the magnetic field lines out to the radius R_{QED}, where the two modes uncouple and the E-mode photons are released. Notice that this involves only a modest expansion (by a factor ~ 2 in radius if the surface field strength is $10B_{QED}$).

In the regime where $T < T_{sp}$, photon splitting is not fast enough to maintain a Planckian spectrum, and the E-mode spectral distribution at the E-mode photosphere is Bose–Einstein with a finite chemical potential (Section 6.3). Most of the E-mode energy can escape by free streaming outside the E-mode photosphere, but streaming across the magnetic field lines is still inhibited for E-mode photons with $\omega > \omega_{sp}$. These high-energy photons carry a fraction

$$\varepsilon_{sp} \equiv \frac{1}{U^{E}}\int_{\omega_{sp}}^{\infty} d\omega \frac{dU^{E}}{d\omega} \tag{190}$$

of the radiant energy. Even at low E-mode scattering depth, photon splitting will fill in the O-mode distribution function on a time-scale

$$\frac{t_{sp}}{R_E} \sim \varepsilon_{sp}^{-1}. \tag{191}$$

So long as the residency time of the O-mode photons is longer than t_{sp}, the high-energy E-mode photons will remain in approximate equilibrium with the O-mode photons. The high-energy E-mode photons can still be released by streaming along the magnetic field lines, although in this regime the streaming velocity will be quite low,

$$V_{stream}/c \sim \varepsilon_{sp}. \tag{192}$$

6.4.1 Polarization and angular distribution of the emergent radiation

What are the relative fractions of the emergent radiative flux carried by E-mode and O-mode photons? When photon splitting is rapid outside the E-mode photosphere ($T_{eff} > T'_{sp}$), the radiative flux is transported mainly by advection along the magnetic field lines. Although the advected E-mode photons are released at radius R_{QED}, the O-mode photons do not couple effectively to the E-mode outside this radius (assuming that the E-mode scattering depth is low). Thus the O-mode photons, together with the entrained electrons and baryons, must continue to stream outward until $\tau_{es}(O)$ drops below unity and the O-mode photons are released. The scattering depth is lower, and the O-mode photons are released sooner, if the bulk streaming motion is relativistic. In this regime, we expect that *comparable* fractions of the emergent flux are carried by the two modes.

When photon splitting is slow ($T_{eff} < T'_{sp}$), only a fraction ε_{sp} of the E-mode radiative flux is advected along the magnetic field lines outside the E-mode photosphere. If these high-energy photons remain in equilibrium with the O-mode,

then most of the *advected* energy is in fact carried by the O-mode. Thus in this regime a fraction $\sim \varepsilon_{sp}$ of the radiative flux is converted to the O-mode outside the E-mode photosphere and is released to the observer.

What is the angular distribution of the emitted radiation? If the exterior field has a simple dipole geometry, then most of the radiation advected along the magnetic field lines will be concentrated about the magnetic axis (where most of the field lines that reach beyond R_{QED} are concentrated), but will not be strongly beamed due to the flaring of the field lines. Thus *the emergent radiative flux should be concentrated about the magnetic axis when* $T > T'_{sp}$, *but not when* $T < T'_{sp}$. Note also that the high- and low-energy E-mode photons have different angular distributions, with the result that the E-mode spectrum will depend somewhat on orientation.

6.4.2 *Spectrum of the emergent radiation*

Given the complicated geometry and radiative physics involved in this model, we will not attempt a detailed calculation of the emergent X-ray spectrum in this paper, and limit ourselves to the following qualitative remarks.

The photon distribution function at the E-mode photosphere is close to Planckian if T_{eff} is larger than the critical value (180), and has a finite chemical potential if T_{eff} is smaller. Because the net splitting rate vanishes in thermal equilibrium, the temperature of the SGR radiation is *not* bounded above by photon splitting. However, blackbody spectra with temperatures less than ~ 10 keV cannot be achieved by photon splitting, and would require another photon creation process such as cyclotron emission (which is not effective when T is much less than the energy of the first Landau level).

When considering spectral evolution outside the E-mode photosphere, we treat the two cases $T_{eff} > T'_{sp}$ and $T_{eff} < T'_{sp}$ separately.

In the regime $T_{eff} > T'_{sp}$ (which applies to SGR 0526 − 66), the O-mode spectrum outside the E-mode photosphere is approximately Planckian. The high-energy ($\omega > \omega_{sp}$) and low-energy ($\omega < \omega_{sp}$) segments of the E-mode spectrum are also approximately Planckian, but with different temperatures. The high-energy E-mode photons advected along the magnetic field lines will, in general, have a lower temperature due to adiabatic expansion. Since the angular distributions and temperatures of the high-energy and low-energy E-mode photons are different, the spectral shape around energy ω_{sp} is hard to predict. The high-energy spectrum should show a suppression from a Planckian distribution as the result of radiative transfer near the splitting photosphere, but only a moderate one. The splitting rate is a strong function of frequency ($\Gamma_{sp} \propto \omega^5$), but it is an even stronger function of radius when $B < B_{QED}$. Thus the position of the splitting photosphere varies rather slowly with frequency, $R \propto \omega^{5/18}$ in a dipole field.

In the regime $T_{eff} < T'_{sp}$ (which applies to the *emergent* spectrum of SGR 1806 − 20), the E-mode spectrum is approximately Bose–Einstein with a positive chemical potential and a suppression at low energies below a Planckian distribution (as observed: Fenimore et al. 1994). The high-energy E-mode photons ($\omega > \omega_{sp}$) are mostly converted to O-mode photons with a Bose–Einstein distribution. Since the O-mode photons are distributed over a broader range of frequencies than the high-energy E-mode photons, the observed (polarization-averaged) spectrum should also show a suppression below a Planckian distribution at $\omega > \omega_{sp}$ as a result of the conversion of E-mode photons to O-mode photons. We find, somewhat paradoxically, that this suppression is most effective when T is slightly smaller than T'_{sp}, and becomes proportionately weaker when $T \gg T'_{sp}$.

There is a third, intermediate, regime where $T_{eff} > T'_{sp}$ at the E-mode photosphere, but $T_{eff} < T'_{sp}$ at the splitting photosphere. SGR 1806 − 20 may fit into this category (Section 7.1), depending on the area of the E-mode photosphere. In this regime, the O-mode photons develop a Bose–Einstein distribution outside the E-mode photosphere where T_{eff} drops below T'_{sp}.

7 CONCLUDING DISCUSSION: MODEL APPLICATIONS TO OBSERVED BURST SOURCES

In this paper, we have elaborated upon the idea (DT92; Paczyński 1992; TD93a; TD93b; DT94) that the soft gamma repeaters are neutron stars endowed with magnetic fields much stronger than those of ordinary pulsars. We have outlined how the decaying magnetic fields of these stars can trigger both extremely luminous outbursts such as the 1979 March 5 event, and much shorter but just as luminous soft repeating bursts (Section 2). The reconnection of a stressed magnetic field, or the excitation of Alfvén turbulence by crustal cracking, inevitably generates an optically thick electron–positron–photon plasma trapped on closed magnetic field lines (Section 3).

A detailed discussion of magnetic field decay in such a magnetar is deferred to a companion paper (TD95), where the resulting luminosities in surface X-rays, magnetospheric Alfvén waves and neutrinos are calculated.

The trapped pair plasma loses energy as its cool, outermost layers (where the opacity is dominated by the electron–baryon contaminant) propagate inward. The determination of the cooling rate turns out to be a subtle problem, and our analysis, although detailed, must be viewed as preliminary. The propagation velocity of this cooling wave is limited *either* (1) by the rate at which the pair plasma can be advected along the magnetic field lines toward the neutron star surface, where the field is strongest and the E-mode opacity lowest; or (2) by the ablation of baryons off the stellar surface by the intense X-ray flux that flows from the surface of the pair plasma. As we now describe for SGR 0526 − 66 and SGR 1806 − 20, the resulting luminosities and cooling times are in agreement with the highly super-Eddington luminosities and measured effective temperatures if the surface magnetic field is stronger than $B_{QED} = 4.4 \times 10^{13}$ G. Perhaps the most intriguing property of this model is that *the emergent spectrum should vary weakly during a burst as the pair bubble contracts and the radiative area drops* (DT94). This property was noted by Mazets et al. (1982) in their analysis of the soft-spectrum, oscillatory tail of the March 5 event, and independently by Kouveliotou et al. (1987) and by Fenimore et al. (1994) in their analyses of the spectra of bursts from SGR 1806 − 20. Weak spectral evolution is also a property of Type II XRBs, upon which we comment below. In addition, the emergent spectrum should depend very weakly on the total burst energy (that is, on the energy

density of the trapped pair plasma) when the radiative flux is limited by ablation of ions and electrons from the neutron star surface (Section 3.5), which provides a simple explanation for the similarity between the spectrum of the soft tail of the March 5 event and the spectra of the repeat bursts.

A small fraction $\sim 10^{-3}$–10^{-2} of the pair plasma energy is conducted into the cold neutron star crust, and is re-radiated on a time-scale comparable to the duration of the SGR burst (Section 4). Neutrino losses from the pair plasma are negligible for SGR bursts, but might be important for the March 5 event (Section 5).

The strong magnetic field controls the spectral evolution of the diffusing photons, in two distinct ways. First, the magnetic field suppresses the electron scattering cross-section of E-mode photons by a large factor with respect to the Thomson value (Herold 1979; Section 3.1). Thus diffusion occurs in the E-mode, while the photon distribution function relaxes to a Bose–Einstein distribution, owing to the large number of scatterings that photons undergo in the O-mode.[22] We have developed a diffusion formalism that generalizes the familiar LTE approximation, and expresses the energy and photon number fluxes as linear superpositions of gradients in temperature T and chemical potential μ (Section 6.3). Secondly, the strong magnetic field catalyses rapid photon splitting and merging, which is the dominant photon-number-changing reaction in this magnetospheric emission model for SGR bursts. We have presented the Boltzmann equation for stimulated photon splitting and photon merging, and discussed how the spectrum evolves outside the E-mode photosphere under the combined effects of photon splitting and O-mode scattering (Sections 6.1 and 6.4).

Let us now apply these results to the SGR sources 1806 − 20 and 0526 − 66.

7.1 SGR 1806 − 20

SGR 1806 − 20 has been observed to burst much more frequently than has SGR 0526 − 66. The burst spectra have been measured well below the spectral peak, down to X-ray energies of ~ 7 keV (Fenimore et al. 1994), as compared with ~ 30 keV for SGR 0526 − 66 (Mazets et al. 1982). This allows a more detailed comparison with spectral models.

The best-fitting blackbody temperature measured for the brightest bursts is $\simeq 9$ keV (Fenimore et al. 1994), which implies a radiating surface of radius $12(D/8\ \mathrm{kpc})$ km.

The similarity between the maximum radiating surface area of the bursts emitted by SGR 1806 − 20 and the area of a neutron star is, of course, entirely consistent with emission from the magnetosphere. In the magnetic confinement model discussed in Section 3, *most of the pair plasma energy leaks out through an annulus of height* $\sim \frac{1}{2}R_\star$ *just above the neutron star surface*, where the magnetic field is strongest and the E-mode scattering opacity lowest. This is the case even if the confinement volume is much larger than the neutron star. It is difficult to deduce a distance to SGR 1806 − 20 from this radiative model, however, because the emergent radiation may be modified by photon splitting outside the E-mode photosphere (out to a radius $R_{\mathrm{QED}} \sim 2R_\star$).

What effective temperature is predicted by the magnetic confinement model? The relevant cooling solution depends on the internal temperature of the pair plasma – which, for a fixed burst energy, is determined by the confinement volume. Recall that, if the pairs are generated by the damping of Alfvén waves of frequency $\nu = \nu_4 \times 10^4$ Hz (a characteristic seismic mode frequency for neutron star crusts; Blaes et al. 1989), the confinement volume can be roughly estimated as [equations (13)–(15)]

$$\Delta R_{\mathrm{max}}^3 \gtrsim \left(\frac{c}{\nu}\right)^3 \sim (30\nu_4\ \mathrm{km})^3. \tag{193}$$

The precise value will depend on the geometry of the external field and of the triggering event; it might vary significantly. In the case of a bright SGR burst ($E_{41} \sim 1$), the internal temperature T_{c} of the pair bubble is then $T_{\mathrm{c}} \sim 70 E_{41}^{1/4} \varepsilon_\gamma^{1/4} (\Delta R_{\mathrm{max}}/30\ \mathrm{km})^{-3/4}$ keV, where the parameter $\varepsilon_\gamma \sim 1$ [cf. the paragraph following equation (61)]. Thus one has

$$T_{\mathrm{eff}} \sim 15.2 \left(\frac{B}{10B_{\mathrm{QED}}}\right)^{1/4} \left(\frac{\Delta R_{\mathrm{max}}}{30\ \mathrm{km}}\right)^{-5/32} E_{41}^{3/32}\ \mathrm{keV} \tag{194}$$

for the emergent radiation from an advection-limited cooling wave [equation (87)], as compared with

$$T_{\mathrm{max}} \sim 15.7 \varepsilon_{\mathrm{b}}^{-1/6} \left(\frac{B}{10B_{\mathrm{QED}}}\right)^{1/3}\ \mathrm{keV} \tag{195}$$

for the magnetic Eddington flux *across* the B-field (Section 3.1). Note that conversion of photons from the E-mode to the O-mode outside the E-mode scattering photosphere reduces T_{eff} by a factor $2^{1/4}$. We conclude that the cooling rate of the pair plasma is limited by advection along $\boldsymbol{B}$ (rather than by ablation) when the pair bubble is larger than

$$\Delta R_{\mathrm{max}} \gtrsim 24 E_{41}^{3/5} \varepsilon_{\mathrm{b}}^{16/15} \left(\frac{B}{10B_{\mathrm{QED}}}\right)^{-8/15}\ \mathrm{km}\,. \tag{196}$$

Note the dependence on the baryon density at the photosphere through the parameter ε_{b} [equation (50)].

The effective temperature of the emergent radiation, as given by equation (194), depends very weakly on both the burst energy E and the confinement radius R_{max}. This contrasts with the ablation-limited cooling wave solution (195), in which there is no dependence (to first order) of T_{eff} on either E or R_{max}. Although E and R_{max} both depend on the specific magnetic field configuration in the SGR source, there may exist some correlation between these quantities which yields a direct relation between T_{eff} and E. We will not try to deduce such a correlation here.

The radiative surface area of the trapped pair plasma is not determined a priori in this model. Indeed, the requirement that the total X-ray luminosity match that observed for the brightest SGR bursts sets interesting limits on the surface magnetic field strength. Radiation escapes from the inner pair bubble through an annulus of area $\sim \frac{1}{2}C_{\mathrm{bubble}}R_\star$ [equation (79)], where C_{bubble} is the circumference of the pair

[22] Ulmer (1994) independently treats the restricted case where the photons relax to a Planckian distribution, which is appropriate for radiation from a neutron star surface. When considering such crustal emissions (Section 7.3.2), however, the dominant photon-number-changing process is free–free emission/absorption of the O-mode, not double Compton scattering (cf. Section 6.2).

bubble at the neutron star surface. We have argued (Section 3.4) that the radiative area of the E-mode photosphere is not much larger than this when $B \gg B_{\rm QED}$. If that is true, then the maximum area of the E-mode photosphere ($C_{\rm bubble} \sim 2\pi R_\star$) is $\sim 1/2$ of the total surface area of the neutron star visible to the observer at any instant. By contrast, one deduces a photospheric radius of $12(D/8\ {\rm kpc})$ km for the brightest burst from SGR 1806 – 20 (Fenimore et al. 1994; assuming spherical emission).

This suggests that, in order to fit the observed peak fluxes from SGR 1806 – 20, the value of $T_{\rm eff}$ at *the boundary of the pair bubble* must be higher by a factor of $\sim 2^{1/4}$ than the best-fitting blackbody temperature of $T_{\rm bb} \sim 9$ keV (Fenimore et al. 1994). (The relation between $T_{\rm eff}$ and the spectral shape, under the combined effects of Compton scattering and photon splitting, is summarized in the next section.) As a result, the surface magnetic field of the neutron star must be

$$B \sim 2 \times 10^{14} E_{41}^{-3/8} \left(\frac{\Delta R_{\rm max}}{30\ {\rm km}}\right)^{5/8} \left(\frac{T_{\rm bb}}{9\ {\rm keV}}\right)^4 {\rm G}. \qquad (197)$$

Note that the required magnetic field would be weaker if the maximum area of the E-mode photosphere were larger than our estimate. In this model, one expects that the surface magnetic field of SGR 1806 – 20 is *weaker* than that of SGR 0526 – 66, since the best-fitting temperature of the bursts is a factor of ~ 0.6 smaller.

7.1.1 *Deviations from a Planckian spectrum*

How is the emergent spectrum expected to deviate from a blackbody? We confine ourselves to a few qualitative remarks. A more complete discussion is given in Section 6.4.2.

First, the dominant photon-number-changing reaction in the magnetosphere is photon splitting.[23] The rate of photon splitting is sufficient to maintain a blackbody spectrum only down to an effective temperature $T_{\rm eff} \sim 10$ keV. At lower $T_{\rm eff}$, a large, positive chemical potential develops, which suppresses the low-energy emission with respect to a Planckian distribution.

Secondly, radiation emerging from the E-mode photosphere at higher effective temperatures ($T_{\rm eff} > 10$ keV) will be degraded to lower temperatures by photon splitting as it propagates outward and the effective radiative area increases. However, only photons with energies greater than ~ 35 keV are able to split across a distance of ~ 10 km in a magnetic field stronger than $B_{\rm QED}$. The splitting probability peaks when the two daughter photons carry half the energy; so splitting will not greatly increase the number of O-mode photons with energies less than ~ 17 keV. None the less, O-mode photons will be Compton down-scattered to a minimum energy $\omega_{\rm min} \sim (n_{\rm e}\sigma_{\rm T} t_{\rm res})^{-1} m_{\rm e}$ outside the E-mode photosphere [where the residency time $t_{\rm res}$ is given by equation (182)], and will form a Bose–Einstein distribution after splitting freezes out.

[23]The baryon density that can be supported by radiation pressure in the magnetosphere is much lower than the baryon density at the surface photosphere, and so free–free absorption can be neglected (Section 6.2).

Both of these effects work in the direction of *suppressing the low-energy emission with respect to a blackbody*, as is observed (Fenimore et al. 1994). It should be emphasized that our estimate of the surface area of the E-mode photosphere (in the brightest bursts from SGR 1806 – 20) implies an effective temperature $T_{\rm eff} \gtrsim 11$ keV. This is close to the value at which a significant chemical potential develops, but is also high enough that photon splitting and merging, combined with rapid Compton scattering in the O-mode [$\sigma_{\rm es}({\rm O}) \sim \sigma_{\rm T}$], will inhibit free streaming of a non-negligible fraction of the E-mode energy across the magnetic field lines (Section 6.4). The effective radiative area increases, and $T_{\rm eff}$ decreases, as the photons stream along the magnetic field lines out to a radius where photon splitting becomes ineffective. The emergent E-mode spectrum is a composite of low-energy E-mode photons (which do not split and propagate across the magnetic field) and high-energy E-mode photons (which do split and are advected along the magnetic field).

Unfortunately, the emergent X-ray spectrum generated in this model depends on a number of complicated geometrical and physical effects, and it will take considerable work to make a realistic calculation.

7.1.2 *Large or small B_{dipole}?*

The discovery that the X-ray error box of SGR 1806 – 20 overlaps with the supernova remnant G10.0 – 0.3 (Kulkarni & Frail 1993; Murakami et al. 1994) caused no surprise in light of the similar association between SGR 0526 – 66 and the N49 nebula in the LMC, and reinforced the idea that the soft gamma repeaters are relatively young, $t \sim 10^4$ yr, neutron stars. Kulkarni et al. (1994), however, also discovered that SNR G10.0 – 0.3 is a centre-filled radio plerion. The radio emission is peaked around the position of SGR 1806 – 20, which indicates that the neutron star is an active source of relativistic particles. Such plerionic structure is absent in the case of supernova remnant N49 (Junkes 1991) which contains SGR 0526 – 66. This has led to the suggestion (Kulkarni et al. 1994) that SGR 1806 – 20 is a relatively young ($t \sim 10^4$ yr), fast pulsar with an ordinary dipole magnetic field ($B \sim 10^{12}$ G).

The detection of a highly reddened optical companion, which is possibly a blue supergiant (Kulkarni et al. 1994b), might suggest that SGR 1806 – 20 is an accreting neutron star. If the radio plerion is powered by the SGR, however, then the quiescent X-ray emission is probably *not* powered by accretion. The luminosity in relativistic particles needed to power the plerion exceeds the quiescent X-ray luminosity (Murakami et al. 1994) by three orders of magnitude. Thus the required mass accretion would easily be choked off by the outward ram pressure of the relativistic wind. Although there is tentative evidence for a jet-like feature in the nebular emission, the radio flux is constant on a $\sim 10^7$-s time-scale (Vasisht, Frail & Kulkarni 1995), as is the X-ray flux (Sonobe et al. 1994). This contrasts with the strong radio flares emitted by accretion-powered sources such as Cir X-1, which also tend to accrete close to the Eddington rate. Finally, we note that the bursts emitted by 1806 – 20 show none of the temporal correlations characteristic of accretion-powered (Type II) X-ray bursts (Laros et al. 1987).

If the radio plerion around SGR 1806 – 20 is powered by rotational energy, we are immediately presented with a

puzzle. The coherent 8-s periodicity of SGR 0526−66 (which probably was the rotation period of the neutron star) is inconsistent with any detectable, rotationally powered plerion. Thus identification of SGR 1806−20 with a young pulsar would imply that two neutron stars of comparable ages but widely differing rotation periods and evolutionary histories are both sources of SGR bursts.

We should therefore consider the possibility that the SGRs are a uniform class of objects, with SGR 1806−20 and SGR 0526−66 having similar, long rotation periods. Weak evidence for a 2.8-s periodicity appears in the summed power spectra of the 20 brightest bursts of SGR 1806−20 (Ulmer et al. 1993).

We doubt that the observed radio plerion could be powered by a second neutron star that was created in the supernova explosion, since the inferred proper motion of SGR 1806−20 would place it in a different part of the nebula, and since SGR 1806−20 would necessarily be much older than the fast pulsar. A more interesting possibility is that the 1806−20 *radio* plerion is powered by the decaying magnetic field of the neutron star, as we conjecture is its continuous X-ray emission [DT92; TD93b; equation (7)]. The required luminosity in relativistic particles is $\sim 1\times10^{37}(D/8\ \mathrm{kpc})^{2.5}(t/10^4\ \mathrm{yr})^{-1}$ erg s^{-1} (as estimated from the data of Kulkarni et al. 1994). When the internal magnetic field is very strong, most of the energy released by its decay is radiated away in the form of neutrinos and Alfvén radiation rather than surface X-ray emission (TD95); much of the Alfvén wave energy is plausibly transferred to relativistic particles. The much greater Alfvén wave luminosity that is deduced for SGR 1806−20, as compared with SGR 0526−66,[24] then implies that the internal magnetic field of SGR 0526−66 is either weaker *or* stronger than the internal field of SGR 1806−20. That is, if the internal magnetic field is stronger than $B_\mu \simeq 6\times10^{15}$ G [equation (12)], magnetic stresses overwhelm lattice stresses, and the crust undergoes a continuous plastic deformation, suppressing seismic activity (TD95). The hypothesis that SGR 1806−20 is much more seismically active than SGR 0526−66 is consistent with the fact that SGR 1806−20 has been observed to emit 10 times more bursts than SGR 0526−66 (which themselves appear to have been 'aftershocks' of the March 5 event).

These two burst sources, however, differ qualitatively in several observational properties. Unlike SGR 1806−20, SGR 0526−66 definitely does not have a supergiant companion (Fishman, Duthie & Dufour 1981) or associated radio plerion emissions (Junkes 1991); and only SGR 0526−66 emitted the extremely luminous 1979 March 5 burst.[25] Thus we will now consider the possibility that SGR 1806−20 is indeed a much more rapid rotator (by a factor of $\gtrsim 100$) than SGR 0526−66.

In this case, a strong magnetic field is still required to enhance burst luminosities to the observed hyper-Eddington values, but in SGR 1806−22 (unlike SGR 0526−66) this field must necessarily be concentrated in high multipoles for the star to maintain a large spin-down luminosity.

One possibility is that 1806−20 is a magnetar which, very early in its life, experienced a large-scale magnetic interchange instability (Flowers & Ruderman 1977) which dramatically reduced the external dipole field, while retaining most of the internal magnetic energy of the star. Although such an instability can be suppressed (at least initially) by the strong internal toroidal field which is generated by an α–Ω dynamo, it is none the less possible that diverse internal magnetic configurations exist among magnetars, on account of differing rotational and convective histories. For example, magnetars that form near the 'strong fizzler' limit (where direct collapse to nuclear density is prevented by centrifugal forces: TD94b) may become convectively unstable in only part of their interiors. Given the complexity of the physics underlying a turbulent dynamo, we cannot rule out the possibility that low-order magnetic moments relax quickly in a subset of magnetars.

The hypothesis that 1806−20 is a magnetar with a reduced dipole field, while 0526−66 has retained most of its original dipole moment to the present era, is consistent with the fact that only 0526−66 has been observed to emit a burst as energetic as the March 5 event, which we have argued is driven by a sudden large-scale interchange instability (Section 2.1).

Another mechanism that could conceivably produce a very strong, small-scale magnetic field is a stochastic (non-helical) dynamo driven by vigorous entropy-driven convection in a new-born neutron star with a spin period in excess of ~ 10 ms (TD93a; TD94a). If the residual small-scale field is as strong as $\sim 10B_{\mathrm{QED}}$ in SGR 1806−20, however, then it is difficult to understand why the field is not so strong in *all* pulsars of comparable age, since all new-born neutron stars probably pass through a similar convective phase. By contrast, a very strong dipole field $B_{\mathrm{dipole}} \gtrsim 10^{14}$ G is generated by a helical dynamo in a new-born neutron star only if its initial spin period is as low as $P_{\mathrm{i}} \sim 1$–3 ms. Note that such a rapid initial spin is unlikely for ordinary radio pulsars (DT92).

An additional problem with this high-multipole scenario arises when one considers the spatial distribution of the radiating pair plasma. If a burst is triggered when the crust cracks and the magnetic field undergoes a small horizontal displacement, then the resulting Alfvén pulse damps at a large radius (31) and most of the plasma is confined by a relatively weak field, $B \lesssim B_{\mathrm{dipole}} \sim 10^{12}$ G. The cooling radiative flux (45) across a field this weak is comparable to the standard Eddington flux, and is much lower than the fluxes inferred for SGR bursts. Thus most of the radiative losses will occur close to the surface of the neutron star, just as in the case where B_{dipole} is very strong. However, the confining magnetic flux emerges from a small fraction $B_{\mathrm{dipole}\star}/B_\star$ of the stellar surface when the rms surface field $B_\star$ greatly exceeds the surface dipole field $B_{\mathrm{dipole}\star}$. Assuming that this flux emerges in N spots of radial extent $\Delta R \sim \frac{1}{2}R_\star$ and area $N^{-1}(B_{\mathrm{dipole}\star}/B_\star)4\pi R_\star^2$, the total radiative surface area at the base of the bubble is

$$A \sim 2\pi N^{1/2}(B_{\mathrm{dipole}\star}/B_\star)^{1/2}R_\star^2. \qquad (198)$$

Thus A is much smaller than the neutron star area, unless N is very large. This disagrees with the inferred radiative

[24]Or as compared with the peculiar X-ray pulsar 1E2259+586, which shares many properties with 0526−66 (TD93a; TD93b; Corbet et al. 1995).

[25]The absence of such an extremely luminous burst from the other SGRs could, of course, be simply an artefact of the small number statistics.

surface area of $2\times10^3(D/8\ \mathrm{kpc})^2\ \mathrm{km}^2$ for SGR 1806 − 20 (Fenimore et al. 1994). In sum, if the strong magnetic field is confined to multipoles, then *it is difficult to obtain both the high effective temperatures and the large total luminosities of the SGR bursts.*

Alternatively, the bursts could be triggered by reconnection of small-scale flux loops, which would generate a much higher frequency magnetospheric disturbance. The danger of such a model is that it is very easy to release too much energy. The reconnecting flux loops can be no larger than $l\sim0.3$ km, given that the magnetic energy contained in a volume l^3 is $\sim2\times10^{41}(B/10B_{\rm QED})^2(l/0.3\ \mathrm{km})^3$ erg. There is then an unfavourable trade-off between a very small radiative area (and long radiative time-scale associated with the high pair density) and an excessive burst energy.

7.2 SGR 0526 − 66

Perhaps the most remarkable feature of the 1979 March 5 burst, aside from its extreme brightness and initial hardness, is the close similarity between the spectrum of the soft, oscillatory tail of that burst and the spectra of the repeat bursts which were typically $\sim10^3$ times shorter and had total fluences $\sim3\times10^3$ times smaller (Mazets et al. 1982). Indeed, the bursts emitted by this source are best described as having a characteristic *temperature* rather than a characteristic *luminosity.* Many of the repeat bursts had peak fluxes within a factor of ~2 of the detection threshold (Norris et al. 1991), which might tend to give the impression of a characteristic luminosity (Paczyński 1992). However, the difference between the peak flux of the first pulse of the soft tail emission and the faintest repeat bursts was a factor of ~10, even though the best-fitting temperatures[26] differed by no more than ~10 per cent (Mazets et al. 1982).

The absence of spectral measurements for the bursts of SGR 0526 − 66 below ~25 keV makes it difficult to fit a Planckian profile reliably to these spectra (as has been done for SGR 1806 − 20: Fenimore et al. 1994). The brightest soft bursts from SGR 0526 − 66 were, however, much brighter than those from SGR 1806 − 20 (even if that source is at a distance $D\sim17$ kpc). For example, we estimate a mean photospheric energy flux of $4\times10^{29}(R/10\ \mathrm{km})^{-2}\ \mathrm{erg\ s^{-1}}$ for the first peak in the soft tail of the March 5 event (assuming quasi-spherical emision from a photosphere with radius of curvature R), which corresponds to a blackbody temperature[27] of $T_{\rm eff}\simeq25\ (R/10\ \mathrm{km})^{-1/2}$ keV, as compared with $T_{\rm eff}\simeq9$ keV for SGR 1806 − 20 (Fenimore et al. 1994). Another way of comparing the spectra is to note that the best-fitting optically thin free–free temperature is $T_{\rm ff}=36.4$ keV for the first peak in the March 5 soft tail, as compared with $T_{\rm ff}\simeq21$ keV for the brightest few bursts from SGR 1806 − 20. Scaling up the $T_{\rm eff}=9$ keV blackbody temperature of the 1806 − 20 bursts by the ratio of $T_{\rm ff}$ in the two sources, one obtains $T_{\rm eff}=16$ keV for the first peak of the March 5 soft tail. *This suggests that the first peak of the March 5 soft tail is radiated from a surface of radius ~ 20 km.*

The cooling wave model (Section 3) provides a simple explanation for the spectral similarity between the March 5 soft tail and the repeat bursts. Comparison of equations (194) and (195) shows that, when the energy of the trapped pair plasma greatly exceeds 10^{41} erg, the cooling rate of the plasma is limited by ablation of ions and electrons from the neutron star surface. In this regime, the effective temperature (195) is entirely independent of $T_{\rm c}$ and variations in luminosity are ascribed to variations in the area of the photosphere (Section 3.7). SGR bursts of energy $\sim10^{41}$ erg lie near the boundary between the two different cooling regimes (ablation-limited versus advection-limited), and thus naturally have similar $T_{\rm eff}$ to the March 5 soft tail. Finally, from equation (197) one sees that the surface dipole field strength of $\sim6\times10^{14}$ G is consistent with an X-ray luminosity of $(5\times10^3\text{–}10^4)\ L_{\rm edd}$ if the magnetic bottle has dimensions $\Delta R_{\rm max}\sim10$ km.

The pronounced modulational depth of the March 5 soft tail also deserves some comment. This indicates, first, that most of the emission was confined to one hemisphere of the neutron star and, secondly, that the radiation was strongly anisotropic and/or the radiative surface was confined to a distance of $\lesssim10$ km above the neutron star. (This is marginally consistent with the photospheric radius of ~20 km derived above.) Magnetospheric emission by a trapped pair plasma is probably consistent with these observations, since most of the radiation escapes from the E-mode photosphere close to the neutron star surface. In addition, one expects that this radiation will be anisotropic, since $T_{\rm eff}$ is high enough that photon splitting combined with rapid Compton scattering in the O-mode will cause bulk streaming of the radiation along the magnetic field lines out to a radius $R_{\rm QED}\sim(B_\star/B_{\rm QED})^{1/3}R_\star\sim24R_{\star6}$ km.

7.3 Alternative models: a critical discussion

7.3.1 Accretion-powered SGR bursts?

Sudden accretion models have been suggested for the March 5 event (Colgate & Petschek 1981; Epstein 1985; Colgate & Leonard 1994; Katz, Toole & Uhruh 1994). These models have the advantage of employing a familiar and well-studied energy source to power the bursts. It is certainly possible that the quiescent X-ray emission $L_{\rm X}\sim7\times10^{35}\ \mathrm{erg\ s^{-1}}$ detected from SGR 0526 − 66 (Rothschild et al. 1993, 1994) is due to accretion. The corresponding accretion rate of

$$\dot M\sim6\times10^{-11}\,\mathrm{M_\odot\ yr^{-1}} \tag{199}$$

implies an equilibrium spin period of

$$P_{\rm eq}=8\left(\frac{B_{\rm dipole}}{1\times10^{12}\ \mathrm{G}}\right)^{6/7}R_{\star6}^{19/7}\ \mathrm{s} \tag{200}$$

(e.g. Bhattacharya & van den Heuvel 1991). The neutron star would then be quite ordinary (albeit extraordinary in that it is actively accreting while residing in a young SNR). Of course, no evidence for a binary companion has been found (Fishman et al. 1981), and the recoil velocity implied by the displacement of SGR 0526 − 66 from the centre of the SNR (Section 1.1) is large enough to disrupt even a tight binary. Nevertheless, it is conceivable that the neutron star accretes from a fossil disc without any binary companion (cf. Colgate & Leonard 1994). In this case, an external trigger for bursts would apparently be required.

[26]Assuming optically thin free–free emission, which is physically inconsistent (Section 3.2).
[27]Emission in two polarization states.

Unfortunately, sudden accretion models have great difficulty in accounting for the 1979 March 5 burst, for a number of reasons. First, accretion of $\sim 3\times10^{24}$ g would be required to power the March 5 burst. This is $\sim 1/30$ the mass of the Moon. Secondly, this mass is far too large to be supported in the magnetosphere of a neutron star with $B_{\rm dipole}\sim 10^{12}$ G. To see this, note that the energy $\Delta E\sim 5\times10^{44}$ erg released in the March 5 burst[28] equals the energy in a dipole field of 8×10^{13} G. Suppose that the accreted mass $\Delta M\sim \Delta E/g_\star R_\star$ is suspended in the magnetosphere at a radius R which lies well inside the Alfvén radius. Then, very roughly, $B^2(\Delta R)/8\pi\sim 3GM_{\rm ns}\Delta M/4\pi R^4$. A similar estimate holds if the accreted material is deflected from a Keplerian orbit to the surface of the neutron star in ~ 1 orbital period, with the excess angular momentum being absorbed by the magnetosphere. One finds the expected result that ΔE is bounded above by the external magnetic energy of the neutron star,

$$\Delta E\sim\frac{GM_{\rm ns}\Delta M}{R_\star}\sim\frac{1}{6}B_\star^2R_\star^3\left(\frac{R}{R_\star}\right)^{-2}, \qquad (201)$$

where we have substituted $B(R)=B_\star(R/R_\star)^{-3}$. Thus a dipole field stronger than $\sim 10^{14}$ G is required to divert as much mass as 3×10^{24} g on to the neutron star surface, to power the March 5 burst. Once such a strong magnetic field is postulated, there is no need for an external burst trigger: the decaying magnetic field itself provides a plausible trigger.

Of course, the bound (201) does not apply if the accreted mass falls on a hyperbolic trajectory; but then two other difficulties arise.

First, the accretion event is a *chance event.* The neutron star presents a small impact parameter, and the probability of such a collision in a ~ 10-yr time interval presumably is very small given its large proper motion (cf. Harwit & Salpeter 1973; Tremaine & Żytkow 1986). Although the SGR bursts emitted by 0526−66 clearly seemed to be aftershocks from the March 5 event, SGR 1806−20 has remained active without emitting any burst remotely close in energy to the March 5 burst. Thus a burst of the March 5 type is not needed to trigger SGR bursts, and it seems more plausible that the triggering mechanism is internal to the star. Indeed, a 6×10^{14} G dipole field is capable of powering ~ 60 March 5 events, which together with the young age t of SGR 0526−66 suggests a recurrence rate of $(17\ {\rm yr})^{-1}\,(N/10)\,(t/10^4\ {\rm yr})^{-1}$ from N sources in the Galaxy.

The second difficulty is one of baryon contamination: the hard initial transient of the March 5 burst could not arise directly from the hot accreted material, since the baryon density in this material would be high enough to cause adiabatic dilution of photons in an expanding fireball to energies well below the hard X-ray and gamma-ray range. The upper bound on the mass carried off with the photons is $\frac{1}{2}\dot{M}V_{\rm esc}^2/L\lesssim 10^{-2}$ for $L\sim 3\times10^6\ L_{\rm edd}$ [cf. Paczyński (1990); equation (13) of Thompson (1994)]. If the accreting material is spread over the neutron star surface, the resulting Thomson scattering depth is $\tau_{\rm T}\sim\sigma_{\rm T}\Delta M/4\pi R_\star^2 m_{\rm n}\sim 1\times10^{11}$ at radius $R_\star$.

[28]The total energy released by the burst could in fact be higher, with a significant fraction being radiated in the form of neutrino pairs (Section 5).

Excess baryon contamination might be avoided if the fireball is powered by the compressed magnetic field of the neutron star. Unfortunately, only a small fraction of the accretion energy is expended by compressing the magnetic field. To see this, note that the pressure at the base of the accreted material is equal to $g\Delta M/4\pi R_\star^2$, again assuming that this material is spread uniformly over the star. The equivalent magnetic pressure is $B^2/8\pi=\Delta E/4\pi R_\star^3$. That is, the compressed field has a strength comparable to that of a dipole field that contains total energy $\sim\Delta E$. The volume of the compressed field is, however, only $\sim(B/B_\star)^{-1}4\pi R_\star^3$, and so the energy in the compressed field is

$$E_B\equiv\int_{R>R_\star}\frac{B^2}{8\pi}\,{\rm d}V\sim\left(\frac{B}{B_\star}\right)^{-1}\Delta E\,. \qquad (202)$$

For the particular case of an accretor of mass 3×10^{24} g on a neutron star with $B_{\rm dipole}=10^{12}$ G, this yields $E_B\sim 10^{-2}\Delta E$.

7.3.2 Alternative radiative mechanism: surface X-ray emission

We now consider SGR models in which the X-rays are emitted directly from the stellar surface, with the Eddington radiative flux being greatly enhanced by a very strong magnetic field (Paczyński 1992). There are several difficulties with such models.

(1) The spectra of the brightest bursts from SGR 1806−20 are depressed below the best-fitting blackbody curve at energies less than ~ 15 keV (Fenimore et al. 1994). In a surface emission model, the large free–free optical depth of the O-mode ensures that the spectrum inside the E-mode photosphere is locally a blackbody (Section 6.2); and so a low-energy cut-off is difficult to explain. By contrast, free–free absorption is ineffective in the magnetospheric emission model, and a low-energy cut-off to the spectrum is a natural consequence of the freeze-out of photon splitting at $T\sim 10$ keV (Section 6.3).

(2) The soft tail of the March 5 event showed very little evidence of spectral reddening over time (Mazets et al. 1982). The best-fitting temperature of the main pulse remained constant even while the total flux dropped by a factor of several. The secondary pulse had a temperature about 10 per cent smaller than the main pulse, but it too showed very little evidence of reddening as the intensity declined. As noted by Mazets et al. (1982), these results are inconsistent with a thermal hotspot model. Such spectral uniformity is expected for magnetospheric emission, however, since the radiating area shrinks as the confined photon-pair plasma cools, with little change in physical conditions at the X-ray photosphere where the spectrum is established. Normal SGR bursts also do not show strong spectral evolution (Kouvelioutou et al. 1987; Golentskii et al. 1987).

Note that, in the magnetospheric emission model which we favour, the neutron star surface emits a significantly fainter photon afterglow following an SGR burst (Section 4). This cooling radiation *is* predicted to soften steadily with time. Such emissions may have been detected (Kouveliotou et al. 1987), but they have been too faint for reliable spectral analysis.

Finally, we consider the possibility of nuclear-powered SGR bursts. A thermonuclear flash seems like an attractive energy source for a crustal burst because it deposits energy in a thin layer, but such an event cannot plausibly release as much as 4×10^{44} erg, the total energy radiated in the March 5 soft tail (cf. Woosley & Wallace 1982; Rothschild et al. 1993). The most energetic bursts are expected from a helium layer (perhaps built up by steady burning of hydrogen). The $3-\alpha$ reaction becomes extremely temperature-sensitive above a density[29] of $\sim10^7$ g cm^{-3}, which corresponds to a total helium mass of $\sim10^{20}$ g and a total of 1×10^{39} erg (e.g. Hameury & Lasota 1986). This is indeed close to the maximum energies of Type I X-ray bursts (e.g. Lewin et al. 1992), but it is implausible that the temperature of the accreted material could be kept low enough to prevent ignition at the accretion rate (199) while its mass grew by another 6 orders of magnitude.

7.4 Type II X-ray bursts

There are a number of remarkable similarities beween SGR bursts and Type II X-ray bursts (which have only been convincingly detected from the Rapid Burster). In particular, individual Type II XRBs show very weak spectral evolution, and often display flat-topped light curves (Lewin et al. 1992). It is clear that these bursts are triggered by the sudden accretion of material from a disc on to a neutron star, since the time-averaged Type II XRB luminosity is comparable to the quiescent X-ray luminosity (in the absence of Type II bursts). These bursts also emit much more energy than the Type I XRBs, in the expected ratio of gravitational binding energy to thermonuclear energy.

It is plausible that the same basic radiative mechanism operates in both Type II X-ray bursts and SGR events. We conjecture that the sudden accretion of material from a disc on to the neutron star excites MHD waves in the magnetosphere which cascade to higher wavenumbers, damp, and generate a trapped pair plasma (cf. Blaes & Thompson, unpublished). The observable burst is emitted as the plasma cools. A large-amplitude magnetospheric distortion is expected in any model where the burst is triggered by a significant departure from Keplerian rotation, the tension of the neutron star's magnetic field being sufficient to overcome the orbital ram pressure of the accreted material (e.g. Spruit & Taam 1993; Kuijpers & Kuperus 1994).

There is evidence that *the triggering mechanism* is different for SGR bursts and Type II XRBs. Unlike Type II XRBs, SGR events do not show any correlation between burst energy and time elapsed to the next (or since the previous) burst (Laros et al. 1987). Instead, the interburst intervals and burst energies manifest a stochastic (uncorrelated) log-normal distribution (Hurley et al. 1994). This is consistent with the hypothesis that SGR bursts are triggered not by accretion, but instead by an instability of the stellar magnetic field.

Type II XRBs range in total energy ΔE from $\sim1\times10^{38}$ erg to $\sim7\times10^{40}$ erg (Lewin et al. 1992). The upper end of this range of ΔE places significant limits on the strength of the neutron star's dipole magnetic field. If the burst is indeed the radiative signature of a cooling pair plasma, then the minimum surface dipole field needed to confine the plasma in the most energetic bursts is $\sim1\times10^{12}$ G. [This assumes an axisymmetric confinement region of outer radius $R_{\rm max}\sim2R_\star$: DT94, see also equation (2).] We obtain a similar estimate of the surface field strength by demanding that the field be strong enough to trigger the most energetic bursts. For a maximum burst energy $E_{\rm max}$, equation (201) implies that the surface dipole field must be stronger than[30]

$$B_{\rm dipole}>8\times10^{11}\left(\frac{E_{\rm max}}{10^{41}\ {\rm erg}}\right)^{1/2}\ {\rm G}, \tag{203}$$

with this bound being saturated only if the accreted material is released close to the stellar surface.

The accreted material will also be a source of X-rays. If this material is released suddenly toward the neutron star surface from a radius not much larger than $R_\star$, the ions will be heated initially by an accretion shock to a temperature $\sim GM_\star m_{\rm n}/R_\star$. The resulting thermal pressure is sufficient to support a cloud of scaleheight $\sim R_\star$. Most of the thermal energy is rapidly converted to photons and pairs, and the scattering depth through the cloud is comparable to the estimate (62). If the photon luminosity were limited by diffusion, then the cooling time of the plasma (64) would be much longer than the observed durations of Type II XRBs, and the cooling luminosity would be far lower than $L_{\rm edd}$.

The cooling luminosity may greatly exceed that expected from diffusion if the plasma is accreted along open field lines. In this case, bubbles of photons can escape buoyantly along the field lines (Arons 1992), since the magnetic field provides lateral support but not radial confinement. A cooling luminosity at high as $L\sim L_{\rm edd}$ cannot be excluded.

Alternatively, the accreted plasma may be largely disconnected from the star's magnetic field, as in the Kuijpers and Kuperus (1994) model. In this second case, the accreted plasma is compressed by the confining magnetic field once the field lines that supported it have reconnected (Fig. 9b). The photon luminosity emitted by the plasma is then strongly suppressed, both because the pair density increases under compression, and because photon bubbles do not transport the radiation effectively across the magnetic field lines. Once the plasma thermalizes, its temperature drops from ~100 MeV to a value given by the pressure balance $(\pi^2/45)T^4=B^2/8\pi$ (we assume $T\ll m_{\rm e}$), which implies that $T=230\,B_{12}^{1/2}$ keV. Because the electron-pair density depends on T in a complicated way, we normalize to $B=10^{12}$ G in what follows. The resulting Thomson depth through the pairs is $\tau_{\rm T}=1\times10^{12}l_6$. Assuming the plasma to be distributed in an equatorial ring of radial and horizontal thickness

[29]This applies to relatively high accretion rates, as is inferred for SGR 0526−66 if the quiescent X-ray emission is powered by accretion [Rothschild et al. 1993; equation (199)].

[30]A similar equation was deduced by Kuijpers & Kuperus (1994), but was not used by them to constrain the dipole field strength of the Rapid Burster. They obtained a similar value of $B_{\rm dipole}$ by a related method. In addition, the magnetic distortion energies estimated by Kuijpers & Kuperus exceed the maximum Type II XRB energy by one order of magnitude. We would argue that most of the distortion energy would in fact be converted to electron–positron pairs via Alfvén wave damping, and then radiated.

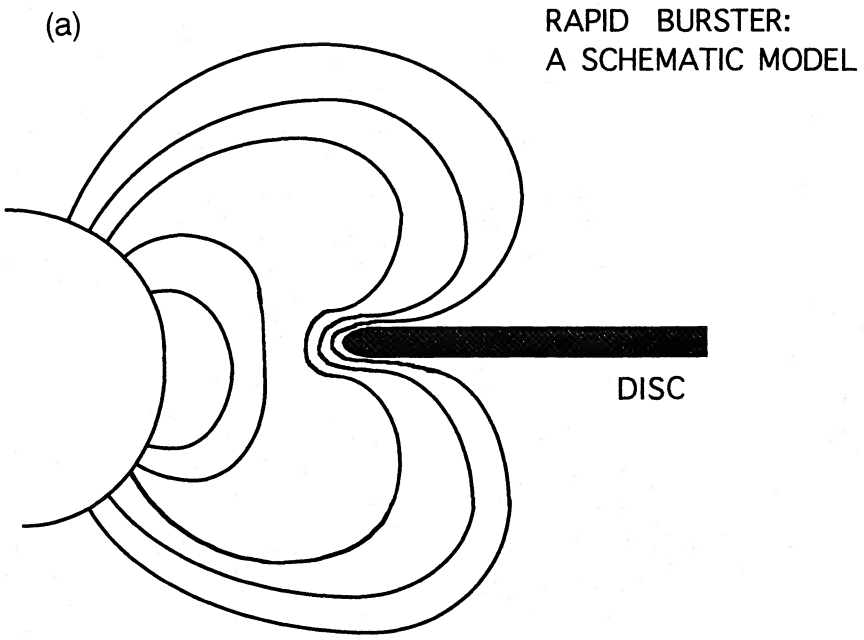

Figure 9. (a) A schematic model for the Rapid Burster (cf. Spruit & Taam 1993; Kuijpers & Kuperus 1994). The accretion disc penetrates inward past the corotation radius, and the magnetic field lines inside the inner disc edge are loaded with plasma.

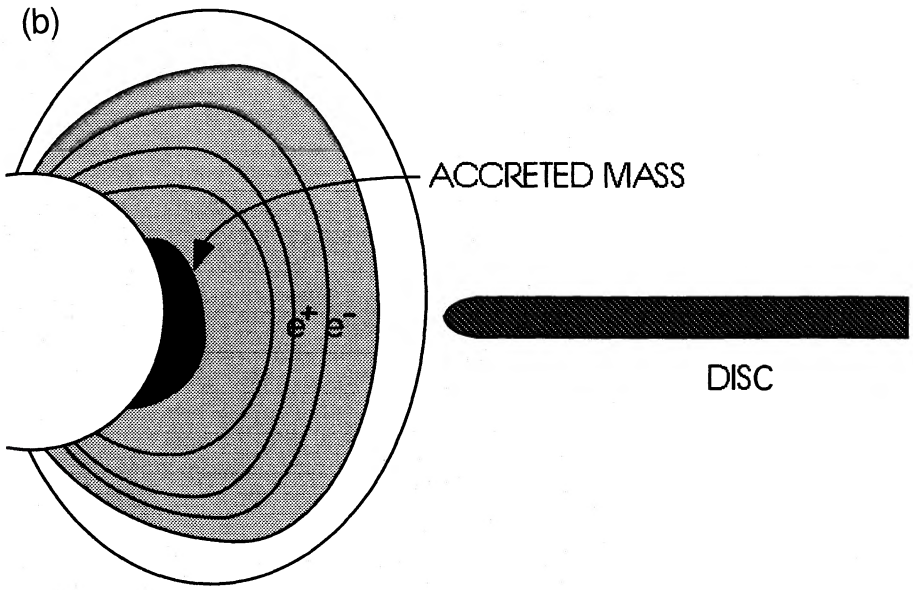

Figure 9. (b) Material from the disc is suddenly diverted toward the neutron star surface, triggering a Type II burst. The simultaneous emission of Type I and Type II X-ray bursts from the Rapid Burster suggests (1) that the surface magnetic field is patchy, with large areas (the sites of the Type I bursts) containing only a weak field $B \lesssim 10^{11}$ G, and (2) that material from the disc is accreted *across* the magnetic field lines, rather than along them. In the illustration, the dipole magnetic flux is concentrated near the magnetic poles.

l, one finds that $\tau_T = 4 \times 10^{11} (\Delta E_{41})^{1/2}$ and

$$L \sim \frac{2\pi R_\star l c}{\tau_T} \left(\frac{B^2}{8\pi} \right) \sim 7 \times 10^{33} \text{ erg s}^{-1}, \tag{204}$$

independent of ΔE. If instead $B = 10^{11}$ G, one finds that $L \sim 5 \times 10^{36}$ erg s^{-1}. In either case, this luminosity is insignificant compared to the persistent emission detected after Type II XRBs, or between periods of Type II XRB activity (Lewin et al. 1992).

If the Rapid Burster does indeed have a dipole field as strong as $\sim 10^{12}$ G, then it is difficult, at first sight, to understand why this object is also a source of Type I XRBs, which are usually associated with weakly magnetized neutron stars ($B \lesssim 10^{11}$ G). It should be emphasized, however, that a field of this strength is needed to explain the highest energy Type II XRBs, if the sudden accretion events are due to a magnetospheric instability. The Rapid Burster is a unique

object, and its surface field may have an unusual structure. A simple explanation for the simultaneous appearance of Type I and Type II XRBs is that *the Rapid Burster is a neutron star the magnetic field of which is in the process of being buried.* We suggest that the accreted matter is deposited mainly in regions of the neutron star surface with a low flux density, where thermonuclear flashes can occur, while strong field patches survive to support the dipole field of $\sim 10^{12}$ G (Figs 9a and b). That is, the Rapid Burster may provide the first detailed evidence for the mechanism of accretion-induced field decay (e.g. Taam & van den Heuvel 1986; Shibasaki et al. 1989; Phinney & Kulkarni 1994) which has long been suggested as the origin of weak-field pulsars.

This also provides some circumstantial evidence that most of the accreted material does flow *across* the dipole field lines, rather than along them. In order to explain the presence of Type I XRBs, the dipole field of the Rapid Burster must be anchored in regions of the neutron star surface that do not receive substantial accreted material. This implies that the accreted material is mainly *disconnected* from the magnetic field of the neutron star, and that *the main energy source for Type II XRBs is the release of magnetic distortion energy, not the direct photon cooling of the accreted material.*

A second, independent, argument suggests that accretion occurs across the dipole field lines (Kuijpers & Kuperus 1994). The maximum burst luminosity of $\sim 7\times 10^{40}$ erg is achievable with a dipole field of order 10^{12} G only if, at the onset of such a luminous burst, the innermost orbit of the Keplerian disc reaches in close to the stellar surface. In such a situation, the disc must strongly compress the dipole field lines in the equatorial plane (Fig. 9a). If the material that triggers the burst is suspended in the magnetosphere just inside the inner radius of the Keplerian disc (and corotates with the neutron star, at an angular velocity well below the local Keplerian angular velocity), then there is a strong energetic barrier against this material flowing along the poloidal field lines (which are directed outward from the star at the inner edge of the Keplerian disc). A burst occurs when the field lines reconnect and the magnetic support is lost.

This model provides a simple explanation for a number of observational features of Type II XRBs. The following should be noted in particular.

(1) The much lower flux of Type II XRBs ($L\sim L_{\rm edd}$) compared with SGR bursts [$L\sim(10^3$–$10^4)L_{\rm edd}$] can be attributed to a weaker confining field, $B\sim 10^{12}$ G. At the observed colour temperatures of ~ 1.5–2 keV (Lewin et al. 1992), the E-mode scattering opacity is reduced below $\kappa_{\rm T}$ at the stellar surface by a factor $\sim 3B_{12}^{-2}$, but is close to $\kappa_{\rm T}$ at a radius $2R_\star$. The radiative solution is therefore a hybrid of the strong-field and weak-field Eddington-limited solutions (B) and (C) of Section 3.4. The magnetic Eddington limit (for diffusion across the magnetic field lines) yields the effective temperature $T_{\rm eff}=3(B/10^{12}\ {\rm G})^{1/3}\,Y_{\rm e}^{-1/6}$ keV at the stellar surface, which is very close both to the observed colour temperatures and to the non-magnetic Eddington effective temperature. Our treatment of the cooling of the trapped plasma (Section 3.4) suggests, first, that the energy that leaks out of the inner, pair-dominated plasma is concentrated in a layer of height $\sim R_\star$ above the stellar surface; but, secondly, that, by the time this energy reaches the photosphere, pressure gradient forces along the magnetic field lines can spread the radiative flux more uniformly.

(2) The radiative area of the Type II X-ray bursts typically exceeds the radiative area inferred for Type I X-ray bursts by a factor of ~ 3 (Lewin et al. 1992), which suggests that the radiation is emitted from the magnetosphere, and not directly from the accreted material.

(3) There is a minimum accreted mass (burst energy) that is sufficient to generate an optically thick electron–positron plasma. The minimum temperature is $T=22$ keV across a distance ~ 10 km, which corresponds to an energy

$$\Delta E\sim 1\times 10^{38}\Delta R_{\rm max\,6}^3\ {\rm erg} \qquad (205)$$

within a volume $\Delta R_{\rm max}^3$. Bursts of lower energy may still generate optically thick plasma, but the dominant source of opacity in that case is the electron–baryon contaminant. The opacity of the electron–positron plasma is much more uniform in local thermodynamic equilibrium. By contrast, the photon bubble instability can segregate the photons and the electron–baryon component (Arons 1992), with the result that the emergent radiative flux may be more intermittent. *This may explain the erratic time profiles of low-energy ($E\lesssim 10^{38}$ erg) Type II XRBs.*

(4) When the photon-pair plasma is confined in a volume much larger than that of the neutron star ($\Delta R_{\rm max}\gg R_\star$), the emergent luminosity hardly changes as the photosphere propagates inward (Section 3.7). If the confined pair plasma is axially symmetric (as is needed in order to explain the absence of a strong rotational modulation of Type II XRBs), a large decrease in the volume of the confined pair plasma is accompanied by only a moderate change in the area A of the radiative surface. Moreover, the increase in A during a burst is largely compensated by a decrease in the Eddington-limited radiative flux associated with the larger temperature gradient scale at the photosphere (Section 3.7). In this model, one also might be able to understand why the most energetic Type II XRBs tend to have flat-topped profiles with *reduced* fluxes (Lewin et al. 1992): when the confining magnetic field lines are anchored close to the rotation axis, the escaping radiative flux peaks along the magnetic axis. Thus the larger the confining volume of the pair plasma, the more strongly peaked is the radiative flux about the magnetic axis, and the lower is the flux detected off-axis. Note that such a correlation would be difficult to understand if the X-rays were emitted from the surface of the neutron star.

ACKNOWLEDGMENTS

CT thanks Omer Blaes for a collaboration on Alfvén wave damping, which has helped make this model more precise, and Robert Nelson for several discussions of Compton scattering in magnetic fields, as well as for a conversation in which the idea for Section 4 was developed. He also thanks Lars Bildsten, Cole Miller, Bohdan Paczyński and Malvin Ruderman for conversations. RCD thanks Anand Kudari for sharing his calculations on magnetized pair bubbles, and Ethan Vishniac for discussions and much-needed encouragement. This work was supported by the NASA Theoretical Astrophysics Program, Grant No. NAGW-2418; by the NSERC of Canada; and by the Texas Advanced Research Program, Grant No. ARP-279.

REFERENCES

Adler S. L., 1971, Ann. Phys., 67, 599
Adler S. L., Bahcall J. N., Callan C. G., Rosenbluth M. N., 1970, Phys. Rev. Lett., 25, 1061
Alexander S.-P., Mészáros P., 1991, ApJ, 372, 545
Arons J., 1992, ApJ, 388, 561
Atteia J.-L. et al., 1987, ApJ, 320, L105
Barat C. et al., 1983, A&A, 126, 400
Baym G., Pines D., 1971, Ann. Phys., 66, 816
Berestetskii V. D., Lifshifz E. M., Pitaevskii L. P., 1982, Quantum Electrodynamics. Pergamon Press, Oxford
Bhattacharya D., van den Heuvel E. P. J., 1991, Phys. Rep., 203, 1
Bisnovaty-Kogan G. S., 1993, Astron. Astrophys. Trans., 3, 287
Blaes O., Blandford R., Goldreich P., Madau P., 1989, ApJ, 343, 829
Burrows A., 1987, ApJ, 318, L57
Burrows A., Lattimer J. M., 1988, Phys. Rep., 163, 51
Cline T. L. et al., 1980, ApJ, 237, L1
Cline T. L. et al., 1982, ApJ, 255, L45
Colgate S. A., Leonard P. J. T., 1994, in Fishman G. J., Brainerd J. J., Hurley K., eds, Gamma-Ray Bursts. Am. Inst. Phys., New York, p. 581
Colgate S. A., Petschek A. G., 1981, ApJ, 248, 771
Corbet R. H. D., Smale A. P., Ozaki M., Koyama K., Iwasawa K., 1995, ApJ, 443, 786
Dicus D. A., 1972, Phys. Rev. D, 6, 941
Dorofeev O. F., Rodionov V. N., Ternov I. M., 1985, Sov. Astron. Lett., 11, 123
Duncan R. C., Thompson C., 1992, ApJ, 392, L9 (DT92)
Duncan R. C., Thompson C., 1994, in Fishman G. J., Brainerd J. J., Hurley K., eds, Gamma-Ray Bursts. Am. Inst. Phys., New York, p. 625 (DT94)
Duncan R. C., Li H., Thompson C., 1993, in Friedlander M., Gehrels N., Macomb R. J., eds, Compton Gamma Ray Observatory. Am. Inst. Phys., New York, p. 1074
Eichler D., Cheng A. F., 1989, ApJ, 336, 360
Epstein R. I., 1985, ApJ, 291, 822
Felten J. E., Rees M. J., 1972, A&A, 17, 226
Fenimore E. E., Evans W. D., Klebasadel R. W., Laros J. G., Terrell J., 1981, Nat, 289, 42
Fenimore E. E., Laros J. G., Ulmer A., 1994, ApJ, 432, 742
Fishman G. J., Duthie J. G., Dufour R. J., 1981, Ap&SS, 75, 135
Flowers E., Ruderman M., 1977, ApJ, 315, 302
Goldreich P., Reisenegger A., 1992, ApJ, 395, 250
Golenetskii S. V. et al., 1982, Sov. Astron. Lett., 8, 354
Golenetskii S. V., Ilyinskii V. N., Mazets E. P., 1984, Nat, 307, 41
Golenetskii S. V. et al., 1987, Sov. Astron Lett., 13, 166
Hameury J. M., Lasota J. P., 1986, in Liang E. P., Petrosian V., Gamma-Ray Bursts. Am. Inst. Phys., New York, p. 177
Harwit M., Salpeter E. E., 1973, ApJ, 186, L37
Hernquist L., 1985, MNRAS, 213, 313
Herold H., 1979, Phys. Rev. D, 19, 2668
Hurley K. et al., 1994, ApJ, 431, L31
Hurley K. J., McBreen B., Rabbette M., Steel S., 1994, A&A, 288, L49
Janka H.-T., Müller E., 1994, A&A, 290, 496
Joss P. C., Li F. K., 1980, ApJ, 238, 287
Junkes N., 1991, in Haynes R., Milne D., eds Proc. IAU Symp. 149, The Magellanic Clouds. Kluwer, Dordrecht, p. 347
Katz J. I., Toole H. A., Unruh S. H., 1994, ApJ, 437, 727
Kouveliotou C. et al., 1987, Nat, 322, L21
Kouveliotou C. et al., 1993, ApJ, 362, 728
Kuijpers J., Kuperus M., 1994, A&A, 286, 491
Kulkarni S. R., Frail D. A., 1993, Nat, 365, 33
Kulkarni S. R., Frail D. A., Kassim N. E., Murakami T., Vasisht G., 1994, Nat, 368, 129
Kulkarni S. R., Matthews K., Neugebauer G., Reid I. N., van Kerkwijk M. H., Vasisht G., 1995, ApJ, 440, L61
Lamb D. Q., 1982, in Lingenfelter R. E., Hudson H. S., Worrall D. M., eds, Gamma-Ray Transients and Related Astrophysical Phenomena. Am. Inst. Phys., New York, p. 249
Laros J. G. et al., 1987, ApJ, 320, L111
Lewin W. H. G., van Paradijs J., Taam R. E., 1992/3, Space Sci. Rev., 62, 223
Li H., Duncan R. C., Thompson C., 1994, in Fishman G. J., Brainerd J. J., Hurley K., eds, Gamma-Ray Bursts. Am. Inst. Phys., New York, p. 600
Lightman A., 1981, ApJ, 244, 392
Loskutov Yu. M., Skobelev V. V., 1986, Sov. J. Nucl. Phys., 43, 964
Lynden-Bell D., Boily C., 1994, MNRAS, 267, 146
Lyne A. G., Lorimer D. R., 1994, Nat, 369, 127
Mazets E. P. et al., 1979, Nat, 282, 587
Mazets E. P., Golenetskii S. V., Guryan Yu. A., Ilyinskii V. N., 1982, Ap&SS, 84, 173
Melia F., Fatuzzo M., 1993, ApJ, 408, L9
Mészáros P., 1992, High-Energy Radiation from Magnetized Neutron Stars. Univ. Chicago Press, Chicago
Mészáros P., Nagel W., Ventura J., 1980, ApJ, 238, 1066
Mikić Z., Linker J. A., 1994, ApJ, 430, 898
Moffatt H. K., 1986, J. Fluid Mech., 159, 359
Murakami T., Tanaka Y., Kulkarni S. R., Ogasaka Y., Sonobe T., Ogawara Y., Aoki T., Yoshida A., 1994, Nat, 368, 127
Narayan R., Popham R., 1989, ApJ, 346, L25
Negele J. W., Vautherin D., 1973, Nucl. Phys., A207, 298
Norris J. P., Hertz P., Wood K. S., Kouveliotou C., 1991, ApJ, 366, 240
Paczyński B., 1990, ApJ, 363, 218
Paczyński B., 1992, Acta Astron., 42, 145
Pethick C. J., Thorsson V., 1994, Phys. Rev. Lett., 72, 1964
Phinney E. S., Kulkarni S. R., 1994, ARA&A, 32, 591
Podsiadlowski Ph., Rees M. J., Ruderman M., 1995, MNRAS, 273, 755
Rothschild R. E., Lingenfelter R. E., Seward F. D., Vancura O., 1993, in Friedlander M., Gehrels N., Macomb R. J., eds, Compton Gamma Ray Observatory. Am. Inst. Phys., New York, p. 808
Rothschild R. E., Kulkarni S. R., Lingenfelter R. E., 1994, Nat, 368, 432
Ruderman M., 1991, ApJ, 382, 587
Schmidt G. D., 1989, in Davies-Phillip A. G. D. et al., eds, Proc. IAU Colloq. 95, Faint Blue Stars. L. Davis Press, Schenectady, NY, p. 377
Schmidt G. D., Liebert J., 1987, Ap&SS, 131, 549
Shibasaki N., Murakami T., Shaham J., Nomoto K., 1989, Nat, 342, 656
Silant'ev N. A., Yakovlev D. G., 1980, Ap&SS, 71, 45
Sonobe T., Murakami T., Kulkarni S. R., Aoki T., Yoshida A., 1994, ApJ, 436, L23
Soyeur M., Brown G. E., 1979, Nucl. Phys., A324, 464
Spruit H., Taam R. E., 1993, ApJ, 402, 593
Sturrock P. A., Kaufman P., Moore R. L., Smith D. F., 1984, Sol. Phys., 94, 341
Taam R. E., Van den Heuvel E. P. J., 1986, ApJ, 305, 235
Thompson C., 1994, MNRAS, 270, 480
Thompson C., Duncan R. C., 1993a, ApJ, 408, 194 (TD93a)
Thompson C., Duncan R. C., 1993b, in Friedlander M., Gehrels N., Macomb R. J., eds, Compton Gamma Ray Observatory. Am. Inst. Phys., New York, p. 1085 (TD93b)
Thompson C., Duncan R. C., 1994a, in Stephan V., ed., Research Trends in Plasma Astrophysics. Am. Inst. Phys., New York, in press (TD94a)
Thompson C., Duncan R. C., 1994b, in Fruchter A. S., Taviani M., Backer D., eds, ASP Conf. Ser. Vol. 72, Millisecond Pulsars: A Decade of Surprise. Astron. Soc. Pac., San Francisco, p. 301 (TD94b)
Thompson C., Duncan R. C., 1995, ApJ., submitted
Tohline J. E., 1984, ApJ, 285, 721

Tremaine S., Zytkow A. N., 1986, ApJ, 301, 155
Ulmer A., 1994, ApJ, 437, L111
Ulmer A., Fenimore E. E., Epstein R. I., Ho C., Klebesadel R. W., Laros J. G., Delgado F., 1993, ApJ, 418, 395
Urpin V. A., Yakolev D. G., 1980, SvA, 24, 126
Van Riper K. A., 1991, ApJ, 372, 251
Van Riper K. A., Epstein R. I., Miller G. S., 1991, ApJ, 381, L47
Vancura O., Blair W. P., Long K. S., Raymond J. C., 1992, ApJ, 394, 158
Vasisht G., Kulkarni S. R., Frail D. A., Greiner J., 1994, ApJ, 431, L35
Vasisht G., Frail D. A., Kulkarni S. R., 1995, ApJ, 440, L65
Wilson J. R., Mayle R. W., 1989, preprint
Woosley S. E., Wallace R. K., 1982, ApJ, 258, 716

APPENDIX A

In this appendix, we derive the depth to which a neutron star crust is heated when exposed to a hot pair plasma above its surface for a time Δt.

We first treat the case where the crustal electrons dominate the heat capacity. The characteristic radiative diffusion scale $(\chi\Delta t)^{1/2}$, in the presence of a very strong vertical magnetic field, is given by equation (108). As the density in this expression is unknown, we require a relation between density and depth. We use, for simplicity, the $\rho(\Delta z)$ relation for a cold crust supported by electron degeneracy pressure. This is reasonable since the electrons at depth $(\chi\Delta t)^{1/2}$ become only moderately non-degenerate (as we can demonstrate below). The strong density dependence of χ [equation (105)], combined with the exponential decrease of the mean electron thermal energy beyond the characteristic diffusion depth, implies that the electrons rapidly become non-degenerate at $\Delta z \gtrsim (\chi\Delta t)^{1/2}$.

The pressure of a degenerate, relativistic Fermi gas in a very strong magnetic field is $P_e = p_{F,e}^2 eB/12\pi^2 = (\pi Y_e \rho)^2/3eBm_n^2$, where $p_{F,e}$ is the one-dimensional electron Fermi momentum. Substituting this expression into the equation of hydrostatic equilibrium, we find

$$\Delta z = \frac{2\pi^2 Y_e^2}{3}\frac{\rho}{eBm_n^2 g} = 4.6\times 10^2 (B/B_{QED})^{-1}\rho_6 (g_{14}/2)^{-1}. \quad \text{(A1)}$$

Setting $\Delta z = (\chi\Delta t)^{1/2}$, we obtain the depth of the heated layer,

$$(\chi\Delta t)^{1/2} = 2.5\times 10^2 \Delta t_{-1}^{1/4} T_{MeV}^{1/4} (g_{14}/2)^{-1/2}\ \text{cm}, \quad \text{(A2)}$$

as well as the density at this depth,

$$\rho = 5.3\times 10^6 \Delta t_{-1}^{1/4} (B/10B_{QED}) T_{MeV}^{1/4} (g_{14}/2)^{1/2}\ \text{g cm}^{-3}. \quad \text{(A3)}$$

Note that the depth (A3) is independent of B. This is in accord with detailed calculations of radiative transport in neutron star crusts, which indicate that the temperature contrast across the crust is only weakly dependent on B (Hernquist 1985).

Finally, we show that the electrons are only mildly non-degenerate. The one-dimensional electron Fermi energy at depth $(\chi\Delta t)^{1/2}$ in a cold neutron star crust is

$$\frac{E_{F,e}}{T} = \frac{2\pi^2 Y_e \rho}{eBm_n T} = 0.08\,\Delta t_{-1}^{1/4} T_{MeV}^{-3/4} (g_{14}/2)^{1/2}. \quad \text{(A4)}$$

This yields $E_{F,e}/T \sim 0.3$–0.5 for parameters applicable both to the March 5 event and to SGR bursts.

Next, we treat the case where the photons dominate the heat capacity, as appropriate for the model of the March 5 event which indicates that $T \sim 1$ MeV. From equation (107) for the radiative diffusivity χ, the characteristic diffusion depth is

$$(\chi\Delta t)^{1/2} = 5.2\times 10^1 \Delta t_{-1}^{1/2} (B/10B_{QED}) T_{MeV}^{1/2} \rho_6^{-1}\ \text{cm}. \quad \text{(A5)}$$

Equating this to the depth (A1) of the cold crust at density ρ, we obtain

$$(\chi\Delta t)^{1/5} = 5.0\times 10^1 \Delta t_{-1}^{1/3} (B/10B_{QED})^{1/3} T_{MeV}^{-2/3} (g_{14}/2)^{-1/3}\ \text{cm}. \quad \text{(A6)}$$

We then have the total energy absorbed by the cold crust,

$$E_{th} = A(\chi\Delta t)^{1/2}\times\frac{\pi^2}{15}T^4 = 7\times 10^{40}\Delta t_2^{1/3}(B/10B_{QED})^{1/3} T_{MeV}^{10/3} A_{12}\ \text{erg}, \quad \text{(A7)}$$

where we now normalize Δt to $\Delta t_2 \times 10^2$ s. This energy is much smaller than the total energy radiated in the soft tail of the March 5 event. One may express this result in terms of an absorption luminosity,

$$L_{absorb} = 7\times 10^{38}\Delta t_2^{-2/3}(B/10B_{QED})^{1/3} T_{MeV}^{10/3} A_{12}\ \text{erg s}^{-1}, \quad \text{(A8)}$$

which lies well below the magnetic Eddington limit (42).

APPENDIX B

The Rosseland mean coefficients defined in equations (164) and (165) are

$$\frac{1}{\alpha_T(B,T,\mu)} = \frac{1}{\alpha_T(B,T,0)}\frac{\int_0^\infty d\nu\,\nu^{-2}\frac{\partial B_\nu(T,\mu)}{\partial T}}{\int_0^\infty d\nu\,\nu^{-2}\frac{\partial B_\nu(T,0)}{\partial T}} \times \frac{\int_0^\infty d\nu\frac{\partial B_\nu(T,0)}{\partial T}}{\int_0^\infty d\nu\frac{\partial B_\nu(T,\mu)}{\partial T}} \quad \text{(B1)}$$

and

$$\frac{1}{\alpha_\mu(B,T,\mu)} = \frac{1}{\alpha_T(B,T,0)}\frac{\int_0^\infty d\nu\,\nu^{-2}\frac{\partial B_\nu(T,\mu)}{\partial \mu}}{\int_0^\infty d\nu\,\nu^{-2}\frac{\partial B_\nu(T,0)}{\partial T}} \times \frac{\int_0^\infty d\nu\frac{\partial B_\nu(T,0)}{\partial T}}{\int_0^\infty d\nu\frac{\partial B_\nu(T,\mu)}{\partial \mu}}. \quad \text{(B2)}$$

Similar expressions for $\beta_{T,\mu}$ are obtained by substituting $(B_n)_\nu(T, \mu)$ for $B_\nu(T, \mu)$ in these expressions. These expressions may be easily evaluated in terms of the coefficients $I_1(\mu/T)$–$I_4(\mu/T)$ given in equation (168). At small μ/T, one finds the following relation:

$$\frac{1}{\alpha_\mu(B, T, \mu \simeq 0)} = \frac{1}{\beta_T(B, T, \mu \simeq 0)} = \frac{2\pi^2}{15\zeta(3)} \frac{\ln(T/\mu)}{\alpha_T(B, T, 0)}. \quad \text{(B3)}$$